

**CHARACTERISATION OF A SNARE-COMPLEX
INVOLVED IN GOLGI-TO-ER RETROGRADE TRANSPORT
IN MAMMALIAN CELLS**

Dissertation for the degree of PhD
at the Georg-August-University of Göttingen
Faculty of Mathematical and Natural Sciences

submitted by

Sophie Verrier

born in Decize, FRANCE

Göttingen November 2005

Examiners:

Prof. Dr. H.D. Söling
Prof. Dr. F.W. Schürmann
Prof. Dr. G.H. Braus

ACKNOWLEDGEMENTS

I would like to express my gratitude to Prof. Dr. Hans-Dieter Söling for the opportunity to perform my PhD within his laboratory, for his interest, support and enthusiasm. I am also grateful for his critical reading of the manuscript.

I am also grateful to Prof. Dr. Reinhard Jahn for his support and for providing the working environment at the Dept. of Neurobiology, Max Planck Institute of Biophysical Chemistry.

I would like to thank Prof. Dr. Friedrich-W. Schürmann of the Dept. of Cell Biology, and Prof. Dr. Gerhard H. Braus of the Dept. of Molecular Microbiology, for being my co-referee and examiner, respectively.

I would like to acknowledge all the people who have been working with me and all those that have honoured me with their friendship and their presence.

Finally, I wish to say an enormous “MERCI” to my family and my friends for constant support and encouragement throughout my PhD and previous studies.

*„Auch aus Steinen, die einem
in den Weg gelegt werden,
kann man Schönes bauen“
Goethe.*



SUMMARY

The intracellular trafficking allows dynamic flux of proteins and lipids between different compartments. This is largely mediated by the budding of vesicles from a donor compartment, followed by their transport to an acceptor compartment membrane and subsequent fusion. Nevertheless, tubular transport still has to be considered as an additional mode of transport throughout the cell.

The SNARE-proteins have been characterized as playing an essential role in docking and fusion events occurring between two organelles. Four α -helices from SNARE-proteins form a stable, parallel four-helix bundle that facilitates lipid bilayer fusion. The first SNARE complex to be identified was the synaptic complex. A SNARE-complex homologous to the synaptic complex has been shown to be involved in Golgi-to-ER retrograde transport in yeast. By homology with this complex, we assumed the participation of the following SNAREs in Golgi-to-ER traffic in mammalian cells: mSec22b as the R-SNARE, Syntaxin18, mUse1 and mSec20 as the three Q-SNAREs. Even though this putative retrograde Golgi-ER SNARE-complex does not follow the “1R-3Q rule” previously defined for other SNARE-complexes, the data obtained here by live cell fluorescence measurements (FRET and BiFC) and coimmunoprecipitation showed that the addressed mammalian SNARE-homologs indeed form a SNARE-complex.

The cellular machinery for COPI-dependent Golgi-to-ER retrograde transport regulates the exit of specific cargo from the Golgi to the ER. The KDEL receptor Erd2 is known to cycle between the Golgi and the ER following the COPI-pathway. It serves the continuous recycling of escaped ER proteins which contain a KDEL motif at their C-terminus. Using live cell FRET measurements, mSec22b, mUse1 and mSec20 were found to individually interact with Erd2. Moreover, the combination of a cell-free budding assay for Golgi-derived vesicles with immuno-electron microscopy revealed the presence of mSec22b and mUse1 in COPI-coated vesicles. Additionally, mUse1 antibodies co-precipitated β' -COP (a COPI-subunit) as well as KDEL-R. Finally, using the cholera toxin (CTX) as an external KDEL-protein, I was able to show that the down-regulation of mSec22b using siRNA disturbs Golgi-to-ER retrograde transport.

In summary, my results strongly suggest the involvement of the SNAREs mSec22b, mUse1, mSec20 and Syntaxin18 in various steps of the retrograde Golgi-to-ER transport in mammalian cells.

Table of contents

1. INTRODUCTION	5
1.1. The intracellular traffic	5
1.1.1. Vesicular transport.....	6
1.1.2. Tubular transport	7
1.2. Role of the coat-proteins : focus on COPI-vesicles	8
1.3. Structure and function of the SNARE-proteins	12
1.3.1. Discovery of the SNAREs.....	13
1.3.2. Definition and structural features	13
1.4. Accessory and regulatory proteins	17
1.5. Golgi –ER cycle	20
1.5.1. The Endoplasmic reticulum.....	20
1.5.2. The Golgi apparatus	21
1.5.3. The Intermediate Compartment.....	22
1.5.4. Retrograde pathways	23
1.5.4.1. COPI dependent and independent transport pathways.....	23
1.5.4.2. Golgi-ER SNAREs.....	25
1.5.4.3. The cholera toxin as external cargo protein	26
2. AIM OF THIS WORK	29
3. MATERIALS	31
3.1. Materials for culture	31
3.1.1. Bacterial <i>E. Coli</i> strains.....	31
3.1.2. Bacterial growth media.....	31
3.1.2.1. Bacterial media.....	31
3.1.2.2. Additives for bacterial culture.....	32
3.1.3. Mammalian tissue culture cell lines	32
3.1.4. Mammalian cell medium and additives.....	32
3.2. Proteins, kits, enzymes and substrates	33
3.3 Filter materials and chromatography media	33
3.4. cDNA	34
3.5. Plasmid vectors	34
3.6. siRNA and primers	34
3.7. Buffers and solutions	35
3.8. Material for fluorescence microscopy	35
4. METHODS	37
4.1. cDNA cloning and construction of expression vectors	37
4.1.1. cDNA constructs	37
4.1.1.1. Constructs for expression of fluorescent fusion proteins in mammalian cells.....	37
4.1.1.2. Constructs for protein expression in bacteria	37
4.1.1.3. Construct pCMV-TNT-Sec20 for in vitro transcripton/translation.....	38

Table of contents

4.1.2. PCR amplification of DNA.....	38
4.1.3. DNA gel electrophoresis.....	39
4.1.4. Estimation of DNA purity and quantitation.....	40
4.1.4.1. Spectrophotometric Determination.....	40
4.1.4.2. Ethidium bromide fluorescent quantification	40
4.1.5. Competent E.coli	41
4.1.5.1. Preparation and transformation by heat shock.....	41
4.1.5.2. Preparation and transformation by electroporation	41
4.1.6. DNA preparation.....	42
4.2. Expression and purification of recombinant proteins	42
4.2.1. Expression and purification of GST-Sec22b and GST	42
4.2.2. Expression and purification of His6-mUse1	43
4.2.3. Expression and purification of His6-Syntaxin18.....	44
4.3. Protein quantitation.....	44
4.4. Denaturing polyacrylamide gel electrophoresis (SDS-PAGE).....	45
4.5. Generation of antibodies.....	47
4.5.1. Production and purification	47
4.5.1.1. IgG purification using protein A Sepharose	47
4.5.1.2. Purification of antibodies over antigen-bound Sepharose	48
4.6. Western blotting.....	49
4.6.1. Protein transfer onto nitrocellulose membranes	49
4.6.2. Immunoblot and detection	49
4.7. Mammalian cell culture techniques.....	50
4.7.2. Starting a culture from frozen cells.....	50
4.7.2. Cell culture.....	50
4.7.3. Transfection of cultured VERO cells.....	50
4.7.3.1. cDNA.....	50
4.7.3.2. si RNA.....	51
4.8. Application of cholera toxin on cells.....	52
4.9. Immunostaining.....	52
4.10. Protein-protein interaction assays	53
4.10.1 Immunoprecipitation.....	53
4.10.1.1. Using in vitro synthesized [S35] methionine-labeled mSec20.....	54
4.10.1.2. Disassembly experiments	54
4.10.2. Live cell FRET experiment.....	54
4.10.2.1. Principle of FRET.....	54
4.10.2.2. Live cell FRET measurements	55
4.10.2.2.1. Spectrofluorimetry : GFP2 / venus YFP as FRET pair	55
4.10.2.2.2. Microscopy : CFP / YFP as FRET pair.....	56
4.10.2.3. Analysis	58
4.10.3. BiFC experiments	59
4.11. In vitro vesicle release assay from isolated rat liver Golgi	61
5. RESULTS.....	63
5.1. Mammalian Golgi-to-ER SNAREs homologs.....	63

Table of contents

5.2. Purity of the proteins and of the antibodies produced and used in this study	66
5.3. Expression level and localization of endogenous proteins and various overexpressed GFP-fusion proteins expressed in Vero cells.	67
5.4. Detection of interactions between Sec22, Sec20 and Use1 with live cell FRET spectroscopy.	69
5.5. Localization of the specific interactions between Sec22, Sec20 and using with live cell FRET and BiFC imaging.....	73
5.5.1. Single live cell FRET microscopy.....	73
5.5.2. Bimolecular Fluorescence Complementation (BiFC).	76
5.6. Immunoprecipitation of the native retrograde SNARE complex.....	80
5.7. Interaction of the SNARE-proteins mUse1, mSec20 and mSec22b with the KDEL-receptor Erd2.	82
5.8. Presence of the SNARE-proteins in COPI vesicles.	84
5.9. Effects of down-regulation of mSec22b, mUse1, or mSec20.	87
6. DISCUSSION	89
6.1. Characterisation of a new mammalian SNARE-complex	89
6.2. Distribution of the retrograde Golgi-ER SNARE-proteins.....	90
6.3. Role of the Golgi-ER retrograde SNARE-proteins in the COPI-dependent pathway.....	92
6.4. Golgi-to-ER retrograde pathways	97
6.5. Perspectives for a better understanding of intracellular trafficking.....	99
7. REFERENCE	101
ANNEX I.....	117
ANNEX II	120

1. INTRODUCTION

1.1. The intracellular traffic

The secretory apparatus within all eukaryotic cells comprises a dynamic membrane system with multidirectional membrane transport pathways and overlapping compartmental boundaries. Thirty years ago, the work of George Palade and colleagues [1] on protein secretion established that newly synthesized secretory proteins pass through a series of membrane-enclosed organelles, including the endoplasmic reticulum (ER), the Golgi complex, and secretory granules, on their way to the extracellular space where they are released (figure 1). Proteins destined for residence at the plasma membrane, within endosomes, or within lysosomes, share the early stations of this pathway with secretory proteins.

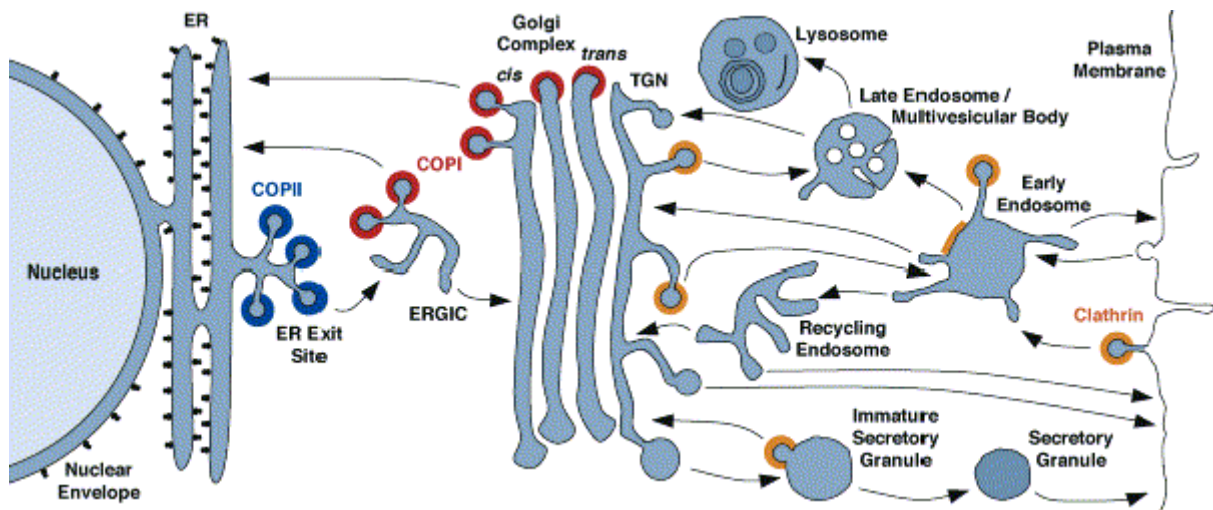


Figure 1. Intracellular pathways (Bonifacino and Glick, 2004). The scheme depicts the compartments of the secretory, lysosomal/vacuolar, and endocytic pathways. Arrows indicate transport steps and colors show the known or presumed locations of COPII (blue), COPI (red), and clathrin (orange). Clathrin coats are heterogeneous and contain different adaptor and accessory proteins at different membranes. Only the functions of COPII (in ER export) and of plasma membrane-associated clathrin (in endocytosis) are known with certainty. Less well understood are the exact functions of COPI at the ERGIC and Golgi complex and of clathrin at the TGN, early endosomes, and immature secretory granules. The pathway of transport through the Golgi stack is generally believed to involve a combination of COPI-mediated vesicular transport and cisternal maturation [2].

The basic eukaryotic secretory apparatus consists of a transport machinery that performs three fundamental tasks: (i) sorting and concentration of secretory products for exit out of the ER; (ii) changes in composition of membrane-bound transport intermediates; and (iii) regulated fusion of transport intermediates with target membranes.

The transport of proteins can be mediated by distinct vesicles as well as by continuous tubular connections (such as between the ER and the Golgi complex). Many aspects of secretory traffic vary considerably in different cell types (e.g. the roles of cytoskeletal elements and the sizes, shape, and location of organelles). Nevertheless, intracellular transport and sorting events work similarly for most of them. Intracellular traffic is rapid and very selective, with some carriers only needing seconds to transport a selected subset of proteins and lipids from the donor membrane to the acceptor organelle, thus preventing the homogenization of membrane components and permitting the maintenance of cellular organization.

Compartmental specificity is provided by distinct members of protein families, such as those involved in sorting (e.g. membrane coats, adaptor proteins, and cargo receptors; [3, 4]) and membrane fusion (Rabs, SNARES; [5, 6]). The compartment-specific docking is likely accomplished by facilitating the interaction between members of the docking/fusion machinery, the t-SNARES and v-SNARES [7], an interaction that in some cases can be inhibited by another family of proteins, the Sec1 proteins [8, 9]. Together with the other members of the docking/fusion machinery (NSF/SNAP;[10]), these molecular components regulate fusion and assembly of membranes and establish trafficking patterns.

1.1.1. Vesicular transport

How are the secretory proteins transported in the different pathways? As they are often found within small, membrane-enclosed vesicles present among the major organelles of the pathway [11], the vesicular transport hypothesis was put forward, stating that the transfer of cargo molecules between organelles of the secretory pathway is mediated by shuttling transport vesicles. According to this hypothesis, vesicles form from a donor compartment (budding) by a process that allows selective incorporation of cargo into the forming vesicles while retaining resident proteins in the donor compartment (protein sorting). The vesicles are subsequently targeted to a specific acceptor compartment (vesicle targeting), into which they unload their cargo upon fusion of their limiting membranes (vesicle fusion).

The processes of budding and fusion are repeated in the consecutive transport steps until the cargo reaches its final destination within or outside the cell. To balance this forward movement of cargo, organelle homeostasis requires the retrieval of transport machinery components and escaped resident proteins from the acceptor compartments back to the corresponding donor compartments (retrograde transport), a process that is also proposed to occur mainly by vesicular transport [12, 13]. All of these steps are tightly regulated and

balanced so that a large amount of cargo can flow through the secretory pathway without compromising the integrity and steady-state composition of the constituent organelles. Interestingly, yeast and mammals share conserved vesicular transport machineries [14, 15].

The best-studied traffic pathways are those that use carrier vesicles that are clearly identifiable by their coats, made of the coatomer COPI, of COPII, or of clathrin and its partners. However, the possible existence of a transport mediated by tubular structures cannot be excluded.

1.1.2. Tubular transport

Although budding of vesicles is widely believed to occur from ER exit sites [1, 16, 17]), ultrastructural studies have shown these sites sometimes consist of permanent/intermittent connections with the ERGIC (ER-Golgi Intermediate Compartment) or with the first cisternae of the Golgi stack itself [13, 18]. This indicates that the boundary separating the ER from the rest of the secretory pathway is not always distinct and that export of protein out of the ER does not necessarily rely on the production of small vesicles. It however, depends on energy since all protein export out of the ER ceases in the absence of ATP, or when energy-coupled regulatory molecules are inactivated or depleted [19, 20].

The same holds for the intra-Golgi transport. The standard view of Golgi traffic is that it is mediated primarily by vesicles that pinch off from one cisterna and then become targeted to and fuse with a different cisterna [21]. Unidirectional transport of protein and lipid is thus achieved with no intermixing of donor and acceptor compartments. Besides the vesicles, tubule connections between Golgi stacks are frequently observed in electron micrographs [22, 23] and the *cis* - and *trans*- most cisternae of the Golgi complex appear to be composed of extensive tubular (50-100nm diameter) networks [24, 25]. Tubules can be rapidly generated by Golgi membranes *in vivo* and *in vitro* under various conditions [26, 27].

Membrane traffic has been shown to be mediated by tubules extending between organelles in cells expressing GFP tagged markers or/and treated with the drug brefeldin A (BFA). BFA blocks membrane export out of the ER *in vivo* [28, 29] and inhibits vesicle formation both *in vivo* [30] and *in vitro* [31]. This is likely due to BFA's inhibition of nucleotide exchange onto ADP-ribosylation factor (ARF), a low-molecular weight GTPase [32], by which this BFA prevents assembly of cytosolic coat proteins (including COPI components) onto target membranes [31]. At the same time, extensive retrograde transport of Golgi components to the ER, mediated by growth of Golgi tubules, occurs with BFA treatment, leading to the complete

loss of Golgi structure [33]. Whether the formation of tubular structures reflects what occurs under normal physiological conditions, is a matter of discussion.

Other structures that do not have COP or clathrin coats have been observed in the cell. Internalization from the plasma membrane can also occur via macropinocytosis, phagocytosis and probably through caveolae [34]. In the secretory pathway, poorly understood tubular structures connect the Golgi with the plasma membrane and the ER [35, 36]. In the endocytic pathway, tubules emerge from early endosomes and participate in recycling to the plasma membrane [37]. These carrier structures tend to be heterogeneous and in some cases, they might be used for large-scale movement of selectively captured membrane components [38, 39]. Other organelles appearing like elongated vesicles could act in Golgi traffic, migrate within the cytoplasm or translocate along microtubules to their target membranes, unidirectionally and without causing mixing. They could also establish connections between the same or different compartments but certain mechanisms would be necessary to maintain chemically distinct compartments and to achieve directed transport of protein and lipid.

Recently, other carriers called large pleiomorphic carriers (LPCs) have been described as responsible for moving the bulk of the secretory traffic between distant compartments. LPCs are much larger and more variable in shape than vesicles, and they have evident interconnected tubular and saccular/cisternal components. The process of formation of LPC and its function need to be further characterized [40].

1.2. Role of the coat-proteins : focus on COPI-vesicles

The budding of transport vesicles and the selective incorporation of cargo into the forming vesicles are both mediated by protein coats [41, 42]. These coats are supramolecular assemblies of proteins that are recruited from the cytosol to the budding vesicles.

The first group of reactions forms the initiation step; it leads to the specific recruitment of coat components to the corresponding donor membrane. This step is energy dependent and includes sorting of cargo to the forming coat. Coat propagation, the second step in the process, couples further addition of coat components and additional recruitment of cargo with invagination of the underlying membrane. When formation of the coat ends, the vesicle buds by scission of the neck connecting the invaginated membrane to the donor surface. Finally, by a process of uncoating, the coat components are released so that membrane fusion can occur between the uncoated vesicle and the target organelle (Figure 2).

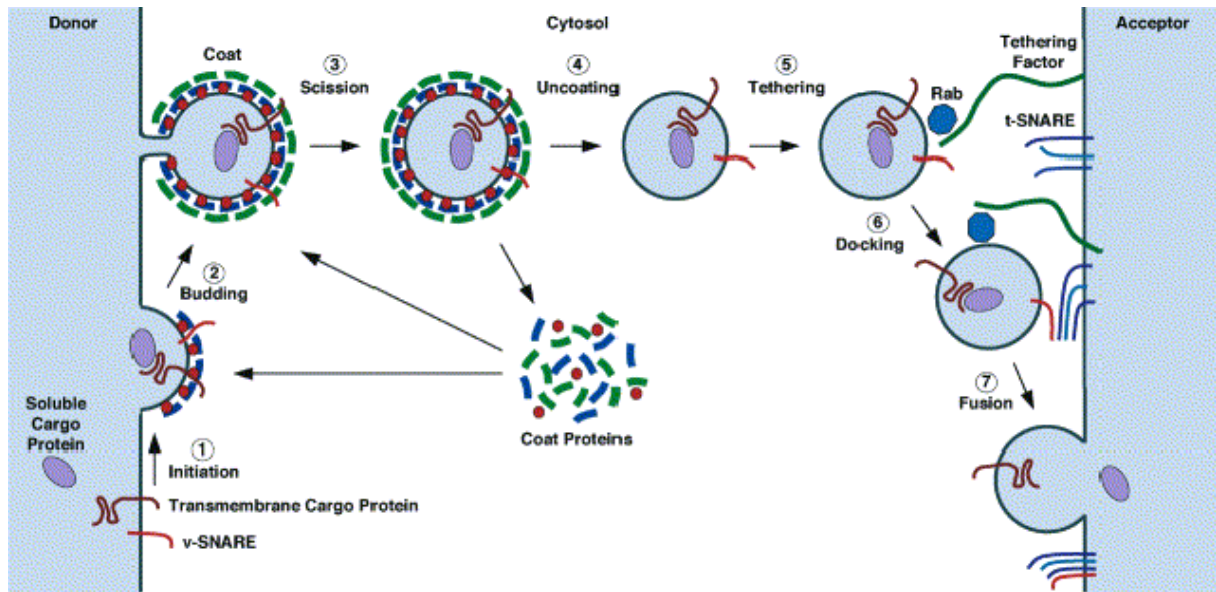


Figure 2. Steps of vesicle budding and fusion (Bonifacino and Glick, 2004). This scheme shows the different proteins involved in the vesicular transport machinery (1) **Initiation**. The membrane-proximal coat components (blue) are recruited to the donor compartment by binding to a membrane-associated GTPase (red). Transmembrane cargo proteins and SNAREs begin to concentrate at the assembly coat. (2) **Budding**. The membrane-distal coat components (green) are recruited and polymerize. Simultaneously, cargo gets concentrated and membrane curvature increases. (3) **Scission**. The neck between the vesicles and the donor compartment is severed either by direct action of the coat (for COPI- and COPII-coated vesicles) or by accessory proteins (for clathrin-coated vesicles). (4) **Uncoating**. The vesicle loses its coat partly due to inactivation of a small specific GTPase, phosphoinositide hydrolysis, and the action of uncoating enzymes. Cytosolic coat proteins are then recycled for additional rounds of vesicle budding. (5) **Tethering**. The "naked" vesicle moves to the acceptor compartment, possibly guided by the cytoskeleton, and becomes tethered to the acceptor compartment by the combination of a GTP bound Rab and a tethering factor. (6) **Docking**. The v- and t-SNAREs assemble into a four-helix bundle. (7) **Fusion**. This "trans-SNARE complex" promotes fusion of the vesicle and acceptor lipid bilayers. Cargo is transferred to the acceptor compartment, and the SNAREs are recycled.

The coats also participate in cargo selection and concentration by recognizing sorting signals present in the cytoplasmic domains of transmembrane cargo proteins. During the formation of a vesicle, coat proteins carry out sequential interactions that lead to budding from the donor membrane, uncoating, fusion with a target membrane and recycling of the coat components. Different coats and specific sorting signals mediate vesicle budding and cargo selection at different stages of the exocytic and endocytic pathways.

Cell-free systems have been useful in demonstrating transport of proteins from various donor organelles to acceptor organelles. They have been used to identify various proteins

required for formation of different transport vesicles and to study their function, their targeting to appropriate organelles, and their fusion with acceptor membranes.

The first coats to be identified and characterized contained a scaffold protein, clathrin, as their main constituent [43]. Clathrin coats were initially assumed to participate in most vesicular transport steps within the cell. However, later studies demonstrated that the function of these coats was restricted to post-Golgi locations including the plasma membrane, the trans-Golgi network (TGN), and endosomes. Non-clathrin coats, called COPII and COPI, were later discovered to be involved in vesicular transport in the early secretory pathway [16, 44] (see chapter 1.5.). There are clear similarities and differences between the ways that COPI, COPII and clathrin coats handle these steps [41, 42]. The coat proteins surrounding many other types of transport vesicles have not been identified yet. This is the case for instance for those moving from late endosomes to lysosomes or the constitutive secretory vesicles that move proteins from the trans-Golgi to the plasma membrane.

The COPI-coatomer complex was first isolated from cytosol of bovine brain. It is present in all eukaryotic cells examined so far, including *Drosophila* and yeast. The COPI coat has been localized to the ERGIC, along the *cis* face of the Golgi, and associated with the rims of subsequent cisternae [45, 46]. The discovery of a membrane-bound form of coatomer on Golgi derived transport vesicles was the first hint for a role of this complex in intracellular trafficking.

The COPI coatomer (700kDa) is a cytoplasmic complex of seven protein subunits: α -COP, β -COP, β' -COP, γ -COP, δ -COP, ϵ -COP and ζ -COP [47]. In *S.cerevisiae*, homologues of α -, β -, β' - and γ -COP are the products of the genes RET4, SEC26, SEC27 and SEC21, respectively. The primary structure of α - and β' -COP presents four or five WD-40 repeated motifs (a conserved ~ 40 amino acids stretch terminating with the residues Trp, Asp), respectively. WD-40 repeats are typically found in β -subunits of trimeric G proteins but also in other subunits of various hetero-oligomeric protein complexes. This motif might represent an oligomerization motif or might be involved in the binding of coatomer to membranes. Interestingly, β -COP, δ -COP and ζ -COP show weak homologies to subunits of the adaptin complexes of clathrin-coated vesicles. Similar to the clathrin-coated vesicle, they act as a bridge between the cytosolic tails of membrane proteins and the fibrous cage that surrounds the vesicles; they also mediate the specific incorporation of proteins into these coated vesicles. Like COPII, COPI recognizes specific signals in the cytoplasmic domains of transmembrane cargo proteins, although in this case the signals function to retrieve proteins

from the ERGIC or the Golgi complex to the ER [48, 49]. γ -COP seems to be the component responsible for cargo recognition because it recognizes the cytoplasmic carboxyterminal domain sorting signals KKXX (the dilysine motif) or KKKXX (X is any amino acid). Finally, ϵ -COP is not related to any known protein.

The KDEL receptor, a 7-fold-spanning membrane protein that binds and retrieves luminal proteins containing the KDEL carboxy-terminal sequence, is transported along the COPI pathway (though it is not known whether it is recognized by the γ subunit) [50]. Additional constituents of the COPI-coated transport intermediates are the p24 family proteins, which are type I transmembrane proteins that have been proposed to function in both cargo selection and coat recruitment [51].

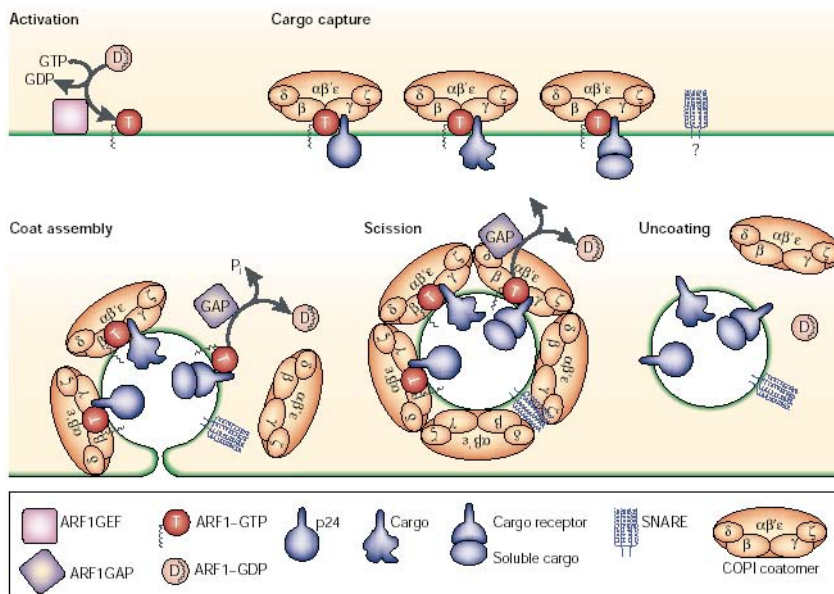


Figure 4. COPI-vesicles assembly and uncoating (Kirchhausen T., 2000).

Coat assembly is activated by the recruitment of ARF1-GTP to the membrane. This allows the binding of the COPII coatomer and the recruitment of cargo. Membrane deformation occurs at the same time as coat recruitment. When the coat is complete, the vesicle buds. The GTPase activity of ARF1

is enhanced by ARF1-GAP leading to inactivation of ARF1 and uncoating. (ARF1, ADP-ribosylation factor 1; ARF1-GAP, ADP-ribosylation factor 1 GTPase activating protein; ARF1GEF, ADP-ribosylation factor 1 guanine exchange factor.)

The initial event in the COPII pathway that leads to recruitment of the coat requires the association of the GTPase ARF1 (ADP-ribosylation factor 1) in its active GTP-bound form to the membrane. ARF1 is myristoylated to allow its membrane association. In the GTP-bound state, the myristoyl group is exposed and ARF1 becomes membrane bound. When the GTP is hydrolyzed, the protein undergoes a conformational change, developing a myristoyl-binding pocket that covers the tail, solubilizing the protein. The GDP-GTP exchange is regulated by a Golgi-associated GTPase-activating protein, ARF-GAP [52] which apparently receives and integrates multiple signals from the cytosol, such that the amount of ARF-GTP, and thus the rate of formation of COPII vesicles is appropriate to the needs of the cell. Recent studies

indicate that this activity is also required for cargo sorting and budding [53, 54]. During COPI coat assembly, ARF-GTP simultaneously recruits the membrane-proximal $\beta\gamma\delta\zeta$ and the membrane-distal $\alpha\beta'\epsilon$ subcomplexes [47], contrary to the stepwise assembly of COPII. ARF1 and the COPII-associated small GTPase Sar1p are closely related [32, 55]. But unlike Sar1p, ARF proteins have many effectors, including COPI and other coats as well as lipid-modifying enzymes [56]. The ARF protein family consists of several members, and targeting of ARF1 to the correct membrane involves specific association with its appropriate GEF. Several GEFs for ARF1 have been identified, one of which (known as ARF1GEF, ARNO3 or GRP1) seems to be specifically associated with the COPI pathway [57]. Many different GEFs and GAPs activate and inactivate ARF binding, respectively, in an effector- or compartment-specific fashion [56]. Once the COPI vesicles are released from the donor membrane, the COPI coat dissociates. This step is triggered by the hydrolysis of the GTP bound to ARF proteins in the vesicles; accordingly when COPI vesicles are formed *in vitro* in the presence of a non hydrolysable GTP analog, the COPI coats do not dissociate [58].

It has been suggested that hydrolysis of GTP and release of ARF1 from the membrane act as a timer, triggering (as with Sar1p and COPII vesicles) the release of the other coat components and preparing the vesicle for fusion with its target membrane. The rate at which ARF1 hydrolyses GTP depends on its association with ARF-GAP and the COPI complex [59], both of which are required for full GTPase activation. Recently, it has been shown that vesicles that capture preferred cargo (such as the FFXXRRXX sorting signal containing p24 protein hp24a [60]) will retain their ARF1 protein long enough to complete coat assembly, whereas vesicles that capture other proteins will not. In other words, GTP hydrolysis is slow when ARF1 is bound to its preferred cargo, allowing kinetic regulation of coat recruitment.

1.3. Structure and function of the SNARE-proteins

Despite the variety of coat proteins that mediate formation of transport vesicles, fusion of all vesicles with their target membranes exhibits several common features. In all cases, fusion occurs after the coats have depolymerized and seems to involve a conserved set of proteins that (a) mediates targeting of vesicles to the appropriate fusion partner and (b) triggers the fusion process itself. Fusion and part of targeting reactions rely on so called SNARE-proteins [61].

1.3.1. Discovery of the SNAREs

An early contribution of the cell-free intra-Golgi transport assay was the identification of an “N-ethylmaleimide-Sensitive Factor” (NSF), which could exist in cytoplasmic or membrane bound forms [62]. Accumulation of uncoated vesicles on Golgi membranes was observed by electron microscopy when NSF was inactivated, implying that NSF is required for membrane fusion [63]. The yeast ortholog of NSF, Sec18p, had been implicated in ER-to-Golgi transport [64]. It became soon apparent, that NSF is involved in a wide range of membrane fusion steps in the secretory and endocytic pathways [65, 66]. NSF forms a homohexameric ring [67] and is a founding member of the AAA protein family (“ATPases associated with diverse cellular activities”), a group of enzymes that catalyze the structural remodeling of protein complexes [68]. α -SNAP (“soluble NSF association protein”), the mammalian ortholog of Sec17p [15], was identified as a binding partner for NSF, which links NSF to membranes [10]. Using NSF/ α -SNAP as an affinity reagent to fractionate a brain lysate, Söllner and colleagues identified a set of three membrane-associated “SNAP Receptors,” or SNAREs [61], which had previously been implicated in linking synaptic vesicles to the plasma membrane [69]. One of them, Synaptobrevin, was known to be associated with synaptic vesicles, whereas the other two, Syntaxin and SNAP-25, had been localized to the presynaptic plasma membrane. The data suggested the presence in the Golgi of synaptic SNARE-proteins homologs which could bind NSF/ α -SNAP and be related to membrane fusion events.

1.3.2. Definition and structural features

The SNAREs represent a superfamily of proteins that is thought to play a key role in most of intracellular membrane fusion events within eukaryotes [5, 7, 70, 71]. SNAREs are generally small proteins of around 100–300 amino acids in length. They possess homologous domains of approximately 60 amino acids referred to as the “SNARE motif” [72, 73]. Most SNAREs contain only one SNARE motif near the C-terminal tail anchor or the C-terminus, but 3 of them (SNAP-23, SNAP-25, and SNAP-29) contain two tandem SNARE motifs separated by a linker region. 36 distinct SNAREs are known in mammalian cells [74, 75] and most of them (31) are C-terminally anchored transmembrane proteins, with their functional N-terminal domains facing the cytosol. The other five SNAREs (SNAP-23, SNAP-25, SNAP-29, Syn11, and Ykt6) are instead attached to the membrane by prenylation (Ykt6) [76], palmitoylation of Cys residues (SNAP-25, Ykt6, and Syn11) [76-78], and/or interaction with

other SNAREs that are anchored by C-terminal tails [79]. Most SNAREs are also characterized by an extended N-terminal domain with coiled-coil regions (for review see [80]).

Certain sets of SNARE proteins form stable complexes through assembly of their SNARE motifs into a parallel four-helix coiled-coil structure [70, 81]. The best characterized SNARE complex is the one mediating exocytosis of synaptic vesicles in neurons. A crystal structure of the neuronal SNARE complex consisting of synaptobrevin-II (VAMP2), syntaxin 1A, and SNAP-25B revealed a four-helix bundle. The four helices are connected by 16 layers of interacting surfaces mediated by the side chains of the residues which are mostly hydrophobic and are arranged perpendicular to the axis of the four-helical bundle. The middle of the bundle is usually characterized by a layer (defined as the 0 layer) of interaction mediated by hydrophilic residues: three Gln (Q) (contributed one each by Syntaxin1 and the N- and C-terminal parts of SNAP25 called S25N and S25C respectively), and one Arg (R) (contributed by VAMP2) [73, 82].

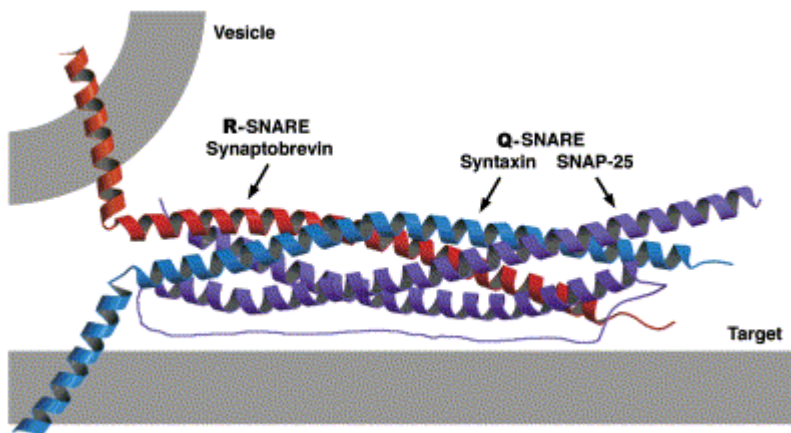


Fig 4: Crystal structure of a synaptic *trans*-SNARE complex drawn after Sutton et al.[82]. The structures of the two membrane anchors and of the peptide that links the two SNAP-25 α -helices are hypothetical.

SNAREs are thus structurally classified as Q-SNAREs and R-SNAREs dependent on the presence of either Q or R at this position, with the Q-SNAREs further divided into Qa (for Syntaxin subfamily), Qb (for S25N subfamily), and Qc (for S25C subfamily) SNAREs [73]. It is now generally believed that one member of each subfamily contributes a single SNARE motif, resulting in the Qa:Qb:Qc:R configuration of a SNARE complex. Solution of the crystal structure of an endosomal SNARE complex consisting of the SNARE domains of Syn7 (Qa), Vti1b (Qb), Syn8 (Qc), and VAMP8 (R) supports this stoichiometric principle derived from analysis of the neuronal SNARE complex [83]. The ionic layer seems to be a conserved feature of many different SNARE complexes and consists in most cases of one arginine residue contributed by an R-SNARE and three glutamine residues contributed by three Q-SNARE helices [73]. However, recent studies show the existence of SNARE complexes formed between an R-SNARE, 2 Q-SNAREs and a fourth SNARE helix carrying

an aspartate or a serine in its zero layer such as ER-to-Golgi [84] and Golgi-to-ER [85] SNARE complexes in yeast and the early endosomal SNARE complex in mammals [83].

The current concept of the action of SNAREs is that the combinatorial use of the various members of the Qa-, Qb-, Qc-, and R-SNAREs gives rise to a wide array of SNARE complexes, whose functions are determined in part by the subcellular targeting of newly-made uncomplexed SNAREs. The composition of many complexes is not known with certainty in mammalian cells [86, 87] while defined SNARE complexes can be assigned to most fusion steps in yeast [88-90]. Some SNAREs participate in several fusion events with different partners, such as the yeast R-SNARE Ykt6p, the mammalian Qa-SNARE Syntaxin5 and the yeast Qb-SNARE Vti1p. A SNARE complex mediating a specific fusion reaction may also accept alternative SNAREs such as Ykt6p which can substitute for Nyv1p in traffic to the vacuole [91] and for Sec22p in the fusion of COPII-vesicles with the Golgi [92].

Although SNAREs are structurally distinguished as Q-SNAREs or R-SNAREs, they can be functionally classified into v-SNAREs that are associated with the vesicle/container and t-SNAREs that are associated with the target compartment; this classification, however, is less meaningful when considering homotypic fusion of organelles. There is a rough correspondence of R-SNAREs with v-SNAREs and of Q-SNAREs with t-SNAREs. A major insight from structural analysis of the SNARE complexes was that v- and t-SNAREs pair in a parallel way [82, 93, 94]. During vesicular transport, the vesicle as it buds from the donor organelle, incorporates a v-SNARE which is uncovered when the vesicle coat proteins depolymerize. The specific v-SNARE targets the transport carrier to its correct membrane fusion partner which contains one or more t-SNAREs. These t-SNAREs act cooperatively to specifically bind a particular v-SNARE.

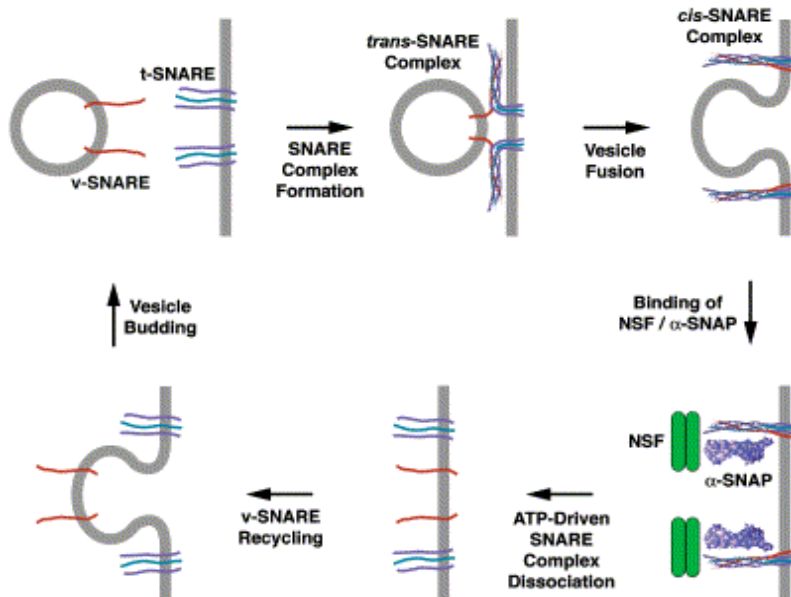


Fig 5: The SNARE cycle (Bonifacino and Glick, 2004). A *trans*-SNARE complex assembles when a monomeric v-SNARE on the vesicle binds to an oligomeric t-SNARE on the target membrane, forming a stable four-helix bundle that promotes fusion. The result is a *cis*-SNARE complex in the fused membrane. α -SNAP binds to this complex [95] and recruits NSF, which hydrolyzes ATP to dissociate the complex. Unpaired v-SNAREs can then be packaged into vesicles again.

Specific interaction between v-SNARE and t-SNARE leads to the formation of the *trans*-SNARE complex (or SNAREpin) [86, 96, 97]. The SNARE motifs are believed to be “unstructured” before complex assembly and become highly organized into a twisted parallel four-helical bundle during the formation of the *trans*-SNARE complex. This conformation persists throughout the fusion reaction to become a *cis*-SNARE complex in the fused membrane (Figure 5). α -SNAP then binds the SNARE complex [95] and recruits the ATPase NSF. Interaction of NSF and three α -SNAPs with the *cis*-SNARE complex leads to the formation of a transient 20 S complex [98, 99]. ATP hydrolysis by NSF leads to the disassembly of the 20 S complex as well as the *cis*-SNARE complex [100]. The freed v-SNAREs can then be recycled to the donor compartment by retrograde transport, while the t-SNARE subunits can be re-organized into functional t-SNAREs for the next round of docking and fusion events.

The formation of the *trans*-SNARE complex generates the energy needed to bring the two negatively charged apposing membranes close enough to fuse. Indeed, the *trans*-SNARE complex with its hydrophobic segments in two apposing membrane bilayers is structurally analogous to the activated form of viral fusion proteins and could act as fusogen [96]. The idea that SNAREs act as fusogens was supported by experiments demonstrating that two populations of liposomes containing either v- or t- purified recombinant SNAREs can fuse [101]. A similar effect was shown with cells engineered to produce either v- or the cognate t- “flipped” SNAREs facing the outside of the cell rather than the cytoplasm [102]. In both cases, fusion was observed suggesting that SNAREs form the conserved, essential core of the fusion machinery.

SNAREs also help to ensure the compartmental specificity of membrane fusion [86, 103, 104]. Different v-/t-SNARE complexes form at different steps of intracellular transport. Surprisingly, purified SNAREs can pair promiscuously in vitro but when used in the liposome fusion assay they form almost exclusively physiologically relevant *trans*-SNARE complexes [103], providing an assay to predict SNARE complexes that form in vivo [105]. However, SNAREs alone cannot be the only components determining the specificity of membrane fusion because a given v-SNARE recycles and is therefore present in both anterograde and retrograde vesicles (Figure 5). Additional specificity is provided by tethering proteins that link the apposing membranes prior to SNARE complex formation. These various tethers assemble with the aid of Rab family GTPases (known as Ypt proteins in yeast) to promote the initial association of two membranes [96, 106] (Figure 2).

All newly-made SNAREs are first delivered to their hosting compartment(s) via the secretory and endocytic pathways. Little is known about how SNAREs are targeted to specific organelles. For the few SNAREs examined so far, targeting determinants are present in the transmembrane sequence, the cytosolic domain, or both [107]. An important mechanism for SNARE localization and possibly for vesicle formation is direct interaction with vesicle coats. For example, SNAREs involved in ER-to-Golgi transport must be packaged into COPII vesicles during ER export and then into COPI vesicles during retrieval from the Golgi [108, 109]. Recent biochemical and structural studies have shown how three *S. cerevisiae* SNAREs involved in ER-to-Golgi transport, Sed5p, Bet1p, and Sec22p, interact with the COPII coat [110, 111]. Distinct sites on the Sec24p subunit seem to bind selectively the uncomplexed, fusogenic forms of the SNAREs [111]. Similarly, Vti1b interacts with epsinR [112], and VAMP2 was suggested to have a role in rapid endocytosis of synaptic vesicles [113]. Thus, SNAREs could also have a role in vesicle budding additionally to their role in vesicle fusion.

1.4. Accessory and regulatory proteins

Biochemical in vitro studies (such as liposome fusion assays) demonstrate that SNARE complexes are sufficient to mediate vesicle fusion. However, the fusion event is much faster in vivo implying that additional components cooperate with SNAREs [101] and regulate fusion.

Although **NSF** and **α -SNAP** represent the most essential regulators of SNAREs, other proteins preventing inappropriate SNARE complex formation are required for regulation of vesicle fusion [114]. For instance, following fusion of two membranes and dissociation of the *cis*-SNARE complex by NSF/ α -SNAP, the SNAREs need to be kept inactive until the next round of fusion. This is done by cytosolic factors such as GATE-16 and LMA1 which bind the individual v- and t-SNAREs and help to keep them separate [115].

Post-translational modifications such as phosphorylation [116-119], palmitoylation [76-78], and prenylation [76, 120] are also likely to regulate the function of SNAREs or of interacting components [114]. Key regulatory elements for SNARE complex assembly are present in the SNAREs themselves as seen previously (the N-terminal three-helix bundle of syntaxins or longin domain of members of the synaptobrevin family; [121]) but they can also come from other factors. In some cases, *trans*-SNARE complex assembly seems to be arrested at an intermediate stage, with accessory proteins preventing the complete “zipping up” of the four-helix bundle until a fusion signal is received [86]. The best candidate for such an accessory protein is the putative Ca^{2+} sensor **synaptotagmin**, which triggers the

complexin-stabilized trans-SNARE complex and promotes synaptic vesicle fusion in response to Ca^{2+} influx [96, 122]. **Complexins** are small cytosolic proteins (134 residues) found in neuronal (complexin I) as well as non-neuronal (complexin II) tissues. Binding of complexins to the SNARE complex competes with binding of α -SNAP, indicating that complexins are involved in regulation of membrane fusion [123]. Complexins are proposed to complete the **Munc13-1/2**-mediated priming process of tethered synaptic vesicles at the presynaptic plasma membrane [97]. The tethering of synaptic vesicles is regulated by **Rab3** and its effector **RIM1** [97]. Further components have been shown to affect SNARE function in synaptic vesicles by inhibiting the formation of a fusogenic SNARE complex (**synaptophysin** [97], **tomosyn** and **amisyn** [124, 125]).

Another important group of SNARE-interacting proteins is the **SM** family, whose founding members are the yeast SEC1 gene product [126] and neuronal Munc-18. Each membrane fusion step requires a specific SM protein [127]. These proteins bind to syntaxins, but the mode of binding is not conserved, and various SM proteins either stimulate or inhibit SNARE complex assembly.

There are at least seven mammalian members of the SM protein family: Munc18-1, Munc18-2, and Munc18-3, VPS33A, VPS33B, VPS45, and SLY1. The Munc18 isoforms are functionally homologous to yeast Sec1p and function at the plasma membrane. They bind to the closed conformation of Syntaxins 1 to 4. This interaction depends on both the N-terminal Habc region and the SNARE motif of Syntaxins [128]. VPS33A and VPS33B correspond to yeast Vps33p and act in the endocytic pathway but they seem to serve unique functions [129, 130]. VPS45 and SLY1 correspond to yeast Vps45p and Sly1p, respectively, and are involved in traffic at the trans- and cis-faces of the Golgi apparatus [131]. SLY1 and VPS45 interact with a short N-terminal region of Syntaxins 5 and 18 and Syn16, respectively, without the involvement of the Habc region or the SNARE motif [132, 133].

A class of small GTPases called **Rab proteins** participates in the control of vesicular traffic in eukaryotic cells. They are found on transport intermediates where they regulate directional movement along microtubules [134] and control the rate of specific fusion [9, 135]. They have an overall structure similar to Ras and, like Ras, purified Rab proteins bind and hydrolyze GTP. Specifically, a cytosolic protein called GEF catalyzes the exchange of GDP, bound to cytosolic Rab, for GTP, inducing a conformational change in Rab which can then bind to a surface protein on a particular transport vesicle. After vesicle fusion occurs, the GTP bound to the Rab protein is hydrolyzed to GDP, triggering the release of the Rab protein, which then can undergo another cycle.

Several lines of evidence support the involvement of specific Rab proteins as timers of specific vesicle fusion events. For instance, Rab5 is localized to early endosomes, and it regulates the sorting endosome via several downstream effectors [136]. Homotypic fusion of early endosomes requires the presence of Rab5 and its rate is increased when adding Rab5 and GTP to cell-free extracts suggesting that Rab5·GTP acts as a timer for vesicle fusion. Similarly, Rab1 (the mammalian homolog of the yeast protein Ypt1) is essential for ER-to-Golgi transport reactions to occur in cell-free extracts, while Rab5 or Rab7 are not. Thus, some individual Rab proteins are essential for specific vesicle fusion reactions to occur.

Various **tethering factors** [137, 138] are also involved in fusion events. They position the vesicles precisely at the region of the target compartment where the t-SNAREs are located. The tethering factors act over a longer distance than the SNAREs and interact with both the vesicle and the target compartment to facilitate the subsequent pairing of the v-SNARE with the cognate t-SNARE. The heteromeric “quatrefoil” tethers are exemplified by the exocyst, which links secretory carriers to the plasma membrane [139]. Six of the original *sec* mutants defined different subunits of the exocyst [140]. Related quatrefoil tethers function in Golgi traffic; for example, the COG complex is believed to mediate the tethering of COPI vesicles to Golgi cisternae [138, 141]. Also, p115 is a tethering factor that functions by simultaneous interaction with giantin on COPI-generated vesicles and with GM130 on the cis-Golgi [142]. A SNARE-related coiled-coil region of p115 interacts with many SNAREs of the Golgi apparatus (Syn5, GS28, GS27, Ykt6, GS15, Bet1, Sec22b), suggesting that p115 modulates the formation of trans-SNARE complexes such as Syn5-GS28-GS15-Ykt6 and Syn5-GS27-Bet1-Sec22b involved in intra-Golgi transport [143]. Like p115, Hrs (endosome-associated hepatocyte responsive serum phosphoprotein) contains a SNARE-like coiled-coil region which is shown to inhibit the incorporation of an R-SNARE into the SNARE complex through competitive binding to a t-SNARE complex. Through this activity, Hrs inhibits early endosomal fusion mediated by Syn13, SNAP-25, and VAMP2 [144]. Other similar coiled-coil tethers called golgins are present in the Golgi [145]. A different type of tether is EEA1 which acts as a Rab5 effector that promotes the homotypic fusion of early endosomes [146].

More generally, an interaction of members of the SM and Rab families with SNAREs might add an additional layer of specificity or serve as a proofreading mechanism to vesicle docking and fusion. Together with tethers, they collaborate to ensure that membranes fuse at the correct time and place. Thus, like many biological processes, membrane fusion employs sequential, partially redundant mechanisms to achieve high fidelity.

1.5. Golgi –ER cycle

Protein transport from the ER to the Golgi occurs in both forward (anterograde) and backward (retrograde) directions. Proteins are transported via the anterograde pathway from the ER to the Golgi, where ER resident proteins are specifically captured in a receptor-dependent manner and retrieved via the retrograde pathway [48, 147-150]. In *Saccharomyces cerevisiae*, more than 15 genes have been identified that are required for membrane traffic between the ER and Golgi complex [151]. Mammalian homologues for many of these genes have been identified biochemically by the use of cell-free systems [10, 65, 152], and through cloning based on sequence similarity with known yeast genes. At least two vesicular coat protein complexes, COPI and COPII, are involved in transport between the ER and Golgi complex [21, 151]. Strong data from yeast genetics and biochemical studies has led to a simple transport model, in which COPII vesicles mediate unidirectional ER-to-Golgi transport and COPI vesicles mediate intra-Golgi and Golgi-to-ER transport [153, 154], maintaining selected molecules within the ER/Golgi system [149, 155]. A putative post-ER-pre-Golgi compartment, designated the intermediate compartment (IC) or ER-to-Golgi IC (ERGIC), was discovered in the early 90s and has been proposed to be a distinct organelle separated from the ER and Golgi by two vesicular transport steps [156]. In this view, COPII was suggested to mediate ER-to-ERGIC transport, COPI would mediate ERGIC-to-Golgi transport [157] and a modified COPI complex would return the transport machinery back to the donor membranes [158]; alternatively, additional vesicular coat complexes that remain to be identified might exist and be involved in traffic between the ER and Golgi complex.

1.5.1. The Endoplasmic reticulum

The ER is the port of entry for all membrane proteins and proteins entering into the secretory pathway. It engages in lipid biosynthesis and metabolism, as well as in protein import, post-translational modifications (which include protein folding, oligomerisation and covalent modifications such as glycosylation and disulfide bonds formation) and degradation [159]. The synthesis and translocation of proteins as well as the release of properly processed, folded and assembled proteins that are transported to their destinations [160], are mainly performed by three sets of specific resident ER components. The **translocation machinery** transports the nascent chain of a growing polypeptide through the ER membrane. In mammalian cells translocation occurs predominantly co-translationally but sometimes post-translationally (e.g. probably for the SNAREs, which do not contain a signal sequence). The

translocation site is composed of membrane proteins that target the ribosome-bound nascent chain to the cytoplasmic face of the ER membrane, and of proteins that form an ER-membrane channel through which the polypeptide is translocated. On the luminal site of the ER membrane, an oligosaccharyl transferase catalyzes co-translational *N*-glycosylation of most polypeptides. **Molecular chaperones** are present as soluble proteins in the lumen of the ER (such as BiP/grp74 and calreticulin) or in a membrane-bound form facing the lumen of the ER (such as calnexin). Chaperones associate with nascent chains or with the polypeptide after its release from the ribosome in order to control and facilitate proper folding and assembly of the newly synthesized protein. A third major group of ER resident proteins comprises **folding enzymes** (such as e.g. protein disulfide isomerase and peptidyl-prolyl *cis-trans* isomerase) that assist the proper folding of newly synthesized proteins. Wrongly folded proteins are rapidly degraded in the ER by a luminal-ER associated degradation apparatus known as **ERAD** (ER Associated Degradation) [161].

The ER is comprised of an extensive array of interconnecting membrane tubules and cisternae which usually extend throughout the cell [162]. The specialized luminal environment of the ER, which is oxidizing (promoting disulfide bond formation) with high ATP and free calcium levels, enable protein folding and assembly of proteins and lipids from monomeric (low energy) forms to multimeric (higher energy) complexes.

Protein export from the ER occurs only when a protein is properly folded and assembled and takes place in specialized regions of the ER, devoid of ribosomes, called ER exit sites [16, 163, 164]. They arise spontaneously throughout the ER [165] and are adjacent to clusters of elaborate membrane tubules/vesicles constituting the IC [166] (also called VTC, Vesicle Tubular Clusters; [17], pre-Golgi intermediates; [165, 167]). Although budding of vesicles is widely believed to occur from ER exit sites [1, 16, 17], ultrastructural studies have shown that ER exit sites sometimes consist of permanent/ intermittent connections with the IC or with the first cisternae of the Golgi stack itself [13, 18, 168, 169].

1.5.2. The Golgi apparatus

While studying nerve cells stained by the metal-impregnation technique, Camillo Golgi discovered a basket-like network surrounding the nucleus in Purkinje cells. A detailed description of this structure called Golgi complex was later provided by electron microscopy (for review see [170]). It revealed a typical stack of 3-8 flattened cisternae which is morphologically and functionally polarised (in the *cis* to *trans* direction). The Golgi stack,

including the *cis*-Golgi, the *medial* (middle) saccules, and the *trans* saccules [170, 171], carries out post-translational processing of newly synthesized proteins and the enzymes involved in these modifications are arranged across the stack in the order in which they function: for instance, phosphorylation occurs in the *cis* region, while in other regions, different types of carbohydrates (like mannose or galactose) are added as a glycoprotein passes through the cisternae [172]. To this ensemble, come two flanking tubular networks of membrane [173]; the *cis*-Golgi network (CGN) and the *trans*-Golgi network (TGN). The CGN comprises vesicular and tubular extensions that may be connected with the first cisternae of the Golgi stack and is located on the entry side of the stack; its role is not only to receive material from the ER but also to participate in the sorting and recycling of proteins and lipids back to the ER. The TGN forms a sacculotubular network extending from the *trans* cisternae and constitutes the sorting station of the Golgi. It has been suggested that the TGN itself is composed of functionally distinct subdomains containing glycosylation enzymes (such as sialyl transferase), as well as enzymes that perform late Golgi modifications (such as tyrosine sulfation). They might also be involved in the segregation of membrane and luminal proteins into different types of transport vesicles destined for endosomes, lysosomes, secretory granules and the plasma membrane. Certain proteins also stay in the Golgi serving in a permanent bidirectional intra-Golgi transport. Thus, the Golgi apparatus appears as a dynamic structure being the main crossroad of the intracellular trafficking; nevertheless, there is an enrichment of lipids and proteins which is constantly maintained from the *cis* to the *trans* compartment. It remains unclear how the different Golgi cisternae interrelate, whether they are stable or not, or what is the exact function of the numerous vesicles and uncharacterized tubules that are always associated with the Golgi apparatus [174].

1.5.3. The Intermediate Compartment

The intracellular traffic between the ER and the Golgi in mammalian cells appears to be complicated due to the existence of the IC which is absent in *Saccharomyces cerevisiae*. The IC has been defined biochemically by marker proteins, most notably ERGIC53, and morphologically by the piling up of secretory proteins in this compartment at reduced temperature: at 15°C, proteins are segregated into tubulo-vesicular structures that are distinct from the typical ER [175]. After its formation, the IC has only a transient existence before delivering its cargo to the Golgi complex in a process involving simultaneously forward secretory transport and Golgi biogenesis. Since its identification [156], it has been matter of debate whether the IC is continuous with the ER [176] or the *cis*-Golgi [173] or is a distinct

organelle separated from the ER and Golgi [156, 177]. In line with the latter, it has been postulated that small vesicles bud from the IC to deliver cargo into the Golgi complex [178] or to recycle proteins back to the ER.

Live cell timelapse imaging following different GFP-tagged secretory markers (e.g. VSVG-GFP; vesicular stomatitis virus G glycoprotein) revealed that the ERGIC is a mobile membrane structure which carries protein and lipid along microtubules from the ER to the Golgi complex [165, 179]; therefore it was called vesicular-tubular transport complex (VTC). VTCs have also been shown to undergo maturation (by recycling of selected components back to the ER; [180]) and to be capable of homotypic fusion [181]. This would fit the hypothesis that the Golgi cisternae form by continuous maturation/ differentiation of VTCs [182, 183]. In this model, the *cis* face of the Golgi complex represents the site where VTCs first merge together, while the *trans* face is where they have to undergo further maturation through recycling pathways [184-186].

1.5.4. Retrograde pathways

1.5.4.1. COPI dependent and independent transport pathways

The continuous flow of membrane from the ER to the Golgi apparatus would finally lead to a depletion of ER membranes and to a steady extension of the Golgi complex. Therefore, in order to maintain the functional and structural identity of the endomembrane system, lipids and proteins must be recycled. At least two retrograde transport routes have been described to be operative in the early pathway. They serve several important functions such as the retrieval of escaped endoplasmic reticulum (ER) proteins [12, 187] and membrane machinery necessary for ER-to-Golgi traffic [188, 189], retention of misfolded proteins [190, 191], recycling of Golgi enzymes [192, 193], the internalization of bacterial and plant toxins [194], and the disassembly of the Golgi complex during mitosis [195].

Among these, the recycling of ER residents has been particularly well studied. During normal anterograde flow a certain number of endogenous ER proteins continuously leave the organelle and reach downstream compartments in the secretory pathway where they are recognized and returned back to their original location [12]. Soluble ER proteins such as chaperones and components of the quality control machinery contain a C-terminal KDEL (HDEL in yeast) sequence that is responsible for their recognition and retrieval from post-ER compartments [196, 197]. Through their association with molecular chaperones misfolded proteins are also efficiently recovered from post-ER compartments and rerouted to the ER

[198]. Many ER transmembrane proteins contain a dilysine (KKXX) motif at their C-terminal cytoplasmic tail which is also a retrieval signal [199, 200]. In addition to KDEL and KKXX sorting signals, retrieval of these proteins depends on receptors that recognize these signals. The role of such receptors is to ensure that there is no net loss of these proteins from the ER. The ligand-receptor complexes are transported back to the ER where they dissociate leading to the release of ligand within the ER and subsequently the empty receptor can be recycled back to the Golgi for further rounds of transport. The affinity between ligand and receptor has been suggested to depend on the pH which is different between the ER and the Golgi [201]. The KDEL motif is recognized by Erd2 (or KDEL receptor) which is located at the Golgi complex and the ERGIC [202]. COPI-coated transport intermediates, believed to be either vesicles or tubules [186, 203, 204], mediate retrograde traffic followed by both the KDEL receptor-ligand complexes and membrane proteins containing a KKXX motif [48, 149, 158, 165]. The A-subunit of Cholera toxin (CTX) which contains a KDEL motif in its C-term is thought to move from Golgi to ER by COPI-dependent transport [205, 206] (see chapter 1.5.4.3.). Upon ligand binding the KDEL receptor oligomerizes and interacts with components of the retrograde transport machinery such as ARF-GAP and ARF1 [207], most likely contributing to the formation at the donor membrane of prebudding complexes that should facilitate evagination. In principle, sorting takes place through the interaction of COPI coat proteins with the cytoplasmic domains of the KDEL receptor [49, 157]. For example, the phosphorylation by cAMP-dependent protein kinase A (PKA) of the C-terminal cytoplasmic domain of the mammalian KDEL receptor seems to favor this interaction of the KDEL receptor with coatomer proteins and ARF-GAP [208].

Another, COPI independent, recycling pathway was claimed to be used by the Shiga toxin or Shiga Toxin B-fragment and to be regulated by Rab6 [209, 210]. Expression of a dominant negative Rab6 form (Rab6-GDP) inhibited redistribution of GFP-tagged Golgi-resident enzymes to the ER [210], which suggests that these enzymes use this or a closely related Rab6-dependent pathway to gain access to the ER. Co-localisation of Shiga-B fragment and GFP-tagged Rab6 on larger tubular structures that do not contain the KDEL-R seems to support these functional studies [209]. These tubules segregate from the Golgi and are believed to fuse with the ER at the cell periphery.

Experiments using GFP-tagged KDEL receptor expressed in HeLa cells showed similar formation of Golgi tubules and subsequent detachment and translocation of these tubules to the cell periphery [204]. These data suggest that both tubular and vesicular carriers could mediate Golgi-to-ER transport. Importantly, in every case, the tubules could be observed as a

result of overexpression of GFP-tagged markers. However, such tubules were also found in untransfected cells by both fluorescence microscopy and immunoelectron microscopy [211]. Interestingly, the effects of the fungal antibiotic brefeldin A (BFA) have been taken as evidence for the existence of a physiologically relevant retrograde pathway from the Golgi to the ER. BFA reversibly blocks transport of secretory proteins to the Golgi apparatus, and induces a dramatic fusion of most of the Golgi membrane with the ER. Treatment of many mammalian cells with BFA leads to an immediate dissociation of Golgi-bound COPI-coats into the cytoplasm resulting in the formation of tubular structures which eventually separate from the Golgi and fuse with the ER [212]. However, a fundamental function of coatamer seems to be the prevention of uncontrolled fusion. Thus, BFA-induced dissociation of coatamer would allow uncontrolled fusion of Golgi with ER membranes rather than retrograde transport.

Recently, Malsam and collaborators [213] demonstrated the existence of subpopulations of COPI vesicles defined by their tethering factors (p115 versus golgin84-CASP). These tethers may differentiate the intra-Golgi and Golgi-ER retrograde COPI vesicles. This work also suggested a two-step retrograde pathway for the Golgi enzymes, the first step mediated by intra-Golgi COPI transport to the CGN, the second by a COPI-independent pathway to the ER. Tubular continuities were previously proposed to mediate the retrograde transport of Golgi enzymes, leaving COPI vesicles to carry the fusion machinery [214].

In principle, vesicles or tubules could also form from the ERGIC in mammalian cells. It has been proposed that a VTC receives cargo from COPII vesicles followed by the exchange of COPII for COPI leading to COPI vesicles which would return recycling material from the ERGIC to the ER [179, 215]. Upon arrival at the cis-Golgi, anterograde cargo must physically segregate from retrograde cargo in order to be delivered for further transit through the secretory pathway, whereas retrograde cargo must be returned back to the ER. Establishment of retrograde- and anterograde-cargo domains [216] was observed within the VTC itself on its way to the cis-Golgi.

1.5.4.2. Golgi-ER SNAREs

Several SNARE complexes have been defined to function in various transport events in the secretory and/ or endocytic pathways of mammalian cells. The complex consisting of Syn5 (Qa), membrin (Qb), Bet1 (Qc), and Sec22b (R) described by Xu et al. [217] as involved in ER to Golgi transport appears to function in mediating homotypic fusion of ER-derived COPII vesicles to form the IC or VTCs [189, 218]. This SNARE complex has a

corresponding yeast homolog formed by Sed5p, Bos1p, Bet1p and Sec22p respectively. The SNARE complex consisting of Syn5 (Qa), GS28 (Qb), Bet1 (Qc), and Ykt6 (R) is suggested to act in the late stage of transport from the ER to the Golgi and is likely to mediate the fusion of matured VTCs with the cis-face of the Golgi apparatus [219]. The SNARE complex consisting of Syn5 (Qa), GS28 (Qb), GS15 (Qc), and Ykt6 (R) functions in intra-Golgi traffic and a similar complex is also found in yeast [105, 220, 221]. Sec22p has been shown to interact with syntaxin 18, the mammalian homologue of Ufe1 [222]. Moreover, in yeast Sec22p recycles from the Golgi back to the ER and this recycling involves retrograde COPI vesicles and the ER transmembrane proteins Ufe1p and Sec20p [223]. Recently, Dilcher et al. demonstrated the existence of an unconventionnal SNARE in the ER called Use1 (also called Slt1, [224]) in yeast which interacts with the SNAREs Ufe1p, myc-Sec20p and Sec22p forming a SNARE complex required for Golgi-to-ER retrograde traffic in yeast [85].

Similar to the interaction of yeast Sec20p with its regulator TIP20 [225], the mammalian Sec20 (also called BNIP) interacts with RINT-1, a mammalian protein homologous to TIP20 [226, 227]. The two SNARE-proteins Sec22 and Ykt6 exhibit a profilin-like structure in their N-terminal extension [228, 229]. Interestingly, the same domain is found in the Trs20/SEDL subunit of the TRAPP complex, which is involved in the tethering process in the early secretory pathway [230]. This raises the possibility that this tethering complex could modulate the function of SNAREs containing profilin-domain through competitive interaction with some unidentified regulators.

1.5.4.3. The cholera toxin as external cargo protein

Cholera toxin (Ctx) from *Vibrio cholerae* is one of the well-characterized virulence factors produced by pathogenic micro-organisms and belongs to the group of so called AB₅-toxins composed of one A-subunit and five identical B-subunits noncovalently associated [231]. Studies on its interaction, uptake and action in epithelial cells have helped to elucidate the mechanisms of toxicity. These toxins move from the plasma membrane through the trans-Golgi and endoplasmic reticulum (ER) to the cytoplasm of host cells. Therefore, they constitute convenient tools to better understand cellular events associated with vesicular movement and targeting.

Cholera toxin begins its journey into the cell by the binding of its B-subunits to the gangliosides GM1 at the cell surface [232] resulting in the association of Ctx with lipid rafts [233, 234], which are required for toxin function [235, 236] and found ubiquitously on the surface of eukaryotic cells [237]. Cholera toxin has been reported to enter cells from non-coated areas of the surface membrane [238], possibly from caveolae [236]. Following

internalization, it can be found in early and recycling endosomes, the Golgi apparatus and the ER [205, 239]. There is evidence to suggest that the A- and B-subunits of the Ctx separate in the Golgi apparatus and that only the A-subunit containing a KDEL motif in its C-term then moves to the ER by binding the KDEL receptor, ERD2 [206, 239]. However, the KDEL motif seems not to be required for toxin function [240], although it improves the efficiency of intoxication [241]. Additionally, recent studies show that the lipid-raft ganglioside, GM1, is responsible for transport into these compartments [240]. Nevertheless, there is evidence to suggest that Ctx might move backwards from the Golgi to ER by COPI-dependent transport [205, 206]. This COPI-dependent pathway might also carry lipid-raft gangliosides back to the ER. Once in the ER, the A1-chain of the Ctx unfolds and enters the cytoplasm by hijacking the cellular machinery that enables misfolded proteins to cross the membrane for degradation, a process termed retro-translocation [242]. Upon entering the cytoplasm, the A1-chain rapidly refolds, avoids the proteasome and induces toxicity by ADP-ribosylating the α subunit of various heterotrimeric G-proteins [231, 243, 244]. This ADP-ribosylation is stimulated by ARF and activates adenylyl cyclase; this induces intestinal chloride secretion that causes the massive secretory diarrhea seen in cholera.

2. AIM OF THIS WORK

The aim of this work was to characterize the SNARE complex(es) involved in Golgi-to-ER traffic and to elucidate a potential role of SNARE-proteins in cargo sorting and budding. By homology with the synaptic SNARE complex and on the basis of previous studies in yeast, we assumed the participation of the following SNARE-proteins in Golgi-to-ER traffic: Sec22b as the R-SNARE, Syntaxin18, mUSE1 and mSec20 as the three Q-SNAREs. The localization and the interaction between SNARE proteins forming the putative retrograde Golgi-to-ER complex were analysed using fluorescence techniques (FRET measurements by spectrofluorimetry and microscopy, bimolecular fluorescence complementation experiments) in living cells, as well as by co-immunoprecipitation.

To study molecular mechanisms involved in retrograde Golgi-to-ER transport which could include the participation of SNARE-proteins, interaction of these SNAREs (except for Syntaxin18) with the KDEL-receptor was measured by FRET experiments. COPI vesicles were released from isolated Golgi apparatus in a cell-free assay and their protein contents were studied by Western-blotting and immuno-electron microscopy. Additionally, the isolated vesicles were used to perform co-immunoprecipitation experiments using mUse1 and mSec22b antibodies. The function of the different SNAREs was further studied using synthesized siRNA. In the case where the cell morphology was not affected by SNARE knock-down, the transport of cholera toxin was followed in transfected and WT cells in parallel.

3. MATERIALS

3.1. Materials for culture

3.1.1. Bacterial E. Coli strains

Strain	Relevant genotype/phenotype	Source
BL21	<i>dcm</i> , <i>ompT</i> , <i>hsdS</i> _(rB-mB-) , <i>gal</i> , F-	Stratagene
DH5 α	F ⁻ , <i>supE44</i> , Δ <i>lacU169</i> , (ϕ 80 <i>lacZ</i> , Δ M15), <i>hsdR17</i> , <i>recA1</i> , <i>endA1</i> , <i>gyrA96</i> , <i>thi-1</i> , <i>relA1</i> , Δ (<i>lacZYA-argF</i>)U169	Gibco-BRL
XL1 Blue	<i>recA1</i> , <i>endA1</i> , <i>gyrA96</i> , <i>thi</i> ⁻ , <i>hsdR17</i> , (<i>rk-</i> , <i>mk+</i>), <i>supE44</i> , <i>relA1</i> , <i>lac</i> ⁻ , [F', <i>traD36</i> , <i>proAB</i> , <i>lacI</i> ^q Z Δ M15, Tn10 (<i>tet</i> ^r)]	Stratagene

For a description of gene nomenclature see Bachmann *et al.* [245].

3.1.2. Bacterial growth media

3.1.2.1. Bacterial media

All cultures were grown on liquid YT or LB media or solid LB medium. Compositions (for 1L) were as noted below.

LB (Luria Bertani) media 10 g Bactotryptone and 5 g Yeast extract (Carl Roth), 5 g NaCl, ad 1 liter with distilled water
12 g agar for solid media

Low salt LB media 10 g Bactotryptone, 5 g Yeast extract, 2.5 g NaCl, ad 1 liter with distilled water
12 g agar (BD Biosciences) for solid media

2X YT 16 g Trypton, 5 g NaCl, 10 g Yeast Extract, ad 1 liter with distilled water

2xYT is richer than LB and therefore allows for higher bacterial densities

All media were autoclaved before use.

3.1.2.2. Additives for bacterial culture

LB-Kan, LB-Zeocin and LB-Amp media were prepared by adding kanamycin (ICM Biomedicals), zeocin (Invitrogen) and ampicillin (Sigma) respectively, from stock solutions of 100 mg/ml H₂O (filtered) to the autoclaved media after the temperature of the media had fallen below 50°C. The working concentration of zeocin was 25 µg/ml, 50 µg/ml for kanamycin and 100 µg/ml for ampicillin.

IPTG (Isopropyl-1-thio-β-D-galactopyranoside) was used for induction of protein synthesis at 0.2-1.0 mM final concentrations for liquid cultures, from 1 M filtered stocks. Tetracycline was prepared as a 1000x stock solution in 50% (v/v) ethanol and used at 12.5 µg/ml.

3.1.3. Mammalian tissue culture cell lines

VERO cells are African green monkey kidney cells and were provided by ECACC (84113001).

3.1.4. Mammalian cell medium and additives

DMEM (Dulbecco's Modified Eagle's Medium) from Cambrex (Biowhittaker)
with 4,5 g/L Glucose, sterile filtered

Trypsin-EDTA (1X) from Cambrex

0.5 gram per Liter Trypsin 1:250, 0.2 gram per Liter Versene (EDTA),
sterile, pH : 7.1-7.9

FCS (Foetal calf serum) for complementation of growth media was purchased from PAA.

L-Glutamine in powder from Cambrex

pH: 5.58-6.78, osmolality : 423-499 mOsm/kg

MEM Na pyruvate from Gibco/BRL

Penicillin-Streptomycin Mixture from Cambrex

pH: 3.61-7.29, osmolality : 287-307 mOsm/kg

Oligofectamin from Invitrogen and **Opti-MEM1** from Gibco/BRL were used for si RNA transfection.

HAM's F-12 from PromoCell was used for its low fluorescence properties for imaging.

Falcon provided all culture dishes used and coverlips were from Menzel-Gläser.

All chemicals used were of analytical grade and were purchased from Boehringer, Merck, Sigma or Serva, unless otherwise stated.

3.2. Proteins, kits, enzymes and substrates

Secondary antibodies (anti-mouse or anti-rabbit) coupled to indigocarbocyanine dyes (Cy3 and Cy5) were purchased from Jackson ImmunoResearch Laboratories. Secondary antibodies (anti-mouse or anti-rabbit) coupled to HRP (HorseRadish Peroxidase) were from Dianova.

Monoclonal antibodies against rBet1 were kindly provided by Dr. Jesse Hay (University of Michigan, Ann Arbor, Mich.), monoclonal antibodies against syntaxin 18 (human) were a kind gift of Prof. Mitsuo Tagaya (School of Life Sciences, Tokyo), polyclonal rabbit antibodies against β' -COP were generously provided by Dr. Britta Brügger (Biochemistry Center, University of Heidelberg) and monoclonal antibodies against ERGIC53 were kindly given by Dr. Hans-Peter Hauri (Biozentrum, University of Basel).

Plasmid DNA extraction from *E. coli*, DNA extraction from agarose gels and purification of PCR products were performed with Qiagen Spin Miniprep or Maxiprep Kits, QIAquick Gel Extraction Kit, PCR Purification Kit and a Nucleotide Removal Kit respectively, from Qiagen.

For chemiluminescence, the Western LightningTM Chemiluminescence Reagent Plus kit from Perkin Elmer was used.

Restriction enzymes were from Fermentas or New England Biolabs. Taq-polymerase, T4-DNA ligase and Pfu-Polymerase were from PAN Biotech, Fermentas and Promega, respectively.

1kb-DNA and Standard-protein MW (Molecular Weight) markers were purchased by Fermentas and Peqlab, respectively.

3.3 Filter materials and chromatography media

Pharmacia's P10 and P20 columns were used for rebuffering of protein and for separating the labeled CTX or antibodies from the fluorescent dye after labeling. Filter paper and nitrocellulose membranes for Western blotting were supplied by Schleicher und Schüll and Sartorius.

All FPLC chromatography media (MonoQ) as well as Q Sepharose FF, and Protein A Sepharose media came from Amersham Pharmacia Biotech. GSH-agarose and CNBr-

activated agarose were also provided by Amersham Pharmacia Biotech, and Ni²⁺-nitrilotriacetic acid-agarose (Ni-NTA) was from Qiagen.

3.4. cDNA

Cloning of mouse Sec20 was performed by Prof. HD. Söling in the laboratory, Rat Use1 was cloned by Dr. Gabriele Fisher von Mollard (Biochemistry II, University of Göttingen), mouse Sec22b was a kind gift from Dr. Jesse Hay (University of Michigan, Ann Arbor, Mich.) and human Syntaxin18 was a kind gift from Prof. Mitsuo Tagaya (School of Life Sciences, Tokyo, Japan).

3.5. Plasmid vectors

For protein expression in bacteria, the vectors pGEX-4T3 and pGEX-6P-2 were obtained from Amersham Pharmacia Biotech.

For in vitro transcription/translation, the pCMV TNT vector was purchased from Promega.

Plasmids coding for GFP variants ECFP, EYFP, EGFP (N1 or C1) were purchased from Clontech (Heidelberg, Germany).

The vectors pC1- and pN3-GFP₂ were from Biosignal Packard and Perkin Elmer respectively.

The plasmid coding for NPY-venusYFP was a kind gift from Dr. Atsushi Miyawaki (RIKEN institute, Hirosawa, Japan) (Nagai T. et al., Nat Biotech 2002) and was used to construct the vectors pN1-venusYFP and pC1-venusYFP.

3.6. siRNA and primers

siRNA duplexes against human Sec22b (5'-CCAGAAGGUGAUGUACGGCdTdT-3' sense and 3'-dTdTGGUCUCCACUACAUGCCG-5'antisense) and human Sec20 (5'-CCAGAAGGUGAUGUACGGCdTdT-3' sense and 3'-dTdTGGUCUCCACUACAUGCCG-5' antisense) were produced by MWG. Stealth siRNA against human USE1 (5'-UCAUCUUCAUAGCA UGAUCCUCUU-3' sense and 3'-AAGAGGAUCAUGC UAAUG AAGAUGA-5' antisense) were produced by Invitrogen. siRNA oligos against lamin (5'-CUGGACUCCAGAAGAACA dTdT-3' sense and 3'-dTdTGACCUGAAGGUCUUCUUG

U-5' antisense) and GL2 (5'-CGUACGCGGAAUACUUCGAdTdT-3' sense and 3'-dTdTG CAUGCGCCUUAUGAAGCU-5' antisense) were produced by Dharmacon Research.

Primers for PCR reaction were produced by either MWG or Invitrogen.

3.7. Buffers and solutions

PBS (phosphate buffered saline): 137 mM NaCl

2.7 mM KCl

8.1 mM Na₂HPO₄

1.4 mM KH₂PO₄ ; pH 7.4

Buffers for specific purposes are to be found in the relevant section, of the Methods chapter.

3.8. Material for fluorescence microscopy

The microscope used for imaging was an Axiovert 200 inverted microscope from Zeiss equipped with an oil-immersion 100× 1.4 NA Plan Apochromate objective lens. A CCD camera provided by Kodak, Princeton Instruments was connected to this microscope and used for imaging. The whole system was monitored by the program Metamorph 6.0 (Universal Imaging Corp.).

All filter sets came from AHF Analysentechnik.

The pictures were analysed with the program Inspector kindly provided by Dr. Andreas Schönle (Department of Nanobiophotonics, Max-Planck Institute for Biophysical Chemistry), unless otherwise stated.

4. METHODS

4.1. cDNA cloning and construction of expression vectors

4.1.1. cDNA constructs

4.1.1.1. Constructs for expression of fluorescent fusion proteins in mammalian cells

mSec22b and mUse1 were subcloned into the different GFP-C1 vectors coding for the GFP variants (including the BIFC vectors) using the restriction enzymes EcoRI and BamHI. For mSec20 subcloning, EcoRI and SalI were used. Syntaxin18 was subcloned into the vector pC1-YFP using the restriction enzymes BglII and EcoRI.

For Erd2, the restriction enzymes PstI and SacI were used for cloning into pN₃-GFP2. For cloning the sequence encoding Erd2 into the N1 vectors coding for ECFP, EYFP and vYFP, Eco47III and AgeI restriction enzymes were used.

Starting from the pNPY-N1-venusYFP plasmid (NPY = Neuropeptide Y) and the primer pair 5'-TAATTAACCGGTCGCCACCATGGTGAGCAAGGGCGA-3' (forward) and 5'-TATAATAGATCTCTTGTACAGCTCGTCCATGCCGAG-3' (reverse), the sequence encoding venusYFP was amplified and ligated into the AgeI/BglII restriction enzyme sites of the expression vector pC1-EGFP previously digested with the same enzymes.

4.1.1.2. Constructs for protein expression in bacteria

Starting from the pEGFP-Sec22 plasmid, the sequence encoding Sec22(Δ TM) was amplified and ligated into the BamHI/NotI restriction enzyme sites of the expression vector pGEX-4T-3. This placed the Sec22 sequence in frame with the upstream GST sequence, allowing for purification of expressed fusion protein over glutathione-agarose columns. In the expressed protein, a thrombin cleavage site between GST and the Sec22 sequence was available.

The sequence encoding Use1(Δ TM) was generated by PCR. This fragment, flanked by restriction sites for NdeI and XhoI, was cloned into pET28 via the NdeI/XhoI sites and transformed into *E. coli* XL1-Blue. This placed the coding sequence for Use1 in frame with, and 3' of, the hexahistidine encoding sequence of pET28. The purification of the His₆-tagged protein was performed over a Ni-beads column.

Starting from the pEGFP-Syntaxin18 plasmid, the sequence encoding Syntaxin18 (Δ TM) was amplified by PCR and ligated into the BamHI/NotI restriction enzyme sites of the expression vector pQE30. This placed the Syntaxin18 sequence in frame with the sequence

encoding a hexahistidine tag immediately upstream, allowing for purification of expressed fusion protein over Ni-beads columns.

4.1.1.3. Construct pCMV-TNT-Sec20 for in vitro transcripton/translation

Starting from the pEYFP-Sec20 plasmid, the primer pair 5'-CTGAATGAATTCG GACCATGGATGGCGGCTCCCCAGGATGTC-3' and 5'-AAGAGGGTCGACTTA CAAAAATGGAAAGAGGCG-3' was designed to insert the kozak sequence ACCATGG upstream of the sequence encoding Sec20 which was amplified and ligated into the EcoRI/Sall restriction enzyme sites of the expression vector pCMV-TNT.

Escherichia coli strain XL1-Blue was used to amplify plasmid DNA. Sequencing of DNA was performed by SeqLab, the files were read with the program DNA-Star and sequences verified with the internet program <http://probes.toulouse.inra.fr/multalin/multalin.html/>.

4.1.2. PCR amplification of DNA

The typical reaction mixture for PCR is composed of 50-100 pmol forward and reverse primers in dH₂O, 1x nucleotide mix (200 μM dATP, dCTP, dGTP, dTTP), 1x PCR buffer with MgCl₂ (20 mM Tris/HCl, pH 8.4; 50 mM KCl; 2.5 mM MgCl₂), ~20 ng template DNA in dH₂O or 10 mM Tris/HCl, pH 8.5, 1 U DNA polymerase and double-distilled H₂O was added to 50 μl final reaction volume.

The primers may have modifications such as extensions at their 5' ends or deletions, insertions and point mutations allowing for specific changes to the amplified sequence.

On a MJ Research Inc. model PTC 150-25 MiniCycler (Biozyme), typical reaction conditions for a primer with modifications that are not present in the initial template are:

Step	T (°C)	time (s)	description
1	95	5	denaturation
2	85	hold	hot start: addition of DNA polymerase
3	94	50	denaturation
4	T ₁	25	partial primer annealing
5	72	t	extension
6	--	--	cycle 5 times to step 3

Methods

7	94	50	denaturation
8	T ₂	25	Full primer annealing, T ₂ > T ₁
9	72	t	extension
10	--	--	cycle 25 times to step 7
11	4	hold	end of reaction

The annealing temperature (T) is determined for each primer pair separately and is dependent on the degree of homology between each primer and its template and the content of high-melting, paired G and C bases. An estimate is given by the following empirical relationship [246]: $T (^{\circ}\text{C}) = 69.3 + 0.41 \times (\text{GC}\%) - 650/l$ where $l =$ (overlap length in bases)

The lower of the two temperature values for a primer pair is used in the reaction. The extension time (t) is dependent on the length of the target sequence and the DNA polymerase used. For Taq DNA polymerase, a rate of 1000 bases per minute was used in computations.

4.1.3. DNA gel electrophoresis

At neutral pH, the negatively charged DNA molecules migrate under the influence of an electrical field from the cathode to the anode. The distance migrated is dependent on fragment size and fairly independent of base or sequence composition. The bands are made visible under ultraviolet light of 302 nm by incubating the gel in a solution of ethidium bromide (0.5 $\mu\text{g/ml}$), which binds to the DNA.

Gels were prepared according to the size of the DNA fragments of interest as follows:

Agarose concentration (%)	Resolving size range (kb)
0.5	1.0-30
0.7	0.8-12
1.0	0.5-10
1.2	0.4-7.0
1.5	0.2-3.0
2.0	0.05-2.0

Agarose gel material was added to an appropriate volume of 1 X TBE and boiled in a microwave oven until all the agarose had dissolved (~ 5 min). The liquid gel was then poured into a horizontal chamber. Two of its sides were sealed with a 2.5 cm wide Drapore[®] and the comb was placed into the chamber for slot formation. The comb was removed after agarose gel polymerisation. The gel was then immersed into an electrophoresis chamber filled with 1

X TBE buffer. The samples were then mixed with gel-loading buffer (stock solution 6 fold) and finally loaded into the slots. The applied current was 85 mA.

10X TBE : 500 mM Tris; 500 mM H₃BO₃; 10 mM EDTA

6X gel-loading solution : 20% (v/v) Ficoll; 0.125% (w/v) bromophenol blue;
0.125% (w/v) Xylene-cyanol in H₂O

Ethidium bromide : 10 mg/ml in H₂O

PCR products, DNA inserts and plasmids were run on a suitable agarose gel. When necessary, the desired bands were excised from the gel with a scalpel and DNA was isolated using a QIAGEN gel extraction kit according to the manufacturers recommendations. The principle of the QIAGEN kit consists in DNA binding to a solid support (a silica-gel membrane) in the presence of chaotropic salts and low pH (pH<7.5) and elution after removal of salt with a buffer of pH>7.5, such as TE-buffer.

4.1.4. Estimation of DNA purity and quantitation

4.1.4.1. Spectrophotometric Determination

For the quantification of the amount of DNA, readings were taken at 260 nm and 280 nm using a GeneQuant II spectrophotometer (Pharmacia). The reading at 260 nm allows the calculation of the concentration of nucleic acid in the sample. An OD of 1 corresponds to approximately 50 µg/ml dsDNA, 40 µg/ml ssDNA and 31 µg/ml oligonucleotide DNA. The ratio OD₂₆₀/OD₂₈₀ provides an estimate of the purity of the nucleic acid. Pure preparations of DNA have ratio values of 1.8. If there is contamination with protein or phenol, the ratio will be significantly less than 1.8.

4.1.4.2. Ethidium bromide fluorescent quantification

In case of a low concentration (<250ng/ml) or heavy contamination of the DNA solution, the concentration can be determined by measuring the ultraviolet-induced fluorescence emitted by ethidium bromide molecules intercalated into the DNA by an using UV light table. Because the amount of fluorescence is proportional to the total mass of DNA, the quantity of DNA (as little as 1 to 5 ng can be detected) in the sample can be estimated by comparing the

fluorescence yield of the sample with that of a series of standards in 1 μ l of a 1 kb ladder solution (0.5mg/ml).

4.1.5. Competent *E.coli*

4.1.5.1. Preparation and transformation by heat shock

The method of Inoue *et al.* [247] was employed. A fresh 250 ml culture, inoculated with cells of the desired strain from an overnight culture, was harvested by centrifugation (10 min at 4,000 x g_{av} , 4°C) upon reaching an A_{600} of 0.5-0.9. The cells were cooled on ice for 30 min and then washed twice with ice cold water. After resuspension in 25 ml sterile filtered TB, the cells were centrifuged again at 7,000 x g_{av} for 5 min, 4°C, and resuspended once more in 5 ml TB. 300 μ l aliquots were taken and stored at -80°C in the presence of 7% (v/v) DMSO unless used immediately.

TB (Transformation buffer) : 10mM PIPES, pH 6.7; 55 mM $MnCl_2$;
15 mM $CaCl_2$; 250 mM KCl
(pH is set before addition of $MnCl_2$)

200 μ l of competent *E. coli* cells were thawed on ice and added to 10-50-ng of plasmid mixture. Cells were incubated for 30 min on ice, then heat shocked for 1.5 min at 42°C in a water-bath. Thereafter, 1 ml LB was added and the samples were incubated at 37°C for 45 min to allow initiation of the expression of selection marker proteins. Finally, 20 μ l and 100 μ l respectively were plated on agar plates containing the appropriate antibiotic of selection and incubated overnight at 37°C.

4.1.5.2. Preparation and transformation by electroporation

A 10 ml overnight culture of *E. coli* XL1-Blue cells in LB-tetracyclin was used to inoculate 1 L of fresh LB medium. The culture was grown at 37°C with agitation for about 2.5 h until an A_{600} of 0.5-0.7 was achieved. The flask was cooled on ice for about 30 min, and the cells were thereafter collected by centrifugation at 4,000 x g_{av} for 20 min at 4°C. The cells were resuspended in 1 L of ice cold, sterile HEPES buffer, spun again as above, resuspended a second time in 500 ml HEPES buffer, spun, resuspended a third time in 20 ml HEPES buffer with 10% (v/v) glycerol, centrifuged again and finally resuspended in 2-3 ml sterile

10% (v/v) glycerol. The cells were then dispensed in 50-100 μ l aliquots and frozen on dry ice. The frozen cells were stored at -80°C .

HEPES buffer: 1 mM HEPES, pH 7.0

10% glycerol: 10% (v/v) glycerol in distilled water

HEPES/glycerol: 1 mM HEPES, pH 7.0; 10% (v/v) glycerol

All solutions were sterilised by autoclaving before use.

For transformation, 50 μ l electro-competent *E. coli* XL1-Blue cells were thawed on ice and transferred to a chilled 0.2 cm electroporation cuvette (Bio-Rad). 1 to 5 μ l salt-free plasmid DNA was added and the sample kept on ice for 1 min. Thereafter, the cuvette was transferred to a Gene Pulser electroporation chamber (Bio-Rad) and pulsed with 25 μ F, 2.5 kV, 200 ohms. The time constant was usually about 4.5-5 ms. 1 ml LB medium was added immediately after pulse and the sample transferred to a 1.5 ml Eppendorf tube and incubated with agitation at 37°C for 1 h. 10-100 μ l of the sample was then plated onto LB-Amp, LB-Kan or LB-Zeocin plates and incubated overnight at 37°C .

4.1.6. DNA preparation

Small- and large-scale plasmid extractions were performed using Plasmid mini- and maxi-prep kits from Qiagen according to the manufacturers recommendations. The basic principle involves alkaline lysis of the cell wall, degradation of RNA by RNase, precipitation of proteins and chromosomal DNA with high salt and binding of plasmid DNA to a silica-gel matrix.

4.2. Expression and purification of recombinant proteins

4.2.1. Expression and purification of GST-Sec22b and GST

One L LB containing ampicillin was inoculated with 10 ml of an overnight culture of *E. coli* BL21 harbouring the vector construct pGEX-mSec22b(Δ TM) or the vector pGEX-6P and the cells were cultured at 37°C till an A_{600} of 0.6-0.9. IPTG was added to 0.5 mM to induce protein expression. After 3 hours, the cells were harvested by centrifugation at $2,500 \times g_{av}$ for 30 min at 4°C . The pellet was resuspended in the following buffer: PBS, pH 7.4; lysozyme 1 mg/ml; DNase 10 μ g/ml; 5 mM MgCl_2 and protease inhibitor (Complete protease inhibitors

cocktail, 1 tablet, Roche) at 40 ml/liter of culture and incubated for 30 min on ice. Thereafter, the cells were disrupted by sonicating in 10 bursts of 30 s at 50% of output and 8 duty cycles using a Branson model 450 Sonifier. This was repeated 5 times.

Triton X-100 was added to 1% (v/v) and the lysate was rotated for 20 min at 4°C. The sample was spun at 30,000 x g_{av} for 30 min at 4°C. The pellet was discarded and the supernatant spun at 180,000 x g_{av} for 30 min at 4°C. The supernatant was bound to 3 ml settled Glutathione-Sepharose, prewashed with PBS, for 30 min at 4°C with end-over-end rotation. After this batch-binding procedure, the sample was transferred to a 10 ml Mo Bi Tec gravity-flow column and washed five times with 10 ml each of PBS. Elution was performed using 10 ml Elution buffer and collecting 1 ml fractions. The eluates, containing eluted GST-mSec22b, were pooled, aliquoted and stored at – 80°C.

Elution buffer : 50 mM Tris/HCl, pH 8.0; 10 mM reduced glutathione (GSH)

4.2.2. Expression and purification of His6-mUse1

A colony from a plate with freshly transformed *E. coli* BL21(DE3) cells harbouring the vector pET28-mUSE1(Δ TM) was used to inoculate 25 ml of 2xYT medium containing kanamycin. The overnight culture grown at 37°C was then added to 500 ml of fresh 2xYT containing kanamycin and the cells were grown until an A_{600} of 0.6-0.9 was reached. Expression of recombinant proteins was then induced by the addition of IPTG to 0.2mM. After a 4 h induction period at 30°C, the cells were centrifuged for 15 min at 3,000 x g_{av} at 4°C and then resuspended in 20 ml of binding buffer. Protease inhibitors (tablet Complete Roche) were added directly before French Press lysis which was performed cracking twice with 1200 psi. The sample was spun at 4°C 10 min at 17,000 x g_{av} to remove insoluble material. The supernatant was centrifuged a second time. 1 ml of washed (with Washing buffer) Ni-NTA beads was added to the supernatant. His-tagged proteins were allowed to bind for 1h at 4°C with end-over-end rotation and the solution transferred into a 10 ml Mo Bi Tec gravity-flow column. The beads were washed with 10 ml of washing buffer. Elution was performed using 2 ml of washing buffer containing imidazol, pH 6,0 and collecting 1 ml fractions. This was done four times, each time increasing the amount of imidazol (50mM, 100mM, 250mM and 500mM). Each eluate fraction was then analyzed for purity and yield on SDS-gel. The purified His-Use1 was aliquoted and stored at -80°C.

Binding buffer: 50 mM NaPO₄, pH 8,0; 300 mM NaCl

Washing buffer: 50 mM NaPO₄, pH 6,0; 300 mM NaCl

4.2.3. Expression and purification of His6-Syntaxin18

XL1-Blue bacteria were transformed with pQE30-Syn18 Δ TM. Bacteria (1 clone) were grown in 50 ml LB-Amp at 37°C. The overnight culture was added to 500 mL LB-Amp and bacteria were grown at 37°C to an A₆₀₀ of 0.8. Protein production was induced with 0.25 mM IPTG for 3h at 30°C. The cells were harvested by centrifugation at 2,500 x g_{av} for 30 min at 4°C, and the pellet was resuspended in 25 ml of the following buffer: PBS, pH 7,4, containing Pefabloc 0.5 mg/ml, lysozyme 1 mg/ml, DNase 10 μ g/ml, MgCl₂ 5mM and protease inhibitors with EDTA. The suspension was incubated for 30 min on ice and sonicated as described previously for GST-mSec22b(Δ TM). TritonX-100 was added to 1% (v/v) and the suspension incubated for 30 min on ice. The sample was spun at 40,000 x g_{av} for 45 min at 4°C. The pellet was resuspended in 15 ml PBS containing 8M urea, 0.1% Triton X-100 + 0.5 mg/ml Pefabloc and spun again at 40,000 x g_{av} for 45 min at 4°C. The supernatant was then added to PBS washed nickel beads and rotated for 30 min at 4°C. The sample was spun at 144 x g_{av} for 5 min at 4°C and then the resin was transferred to a column and washed until no more proteins appeared in the flow-through. The bound protein was eluted with elution buffer and 1 ml fractions were collected.

The eluates obtained for His-Syn18 were loaded onto an FPLC MonoQ 10/10HR column. MonoQ is a strong anion exchanger with trimethyl-aminomethyl (-CH₂N⁺(CH₃)₃) moieties as functional groups. The proteins were then eluted with a standard linear gradient with buffer 1 and 2. Protein peaks were identified by SDS-PAGE.

Elution Buffer: 50 mM Tris-HCl, pH 8,0; 8 M Urea

Buffer 1: 20 mM Tris, pH 7.4

Buffer 2: 20 mM Tris, pH 7.4; 1 M NaCl

4.3. Protein quantitation

The determination of the protein concentration was carried out according to Bradford (1976) [248] by measuring the extinction (E) of 1 μ l protein solution in 1 ml of staining solution at 595 nm in a spectrophotometer against a control containing 1 μ l of water in 1 ml

staining solution. Determination of the protein concentration was based on the concentration curve of bovine serum albumin (1 µg to 10 µg) from which the factor of the staining solution was derived. The factor is the ratio of the weight of bovine serum albumin and the extinction in the linear region of the standard curve.

Protein concentration (µg/µl) = ($\Delta E \times \text{Factor} \times \text{Dilution}$) / (Volume of protein solution)

The factor of the staining solution was in the range of 15 to 20 µg/unit of extinction.

Staining solution: 100 mg Coomassie brilliant blue G 250
50 ml 95% (v/v) ethanol, 100 ml 85% (v/v) phosphoric acid
ddH₂O to 1 liter, filter the solution

4.4. Denaturing polyacrylamide gel electrophoresis (SDS-PAGE)

The principle of polyacrylamide gel electrophoresis is separation of a large range of proteins of varying molecular weights under the influence of an electrical field by a continuous, cross-linked polymer matrix. Here, the polymer is polyacrylamide and the cross-linking agent bis-acrylamide. Cross-linking is effected through a radical-induced pathway [249] by the addition of ammonium peroxide sulfate (APS) and TEMED (1,2-Bis-(dimethylamino)-ethane).

Two gels are employed: a stacking gel with a low level of cross-linkage and low pH, allowing protein bands to enter the gel and collect without smearing, and a separating gel with a higher pH, in which the proteins are separated on the basis of size. The proteins migrate under the influence of an applied electrical field from the cathode to the anode.

The detergent sodium dodecyl sulphate (SDS) is known to bind to proteins at an average of one SDS molecule per two amino acid residues, or roughly 1.4g per g protein, when present at concentrations above 0.8mM. SDS is employed to effect denaturation of the proteins, to dissociate protein complexes and to impart upon the polypeptide chains net negative charge densities proportional to the length of the molecule. A reducing agent such as dithiothreitol (DTT) or 2-ME is used to reduce any existing cystines (disulphide bonds).

The electrophoretic mobility of such SDS-protein complexes is inversely proportional to the logarithm of the molecular mass of the protein [250]. For 8x6x0.1 cm gel, the following volumes were used:

Methods

	Stacking gel	Separating gel		
	5 %	10%	12.5%	15%
Separating buffer	--	1.5 ml	1.5 ml	1.5ml
Stacking buffer	625 µl	--	--	--
Acrylamide	375 µl	2.0 ml	2.5 ml	3.0 ml
dH₂O	1.25 ml	2.5 ml	2.0 ml	1.5 ml
TEMED	3 µl	3 µl	3 µl	3 µl
APS	60 µl	60 µl	60 µl	60 µl
5 X sample buffer:	312.5 mM Tris/HCl, pH 6.8;10% (w/v) SDS; 50% (v/v) Glycerol; 1.25% (v/v) 2-Mercaptoethanol; 0.3% (w/v) Bromophenol blue			
Acrylamide/Bis:	29.2% (w/v) Acrylamide; 0.8% (w/v) Bis(N,N'-bis-methylene-acrylamide)			
Stacking buffer:	0.5 M Tris/HCl, pH 6.8			
Separating buffer:	0.5 M Tris/HCl, pH 8.9			
Running buffer:	25 mM Tris; 192 mM glycine; 0.1% (w/v) SDS			
SDS:	10% (w/v)			
APS:	10% (w/v)			

Protein separation was carried out by discontinuous gel electrophoresis according to Laemmli [251]. The gel solution was poured between two glass plates separated by a 0.1 cm spacer and overlaid with 200 µl isopropanol to straighten the surface of the gel. After polymerisation the alcohol was removed with water. When stacking gel was poured appropriate comb were introduced to form wells for sample loading. The samples were diluted with sample buffer and heated for 2 min at 95°C and loaded onto the gel. Molecular weight standards were used for size comparison. Separation was carried out at 20-25 mA constant current for 1 gel.

Staining of the gels was carried out for 2 hours at RT by immersing the gels into staining solution with mild shaking. Destaining was done by immersing the gel first into destaining solution I and then into destaining solution II until the background was completely removed. The gel was then soaked in water for at least three hours and sandwiched between polyester sheets and dried in a gel dryer for further documentation and autoradiography.

- Staining solution :** 0.2% (w/v) Coomassie brilliant blue R250;
50% (v/v) methanol; 10% (v/v) acetic acid;
40% (v/v) ddH₂O
- Destaining solution I :** 50% (v/v) methanol; 10% (v/v) acetic acid
40% (v/v) ddH₂O
- Destaining solution II :** 10% (v/v) methanol; 5% (v/v) acetic acid
85% (v/v) ddH₂O

4.5. Generation of antibodies

4.5.1. Production and purification

For the preparation of polyclonal antibodies against mSec22 and mUSE1, GST-mSec22b(Δ TM) and His₆-Use1(Δ TM) proteins (300 μ g) emulsified in complete Freund's adjuvant were injected subcutaneously into two rabbits each. The polyclonal antibodies against mSec20 were raised against a HPLC purified synthetic peptide corresponding to the N terminal part of mSec20 with an additional N-terminal cysteine (mouse, C-MAAP QDVHVRICNQE, generously synthesised by Kerstin Overkamp, Dept. of NMR II, Max-Planck Institute for Biophysical Chemistry, Göttingen). Booster injections were performed every 2 to 3 weeks for 3 to 4 months. Serum was extracted from ear veins 10 days after the second and subsequent booster injections.

Polyclonal antibodies directed against ERD2 were raised in rabbits using synthetic peptides as described previously[252].

Antibodies against the A-subunit of cholera toxin were raised in rabbits. Traces of antibodies against the B-subunit were removed by passing the antiserum over a column with immobilized cholera toxin B. These antibodies were then labelled with the monofunctional reactive fluorescent dye Cy5 (Amersham Pharmacia Biotech) according to the manufacturer's recommendations.

4.5.1.1. IgG purification using protein A Sepharose

IgG fractions from serum were purified over Protein A-Sepharose columns as follows: 1 ml of serum was spun for 30 min at 14 000 g in a tabletop centrifuge. The pH of the supernatant was set to 8.1 with 1 M Tris/HCl pH 9, and the sample was then applied to a column holding 1 ml of Protein A-Sepharose pre-washed with 10 ml Pi buffer. Binding of IgG proteins was allowed to proceed overnight by slowly (~0.25 ml/min) circulating the

serum repeatedly over the column with the aid of a peristaltic pump. The column was then washed with buffer Pi until all unbound proteins had been washed out (measured at A_{280}). Bound IgG was eluted in one step with Elution buffer. Eluted proteins were collected in 1.5 ml tubes already containing sufficient neutralisation buffer (~300 μ l) for immediate neutralisation.

Pi buffer: 0.1M sodium phosphate, pH 8.0; 0.01% NaN_3

Neutralisation buffer: 1M Tris/HCl, pH 9.0

Elution buffer: 0.2M glycine, pH 3.5

The fractions were further aliquoted and frozen or used for further purification as described below.

4.5.1.2. Purification of antibodies over antigen-bound Sepharose

CNBr-activated Sepharose is supplied freeze-dried (1g was suspended in 5ml of 1mM HCl) in the presence of additives. These additives were washed away at low pH with an excess of 1 mM HCl (pH 2-3) before coupling the desired ligand. The use of low pH preserves the activity of the reactive groups, which otherwise hydrolyze at high pH.

The solutions containing the proper antigen were dialyzed against coupling buffer and coupled to CNBr-activated Sepharose (2 to 3 mg of antigen were coupled per ml gel), rotating 1 hour at room temperature. The excess of ligand was washed away with at least 5 gel volumes of coupling buffer. Remaining binding sites were blocked and the resin was then washed with washing buffer 1 followed by a wash with buffer 2, this cycle was repeated 3 times. Antiserum (3 to 4 ml) was incubated overnight at 4°C rotating with the resin (1 ml). The mixture was transferred to a suitable column (5ml Mo Bi Tec column, Mo Bi Tec). This column was washed with PBS until the A_{280} dropped to zero. The specific antibodies were eluted with elution buffer and collected fractions (1 ml) were immediately neutralized with 50 μ l of neutralisation buffer. BSA (about 1mg/ml) was added for stabilization. The antibodies were aliquoted and stored at 4°C or at -80°C.

The antibodies raised against GST-mSec22b(Δ TM) were previously passed through a GST-column to remove the antibodies raised against the tag.

Coupling buffer:	0.1M NaHCO ₃ , pH 8.3; 0.5M NaCl
Blocking:	0.2M glycine, pH 8.0
Washing buffers:	1: 0.1M Na-acetate, pH 4.0; 0.5M NaCl 2: 0,1M Tris/HCl, pH 8.0; 0.5M NaCl
Elution buffer:	0.1M glycine, pH 3.0
Neutralisation buffer:	1M Tris/HCl, pH 9.0

4.6. Western blotting

4.6.1. Protein transfer onto nitrocellulose membranes

A semi-dry set-up (Millipore Milli-Blot SDE-System) was employed. One piece of pre-cut Whatman filter paper was equilibrated in blot buffer and placed on the cathodic plate. The electrophoresed separating gel and then, the nitrocellulose membrane were equilibrated in blot buffer and added on top. Two more pieces of blot buffer-wetted Whatman filter were layered on top of this sandwich. Finally, this sandwich was positioned between two closely spaced solid phase electrodes with were in direct contact with the buffer-wetted Whatman filter paper. For an 8x6x0.1 cm gel, transfer was carried out at 100 mA constant current for 1 hour. To test the quality of transfer, the proteins on the blot membrane were stained with Ponceau-S and destained with PBS.

Blot buffer : 25 mM Tris/HCl; pH 8.3
192 mM glycine
20% (v/v) methanol

Ponceau S solution : 0.1% (w/v) Ponceau S; 5% acetic acid

4.6.2. Immunoblot and detection

After transfer of proteins, the nitrocellulose membrane was incubated under mild shaking in PBS containing 0.5%(w/v) dry milk for 2 hours at RT or overnight at 4°C. The membrane was then incubated with the first antibody diluted in PBS containing 0.5%(w/v) dry milk. It was washed twice each for 5 min with PBS, followed by incubation with the secondary antibody (conjugated to horseradish peroxidase) diluted 1:10000 in PBS containing 0.5% (w/v) dry milk. It was then washed three times each for 10 min with PBS containing 0.05% (w/v) Tween20 and finally incubated with Chemiluminescence substrate for exactly 2 min. This substrate was prepared by mixing a peroxide solution as substrate for horseradish

peroxidase and a Luminol/enhancer solution for amplification of the signal according to the manufacturer's recommendation. The membrane was immediately wrapped with plastic sheet and the signal recorded on a Fujifilm LAS-100 cooled CCD instrument using Image Reader and Raytest Aida image analysis software (Fuji).

4.7. Mammalian cell culture techniques

4.7.2. Starting a culture from frozen cells

Frozen cells were thawed in a waterbath (37°C) and transferred rapidly to a 15 ml centrifuge tube. Ten ml of the appropriate, pre-warmed medium was added; the tube was mixed gently, and then centrifuged at 200 x g_{av} for 5 min. The supernatant was decanted, the cells resuspended in fresh medium and the tube centrifuged again as previously. The cell pellet was resuspended in a defined volume of medium including the recommended additives and then transferred to the appropriate culture vessel

4.7.2. Cell culture

VERO cells were cultured in Dulbecco's MEM, with 10% (v/v) heat inactivated FCS, with 2 mM glutamine, 100 U/ml penicillin, 0.1 mg/ml streptomycin and Na pyruvate, in humidified incubators with 10% CO₂ at 37°C. For splitting, cells were washed twice in PBS, and then treated with trypsin/EDTA until they no longer adhered to the plate. They were split 1:5 every 2 days or upon reaching confluency unless otherwise stated.

4.7.3. Transfection of cultured VERO cells

4.7.3.1. cDNA

For DNA transfection, Vero cells were split 2 days before transfection, so that they reached 90% confluency on the day of transfection. Cells were then trypsinized, washed with PBS, and the pellet was resuspended in the DNA solution containing 1 to 3 different cDNAs of interest in 300µl transfection buffer. The suspensions were transferred to an electroporation cuvette and cells were immediately electroporated with a Gene Pulser II device (Bio-Rad, pulse 0.7 kV, 200 ohms, 50 µF, 1–2 ms). The cells were thereafter transferred to 6-well plates or culture dishes depending on the experiments to be performed and grown until the experiment.

For transfection of Vero cells, endotoxin-free plasmid DNA was prepared from *E. coli* strain XL1-Blue using the Endotoxin-free Plasmid Kit (Qiagen).

Transfection buffer : KCl 120mM, KH₂PO₄ 10 mM, K₂HPO₄ 10 mM, EGTA 2 mM,
MgCl₂ 5 mM, HEPES 25 mM, CaCl₂ 0,15 mM,
pH adjusted to 7,7 with KOH

For complete cytomix, GSH 5 mM and ATP 2 mM (pH 7) were freshly added.

4.7.3.2. si RNA

For transfection, siRNA duplexes for lamin and GL2 were prepared as follows: sense and antisense oligonucleotides (20µM final concentration) were mixed with 2x annealing buffer, incubated for 1 min at 90°C, followed by incubation for 1h at 37°C. Solutions could be stored at -20°C. SiRNA lamin and siRNA GL2 were used as positive and negative controls respectively. SiRNA for Sec22b, Use1 and Sec20 were received as duplexes.

Vero cells were plated on polylysine-coated coverslips in 24-well plates and cultured in a 37°C incubator in DMEM supplemented with 10% FCS, L-glutamine and sodium pyruvate, but without antibiotics. After 12 hours, cells were transfected with siRNA duplexes according to Elbashir et al. [253]. For each coverslip, 3µl of Oligofectamine reagent were mixed with 12µl of Opti-MEM and incubated for 7-10 min at RT. This solution was then gently mixed with 20 µM of siRNA duplex in 50µl of Opti-MEM 1 and incubated for another 20-25 min at RT. During this incubation, the cells on the coverslips were washed twice using DMEM containing only L-Glutamine and sodium pyruvate and left with 500µl of this medium. 32µl of fresh Opti-MEM were then added to the siRNA reagent tubes and 100µl of this final solution was added per well on the 24 well-plate. After 4 hours at 37°C, 500µl of DMEM containing 20% FCS, L-glutamine and sodium pyruvate were added to the cells. After 72 hours, cells were either fixed for immunostaining or harvested for western-blotting.

For final cell harvest, cells were washed twice with PBS, then trypsinised, spun and resuspended in 100µl homogenization buffer. Cells were then homogenized with syringes (passed through 20-, 23- and 27-gauge needles, 10 times each). Samples were spun 10 min at 4°C at 100 x g_{max} and supernatant were loaded with SDS-sample buffer on SDS-gel.

Homogenization buffer: HEPES 25mM, sucrose 0,25M, protease inhibitors.

4.8. Application of cholera toxin on cells

The cells were washed with PBS to remove the serum. The plates or the culture dish were placed on a thick metal plate that had been cooled to 0°C. The cells were then incubated for 20 min at 0°C with FCS-free DMEM containing 0.5 µg/ml of CTX to allow for binding of the toxin to the plasma membrane. Subsequently, the sample was warmed for 5 min to 37°C to start internalization of CTX. To remove as much free CTX as possible, the cells were rapidly washed three times with PBS. After the addition of DMEM with 10% FCS, the incubation was continued in an incubator (10% CO₂) at 37°C. At the time points indicated, cells were fixed for immunostaining (as described chapter 4.9.) or used for FRET-measurement (as described chapter 4.10.2).

4.9. Immunostaining

To study the cellular distribution of endogenous proteins, Vero cells grown on cover slips in 12- or 24-well plates to about 60% confluency, were washed twice with PBS and fixed with 4% paraformaldehyde for 12 min at 37°C. The fixed cells were then treated for 10 min at 37°C with 50 mM NH₄Cl to block free aldehyde groups from the fixative, and then washed twice in PBS. Permeabilization was done with 0.1% saponin/PBS. Primary and secondary antibody incubations were performed for 1 h at 37°C in 0.1% saponin/PBS/3% BSA. For each SNARE-protein, rabbit antibodies were used at 1:10 dilution and detected with Cy3- or Cy5-labeled goat anti-rabbit secondary antibodies (1:1000). When co-staining was performed Cy3-labeled goat anti-rabbit and Cy5-labeled goat anti-mouse antibodies were used, recognizing rabbit anti-SNARE and mouse anti-specific markers respectively. After washing four times with PBS, the cover slips were mounted in DAKO Fluorescent Mounting Medium and viewed using the Axiovert 200 inverted microscope described in Materials. Cy3 fluorescence was visualized using the following filter set: a 565/30 nm excitation filter, a 595 nm dichroic filter and a 645/75 nm emission filter. For Cy5, the filter set was composed of an excitation filter 620/60 nm, a dichroic filter 650 nm and an emission filter 700/75 nm. When no mouse antibody against the specific marker was available, this marker was expressed as GFP-fusion protein and anti-SNARE antibodies recognised with Cy5-labeled goat anti-rabbit antibodies. Colocalisation of 2 different labels was analysed using the program Inspector.

When cells had been previously treated with CTX, the coverslips were removed and the cells fixed in 4% paraformaldehyde for 10 min on ice and for 20 min at room temperature to prevent toxin translocation during fixation. When first rabbit anti-SNARE and then Cy5-

labeled rabbit anti-CTX were used for co-staining, one incubation step with normal rabbit serum was needed to block the free sites of the secondary anti-rabbit antibody used to recognize the anti-SNARE antibodies, before the anti-CTX antibody was applied.

4.10. Protein-protein interaction assays

4.10.1 Immunoprecipitation

A crude membrane fraction was prepared from rat liver as follows: 5 livers of about 15g each were cut into small pieces with a scapel, washed with ice-cold PBS and homogenized at 4°C in a kitchen blender for 3 periods of 30 seconds each at maximum speed in 2 volumes homogenization buffer. Cell debris was removed by centrifugation at 3,000 x g_{av} for 20 min at 4°C, the pellet was discarded and the supernatant centrifuged again at 10,000 x g_{av} for 20 min. Larger debris and floating fat were removed by filtering the supernatant, and the solvent was finally removed by centrifugation at 100,000 x g_{av} for 90 min at 4°C. The pellet was resuspended in 50 ml Microsome buffer and homogenized with a glass-Teflon Potter, centrifuged again at 100,000 x g_{av} for 1 h. The resulting pellet was resuspended in about 20 ml Microsome buffer and homogenized, the protein concentration was brought to 10mg/ml and the sample were stored in 1ml aliquots at -80°C.

Homogenization buffer : 280 mM sucrose; 50 mM Tris-HCl, pH 7.4; 1 mM EDTA;

Complete protease inhibitors (1 tablet/100ml of buffer)

Microsome buffer : 50 mM Tris-HCl, pH 7.4; 150 mM NaCl; 1 mM EDTA;

Complete protease inhibitors (1 tablet/100ml of buffer)

For immunoprecipitation, the sample was solubilized in extraction buffer at a final protein concentration of 0.3 mg/ml, while rotating for 30 min at 4°C. Insoluble material was removed by centrifugation at 200,000 x g_{av} for 60 min. Excess amounts of antibodies with the following specificities were then added to separate aliquots: mSec22b, mUse1, mSec20, rBet1 and syntaxin 18. After incubation overnight at 4°C, protein A-Sepharose was added in amounts sufficient to bind all IgG quantitatively, followed by incubation for 1 h at 4°C. Protein in the unbound material was precipitated according to Wessel and Flügge [254]. Bound material underwent six wash cycles of the protein A-Sepharose with extraction buffer followed by addition of SDS-sample buffer. Both bound and unbound proteins were analyzed by SDS-PAGE and immunoblotting with the indicated antibodies.

Extraction buffer : 50 mM Tris–HCl, pH 7.4; 150mM NaCl; 1 mM EDTA;
0.1mM PMSF; 1% Triton X-100

4.10.1.1. Using in vitro synthesized [³⁵S] methionine-labeled mSec20

Cell-free systems for in vitro gene expression and protein synthesis have been described for many different eukaryotic systems [255, 256]. The standard reaction conditions for in vitro transcription/translation using the kit from Promega are as follows: 40 μ l of TNT Quick Master Mix, 2 μ l of [³⁵S]methionine (1,000 Ci/mmol at 10mCi/ml), 1 μ g of plasmid DNA template, and nuclease-free water to a final volume of 50 μ l. The immunoprecipitation experiments were performed as described above with the exception that radioactively labeled Sec20 was added to the extraction buffer.

4.10.1.2. Disassembly experiments

For SNARE-complex disassembly, the solubilized samples were treated or not with 50 nM NSF and 2 μ M α -SNAP in presence or absence of other components (ATP 5mM, EDTA 2mM, MgCl₂ 8mM) for 1 h at 16°C. In parallel, excess amounts of antibodies against mUse1 were incubated for 1 h at 4°C with sufficient quantities of protein A–Sepharose previously washed with extraction buffer. The mUse1 antibodies bound to protein A–Sepharose were then added to the different samples and incubated for 90 min at 4°C to allow the binding of antigen to the antibodies. The immunoprecipitation was then continued as described above.

4.10.2. Live cell FRET experiment

4.10.2.1. Principle of FRET

FRET is a process in which energy is transferred nonradiatively (that is via long-range dipole-dipole coupling) from a fluorophore in an electronically excited state (donor), to another chromophore or acceptor. The latter may, but need not, be fluorescent.

Fluorescence Energy transfer (FRET) is a principle used for quantifying the distance between two molecules conjugated to different fluorophores, one is the Donor molecule (D) and the other is the Acceptor molecule (A). The quantitative treatment of FRET originated with Theodor Förster [257]. It is described by the following parameters: k_t which is the rate of radiationless energy transfer, the transfer quantum yield generally denoted as the energy transfer efficiency E and the Förster constant R_0 which is the distance between the donor and acceptor probes at which E is 50% (see annex I for details).

Conformational changes can also be monitored when both probes are present on the same molecule.

4.10.2.2. Live cell FRET measurements

Two ways are exploited in this work to register FRET in living cells.

- (1) measuring the increase of acceptor fluorescence upon excitation of the donor (sensitized emission)
- (2) measuring increased fluorescence of the donor (donor dequenching) after photobleaching of the acceptor.

These measurements were performed using both spectrofluorimetry and microscopy.

4.10.2.2.1. Spectrofluorimetry : GFP2 / venus YFP as FRET pair

For FRET measurement by spectrofluorimetry, GFP₂ was used as donor molecule and venusYFP as acceptor molecule. The FRET pair GFP₂ / YFP has been previously described by Zimmermann et al. [258]. It has an increased FRET efficiency compared to the most commonly used FRET pair consisting of CFP and YFP (Figure 6). Indeed, GFP₂ has a higher quantum efficiency ($Q= 0.55$) compared to CFP ($Q= 0.4$) and a larger overlap integral with the YFP acceptor (66% for CFP-YFP and 87% for GFP₂-YFP). Moreover, GFP₂ has its excitation maximum at 396 nm at which wavelength the excitation of YFP is negligible. The fluorescence yield of venusYFP is higher than that of YFP [259] which makes it a better acceptor for FRET experiments and also allows to decrease protein overexpression without decreasing the fluorescent signal when using venusYFP.

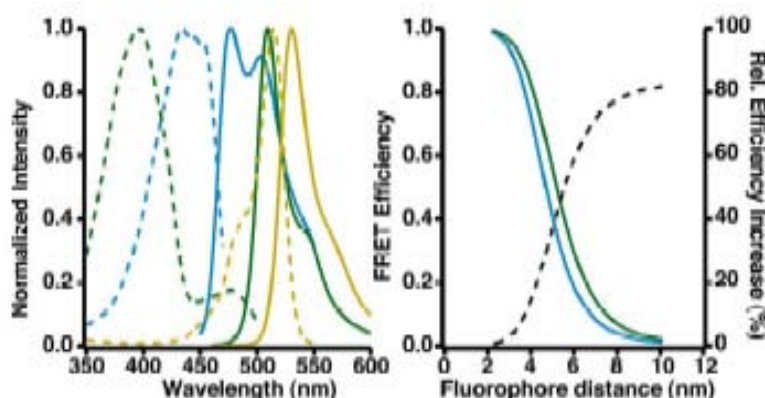


Figure 6: Left panel: **Normalized spectra** of the excitation (dashed lines) and the emission (solid lines) of GFP₂ (green), CFP (blue) and YFP (yellow), respectively. Right panel: **FRET efficiencies** of the GFP₂/YFP and CFP/YFP pairs derived from the spectral properties of the fluorescent proteins. FRET efficiencies for GFP₂/YFP (green) and CFP/YFP

(blue) are plotted as a function of the distance between the fluorescent proteins. Efficiencies at any distance are higher for GFP₂-YFP than for CFP-YFP. The dotted line shows the relative increase in FRET efficiency for GFP₂/YFP as compared to CFP/YFP [258].

Vero cells were expressing either the FRET control construct GFP₂-14AA-vYFP, considered as giving the maximum FRET value measurable in this assay, or co-expressing a GFP₂ fusion protein and a venus YFP fusion protein. Cells co-expressing GFP₂ and venusYFP were used as a negative control as well as cells co-expressing the medial-cis Golgi marker 3'-phosphoadenylyl-sulfate:uronyl-2-O-sulfotransferase (2-OST) coupled to GFP₂ and a lysosomal / endosomal transmembrane protein CD63 coupled to venusYFP. After transfection, Vero cells were grown in 10-cm dishes and on coverslips for expression level control. After 10 to 12 h for SNARE-proteins or 5 h when Erd2 was expressed, the protein expression was visualized with the Axiovert 200 microscope (described in Materials) using an excitation filter 405/20 nm, a dichroic beam splitter 440 nm and an emission filter 525/50 nm for GFP₂ fusion proteins, and an excitation filter 500/20 nm, a dichroic beam splitter 515 nm, and an emission filter 535/30 nm for venus YFP fusion proteins. The cells were then collected with a cell scraper from a 10 cm dish in 500 µl of PBS and transferred into a quartz cuvette for spectrofluorimetry. The emission fluorescence intensities were measured for the donor (GFP₂) after excitation of the sample at $\lambda = 390$ nm and for the acceptor (venusYFP) after excitation of the sample at $\lambda = 498$ nm with a Cary spectrofluorimeter using the program Eclipse (provided by Varian). The spectra were acquired before and after acceptor bleaching which was performed with an Argon laser (Innova 70 from Coherent) emitting at 530 nm while stirring the sample. The wavelength $\lambda = 530$ nm ensures that GFP₂ (maximum excitation 396 nm) is negligibly bleached (see annex II). The spectra obtained with the program Origin were corrected for cell autofluorescence and GFP₂ bleedthrough into the FRET channel. The effect of vYFP bleedthrough on the FRET signal is negligible as there is no direct excitation of vYFP at 390 nm. Normalized FRET values were calculated with Excel according to the equation given below in the analysis chapter (2.10.2.3). The results obtained were shown on a graph (designed with Sigma plot) representing the N_{FRET} values for various transfections.

4.10.2.2.2. Microscopy : CFP / YFP as FRET pair.

The high absorption and quantum yield of YFP [260] make it or its improved variants [259] an attractive FRET acceptor. However, it has limitations for FRET microscopy in its use in combination with optimal donors such as EGFP or GFP₂. Donor and YFP emission spectra show significant overlap, which makes it difficult to separate and quantify the emitted light of the donor and the acceptor. Therefore, the CFP-YFP FRET pair was used for this experiment.

Vero cells were plated in 10 cm dishes and cultured in complete DMEM. After 48 hours cells were co-transfected by electroporation with plasmids coding for the indicated

proteins fused either to CFP or to YFP and grown on coverslips in 6-well plates. Cells expressing CFP-15AA-YFP were considered as giving the maximum FRET values detectable in this type of experiment and cells co-expressing CFP and YFP were used as negative control. After expression for 5 to 8 hours for Erd2 or for 12 to 16 hours for other proteins, transfected cells were transferred to a chamber with 600 μ l of HAM's F-12 medium. FRET measurements were then performed using the inverted microscope described before and equipped with a 37°C thermostated incubator and a 5% CO₂-air mix system (figure 7).

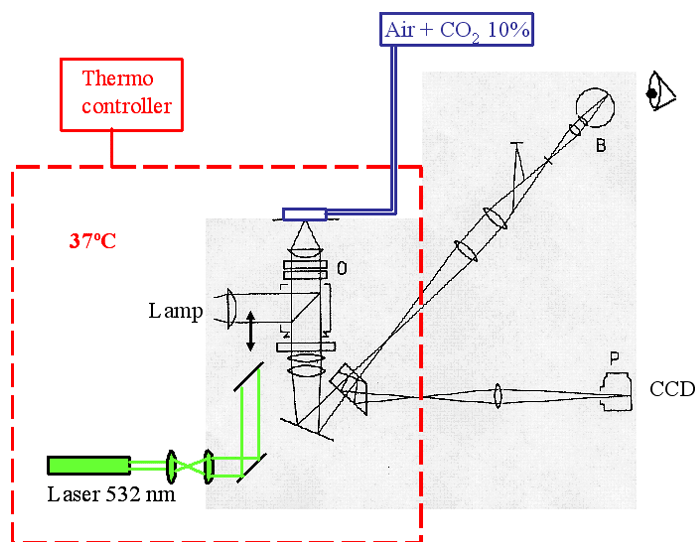


Figure 7: Optical scheme and experimental conditions for FRET measurement with an Axiovert 200 microscope. An incubator and a system with CO₂-air mix were installed on the microscope to maintain the cells viable during the experiment. A laser pointer was inserted into the optical path of the microscope to allow acceptor bleaching in a region of interest (ROI) in the cell.

CFP was detected using a filter set composed of an excitation filter 436/20 nm, a dichroic beam splitter 455 nm, and an emission filter 480/40 nm; for YFP an excitation filter 500/20 nm, a dichroic beam splitter 515 nm, and an emission filter 535/30 nm were used; the FRET filter set consisted of an excitation filter 436/20 nm, a dichroic beam splitter 455 nm and an emission filter 535/30 nm.

Images were acquired into the 3 channels before and after acceptor bleaching which was performed by applying for 1 min to the cell or a cell region of interest a 532 nm low-power laser inserted in the optical path of the microscope (figure 7). The wavelength $\lambda=532$ nm ensures that CFP is negligibly bleached. A filter set, composed of a dichroic beam splitter (595 nm) and a long pass emission filter (570 nm), was used to follow the YFP bleaching.

The results were analysed as described in the analysis chapter (2.10.2.3). The results obtained were shown on graphs (designed with Sigma plot) representing the normalized FRET values for various transfections.

4.10.2.3. Analysis

Steady-state FRET measurements can suffer from several sources of distortion, which need to be corrected for. A simple method, based on the modified Gordon method [261] [262], was used for analysis of FRET data, obtained as described above. This method corrects for cross-talk between donor fluorescence and acceptor fluorescence and between FRET fluorescence and non-FRET fluorescence emitted from donor and/or acceptor, and for the dependence of FRET on the concentrations of the donor and the acceptor.

In the Gordon method mentioned below, the FRET value $FRET_N$ is representative for FRET signals [261]. However, it is limited to samples with comparable donor and acceptor concentrations. Moreover, with this method the authors consider that all the donor- and acceptor-fusion proteins are involved in energy transfer in case of interaction. However, it is likely that free donor- and acceptor-fusion proteins are present in the cell which cannot contribute to the resulting FRET signal. In a recent study, Xia and Liu [262] attempted to provide a reliable FRET value called Normalised FRET value (N_{FRET}) that is also useful for comparison between different cells or samples by arbitrarily inserting a square root of the product ($I_A \bullet I_D$), with I_A and I_D corresponding to the fluorescence intensities in the acceptor (YFP or vYFP) and in the donor (CFP or GFP2) channels respectively. In this way, the dependency of the FRET signal on the donor and acceptor concentrations is reduced and closer to reality.

$$FRET_N = (I_{FRET} - I_A \bullet y - I_D \bullet z) / (I_A \bullet I_D) \quad (\text{Gordon G.W. et al., 1998})$$

$$N_{FRET} = (I_{FRET} - I_A \bullet y - I_D \bullet z) / \sqrt{(I_A \bullet I_D)} \quad (\text{Xia Z. And Liu Y., 2001})$$

where I_{FRET} is the fluorescence intensity in the FRET channel and y and z correspond to acceptor and donor bleed through emissions respectively, into the FRET channel.

To confirm that a FRET signal results from specific interaction between the proteins of interest, acceptor photobleaching can be performed as explained before. When two proteins interact leading to energy transfer, the donor fluorescence after acceptor photobleaching represents the total amount of donor-fusion proteins expressed in the cell. It is therefore more accurate to consider this value (I_{Dab}) to correct for the donor concentration. This led to the following equation used in this work:

$$N_{FRET} = (I_{FRET} - I_A \bullet y - I_D \bullet z) / \sqrt{(I_{Abb} \bullet I_{Dab})}$$

where I_{Abb} is the acceptor fluorescence intensity before bleach
and I_{Dab} is the donor fluorescence intensity after bleach

For the spectral data, the results were analysed with the programs Origin 7.0 and Excel. The values of interest (emission fluorescence intensity at 510 nm and 526 nm when the sample is excited at the donor excitation wavelength at 390 nm) were corrected for background. The bleed through of GFP₂ (called **z** in the formula) was estimated to be about 42% by acquiring spectra of cells expressing GFP₂ fusion protein alone. The bleed through of vYFP (called **y** in the formula) was negligible since it is not directly excited at 390 nm (see Annex II).

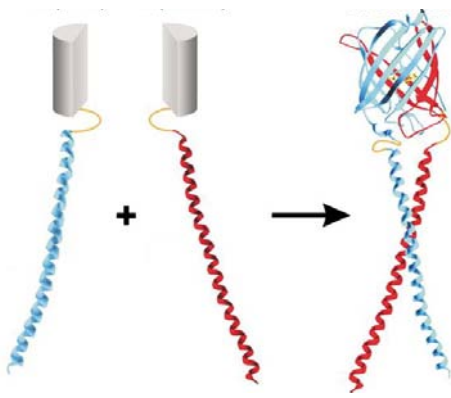
For fluorescence microscopy, the results were analysed according to this formula using the program Inspector provided by Dr. Andreas Schönle. The images were corrected for background, pixel-shift and cross-talks (also called bleedthroughs). The cross-talks between CFP and YFP channels were negligible. The bleed through of CFP (called **z** in the formula) and YFP (called **y** in the formula) into the FRET channel were about 56% and 4% respectively, under our conditions. This estimation was done by taking pictures, in each channel, of cells overexpressing CFP fusion protein and YFP fusion protein alone in the cells.

To define the perinuclear and the peripheral regions, the picture given for the YFP fluorescence was taken as reference. The signal intensity scale was set to saturation limit. The region where the fluorescent signal values exceeded 50 % of the maximal signal was defined as the perinuclear region and the values below were considered to represent the peripheral region.

The results obtained with both spectrofluorimetry and microscopy, were expressed using Sigma Plot on a graph showing the N_{FRET} values for the different samples.

4.10.3. BiFC experiments

The Bimolecular Fluorescence Complementation (BiFC) approach has been recently described by Hu and Kerppola [263]. It is based on the formation of a fluorescent complex by fragments of the enhanced yellow fluorescent protein. They identified nonfluorescent fragments of YFP that could reconstitute the fluorophore only when brought together by interactions between proteins covalently linked to each fragment.



One of the advantages is that BiFC analysis allows direct visualization of protein interactions in their normal cellular environment and the interpretation of the results does not require complex data processing. To construct mammalian expression vectors for bimolecular fluorescence complementation (BiFC) analyses, enhanced yellow fluorescent protein EYFP was dissected into an N-terminal fragment containing

amino acids 1–172 (YN) and a C-terminal fragment containing amino acids 173–238 (YC) as described by Hu et al. [263]. The fragments were amplified by PCR from pEYFP (Clontech) using the following primer pairs: for pC1-YN 5'-TATTATACCGGTCATGGTGAGCAAGG GCGAGGAGCTG-3' (forward) and 5'- TATTATAGATCTGATGTTGTGGCGGATCTTG AAGTT-3' (reverse) for pC1-YC 5'-TATTATACCGGTCATGGAGGACGGCAGCGTGCA GCTCGCG-3' (forward) and 5'-TATTATAGATCTCTTGTACAGCTCGTCCATGCCGAG-3' (reverse). The PCR introduced an Age I site at the 5' end and a BglIII site at the 3' end. This allows exchange of full-length GFP (amino acids 1–238) from pEGFP-vector against the YN and YC fragments.

Different SNARE mutants lacking most of their cytoplasmic parts (Sec20d194, Use1d234 and Sec22-d189), Use1 lacking only its SNARE motif and Sec22 containing point mutations, were constructed and used in the following approach.

Each of our proteins of interest was subcloned into the different vectors and transfected pairwise into Vero cells together with pC1-CFP which was taken as reference for expression level of the fluorescent proteins. Cells were grown on coverslips for 24 h and imaged in PBS at 37°C. CFP and the reconstituted YFP were detected using the same filter sets previously used for CFP and YFP for the FRET experiments. Images were acquired and analysed with MetaMorph 6.0.

The results were calculated using Excel according to the following equation:

$$\text{ratio } R_{\text{BiFC}} = (I_{\text{YFP}} - \alpha * I_{\text{CFP}}) / I_{\text{CFP}}$$

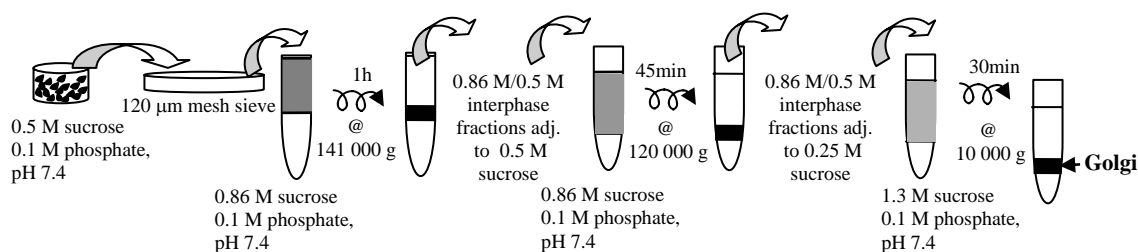
where R_{BiFC} represents the emission fluorescent signal of the reconstituted YFP,

and α corresponds to the CFP bleed through into the YFP channel (equal to 5%)

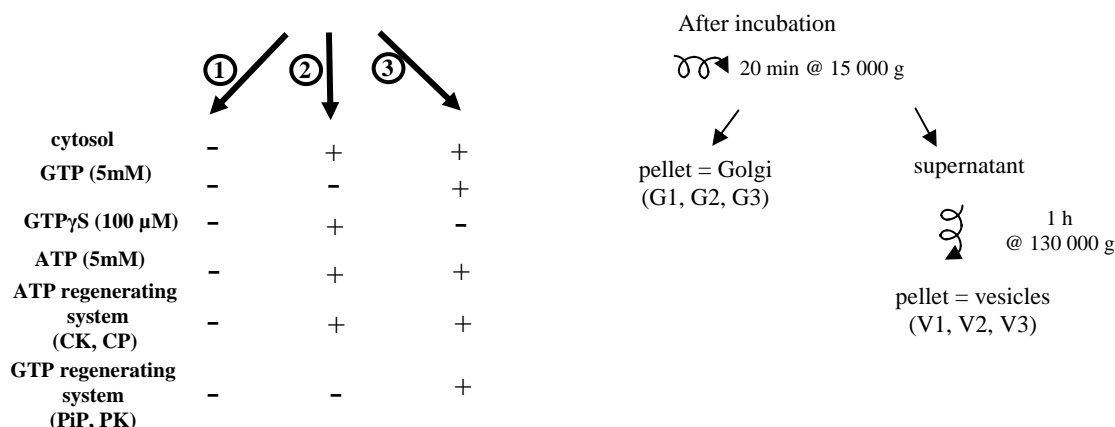
The results obtained are shown on a graph designed with Sigma Plot and were analysed for statistical relevance with the Mann and Whitney test (Matthias Wilmann).

4.11. In vitro vesicle release assay from isolated rat liver Golgi

Golgi stacks were prepared according to Hui et al. [264]. Briefly, rat livers were cut into small pieces in 0.5 M sucrose in 0.1 M phosphate, pH 7.4 and pressed through a 120 µm mesh



Golgi incubated at 37°C for 15 min



sieve. The homogenate was layered over 0.86 M sucrose, 0.1 M phosphate, pH 7.4 and spun at 141,000 x g_{av} for 1 h. The fractions at the 0.86 M/0.5 M interphase were collected, adjusted to 0.5 M sucrose and layered on top of 0.86 M sucrose in 0.1 M phosphate, pH 7.4, and spun at 120,000 x g_{av} (SW 41 rotor) for 45 min. Membranes from the 0.86M/0.5M sucrose interphase were collected, adjusted to 0.25 M sucrose, layered on top of 1.3 M sucrose/0.1 M phosphate, pH 7.4, and spun at 10,000 x g_{av} (SW 41 rotor) for 30 min. The Golgi membranes were finally collected from above the 1.3 M sucrose cushion.

Vesicles were released from Golgi under the conditions described in the scheme. For all the samples, Golgi membranes corresponding to 300 µg protein were incubated in phosphate buffered sucrose. All samples contained 5 mM Mg acetate and 100mM potassium glutamate. Samples were then centrifuged at 15,000 x g_{av} for 20 min to sediment the Golgi membranes. The supernatant was spun for 1 h at 130,000 x g_{av} to obtain the vesicles in the sediment.

Methods

The contents of the different fractions were analysed by western blot and immunoelectron microscopy (Dirk Wenzel, EM facility, Max-Planck Institut Biophysical Chemistry).

5. RESULTS

5.1. Mammalian Golgi-to-ER SNAREs homologs

A SNARE complex involved in the Golgi-to-ER retrograde transport has been recently described in yeast as composed of Sec22p, Ufe1p, Use1p and Sec20p [85]. Mammalian homologs of Sec22p and Ufe1p were already known as Sec22b [265] and Syntaxin18 [222] respectively. To know whether a similar complex exists in mammals, we searched the NCBI database to identify possible mammalian homologues for Use1p and Sec20p. We found one sequence for each protein that we named Use1 (from rat) and Sec20 (from mouse). While this work was in progress, Hirose et al. [227] and Nakajima et al. [226] reported the sequences of the respective human orthologs of Use1p and Sec20p that they called p31 and BNIP1 respectively. The sequence identity between yeast and the corresponding mammalian sequences is significant for all 4 SNARE proteins (fig.8), although it is very low for Sec20. The N-terminal extension of mSec20 is 67 amino acids shorter than that of Sec20p. Moreover, in comparison to mouse Sec20, Sec20p has an 84 amino acid C-terminal extension with a retrieval signal HDEL. The N-terminal domain of Syntaxin18 is involved in the interaction with SLY1 which can open the closed conformation of Syntaxin18 before and/or during the assembly of the t-SNARE complex [133, 266, 267]. mSec22b, as well as Ykt6, have a so called “longin” domain as N-terminal extension [268, 269]. Sec22b is likely to adopt an open conformation [270], while Ykt6p adopts a back folded (closed) conformation in which the N-terminal profilin-like domain binds to its C-terminal SNARE domain [229]. The N-terminal extensions of Sec20 and Slt1 remain to be characterized.

SNARE proteins have been structurally classified according to the central residue of the SNARE motif (0-layer). They can be designated as R-SNAREs and Q-SNAREs which can be sub-classified as Qa, Qb and Qc (see Introduction, chapter 1.3.2). Classically, a ternary SNARE complex as described for the synaptic vesicle [82] contains at its 0-layer one arginine and three glutamines. Among the four SNARE-proteins studied in this work, Sec22 is an R-SNARE, Syntaxin 18 is a Qa-SNARE and USE1 and Sec20 contain respectively an aspartate (D) and a serine (S) at their 0- layer. Based on the homology of SNARE motif sequence between these SNAREs and the mammalian Qb- and Qc-SNAREs which are known to be involved in the formation of a SNARE complex, (such as the synaptic complex, the endosomal complex and the ER to Golgi forward complex, figure 9A), we suggest that USE1 is the Qc-SNARE and Sec20 is the Qb-SNARE in the Golgi-to-ER retrograde transport

Results

SNARE complex (figure 9B). USE1 as a Qc-SNARE was also suggested by Hong W. [80] but in his classification Sec20 remained difficult to define.

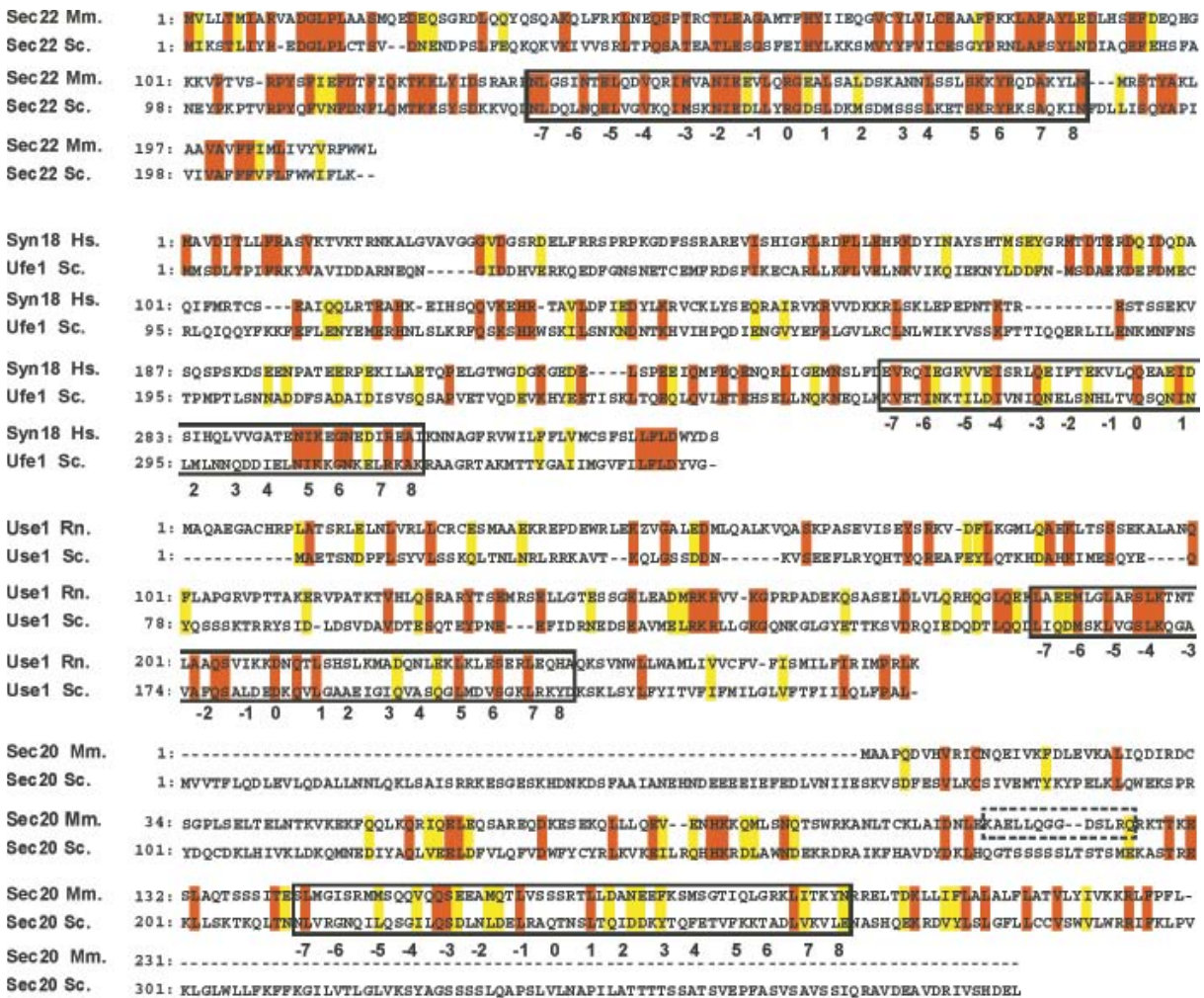


Figure 8: Amino acid sequence alignment of yeast SNAREs involved in Golgi-to-ER retrograde transport and their mammalian homologues identified and used in this study. Red and yellow squares represent identical and similar amino acids respectively, with the following groupings considered similar: R and K; Q and N; T and S; E and D; and V, I, L, F, and M. Pairwise comparisons of yeast and mammalian SNAREs yielded the following results: Sec22 Mm. (*Mus musculus*) shows 44 % homology (37 % identity) with Sec22 Sc. (*Saccharomyces cerevisiae*); Syntaxin 18 Hs. (*Homo sapiens*) versus Ufe1 Sc. and Use1 Rn. (*Rattus norvegicus*) versus Use1 Sc. show 26 % homology (17 % identity); and Sec20 Mm. shows 15 % homology (8% identity) with Sec20 Sc. Note that Syntaxin 18 Hs. and Syntaxin 18 Mm. are highly similar and that USE1 Rn. and USE1 Mm. are 100% identical. The black frames highlight the SNARE motifs. The numbers below the black frames represents the layers of contacting residues on the inner surface by homology with the synaptic complex.

Results

A

			-7	-6	-5	-4	-3	-2	-1	0	1	2	3	4	5	6	7	8																																								
Qa-SNARES	Sx1a	Rn	E	I	K	L	E	N	S	I	R	E	L	H	D	M	F	M	D	M	A	M	L	V	E	S	Q	G	E	M	I	D	R	I	E	Y	N	V	E	H	A	V	D	V	E	R	A	V	S	D	T	K	K	A	V	255		
	Sx7	Rn	S	I	R	Q	L	E	A	D	I	M	D	I	N	E	I	F	K	D	L	G	M	M	I	H	E	Q	G	D	V	I	D	S	I	E	A	N	V	E	S	A	E	V	H	V	Q	Q	A	N	Q	Q	L	S	R	A	A	228
	Sx5	Rn	T	M	Q	N	I	E	S	T	I	V	E	L	G	S	I	F	Q	Q	L	A	H	M	V	K	E	Q	E	E	T	I	Q	R	I	D	E	N	V	L	G	A	Q	L	D	V	E	A	A	H	S	E	I	L	K	Y	F	272
	Sx18	Hs	E	V	R	Q	I	E	G	R	V	V	E	I	S	R	L	Q	E	I	F	T	E	K	V	L	Q	Q	E	A	E	I	D	S	I	H	Q	L	V	V	G	A	T	E	N	I	K	E	G	N	E	D	I	R	E	A	I	306
Qb-SNARES	SNAP25 (N)	Rn	S	T	R	R	M	L	Q	L	V	E	E	S	K	D	A	G	I	R	T	L	V	M	L	D	E	Q	G	E	G	L	D	R	V	E	E	G	M	N	H	I	N	Q	D	M	K	E	A	E	K	N	L	K	D	L	G	82
	Vtilb	Rn	S	I	E	R	S	H	R	I	A	T	E	T	D	Q	I	G	T	E	I	I	E	E	L	G	E	Q	R	D	Q	L	E	R	T	K	S	R	L	V	N	T	N	E	N	L	S	K	S	R	K	I	L	R	S	M	199	
	Membrin	Rn	S	L	Q	N	I	H	H	G	M	D	D	L	I	G	G	H	D	I	L	E	G	L	R	A	Q	R	L	T	L	K	G	T	Q	K	I	L	D	I	A	N	M	L	G	S	N	T	V	M	R	L	I	E	183			
	mSec20	Mm	S	L	M	G	I	S	R	M	S	Q	V	Q	Q	S	E	E	A	M	Q	T	L	V	S	S	R	T	L	L	D	A	N	E	E	F	K	S	M	S	G	T	I	Q	L	G	R	K	L	I	T	K	Y	N	195			
Qc-SNARES	SNAP25 (C)	Rn	N	L	E	Q	V	S	G	I	I	G	N	L	R	H	M	A	L	D	M	G	N	E	I	D	T	Q	N	R	Q	I	D	R	I	M	E	K	A	D	S	N	K	T	R	I	D	E	A	N	Q	R	A	T	K	M	L	203
	Sx8	Rn	G	L	D	A	L	S	S	I	S	R	Q	K	M	G	Q	E	I	G	N	E	L	D	E	Q	N	E	I	D	D	L	A	N	L	V	E	T	N	D	E	K	L	R	T	E	A	R	R	V	T	L	V	D	203			
	mBet1	Mm	L	T	E	S	L	R	S	K	V	T	A	I	K	S	L	S	I	E	I	G	H	E	V	K	N	Q	N	K	L	A	E	M	D	S	Q	F	D	S	T	T	G	F	L	G	K	T	M	G	R	L	K	I	L	S	89	
	mUSE1	Rn	L	A	E	E	M	L	G	L	A	R	S	L	K	T	N	T	L	A	A	Q	S	V	I	K	K	D	N	Q	T	L	S	H	S	L	K	M	A	D	Q	N	L	E	K	L	K	L	E	S	E	R	L	E	E	Q	H	237
R-SNARES	Sb2	Rn	R	L	Q	Q	T	Q	A	Q	V	D	E	V	V	D	I	M	R	V	N	V	D	K	V	L	E	R	D	Q	K	L	S	E	L	D	D	R	A	D	A	L	Q	A	G	A	S	Q	F	E	T	S	A	A	K	L	K	85
	Eb	Rn	R	V	R	N	L	Q	S	E	V	E	G	V	K	N	I	M	T	Q	N	V	E	R	I	L	A	R	G	E	N	L	D	H	L	R	N	K	T	E	D	L	E	A	T	S	E	H	F	K	T	T	S	Q	K	V	A	65
	mSec22b	Mm	N	L	G	S	I	N	T	E	L	Q	D	V	Q	R	I	M	V	A	N	I	E	E	V	L	Q	R	G	E	A	L	S	A	L	D	S	K	A	N	N	L	S	S	L	S	K	K	Y	R	Q	D	A	K	Y	L	N	188

B

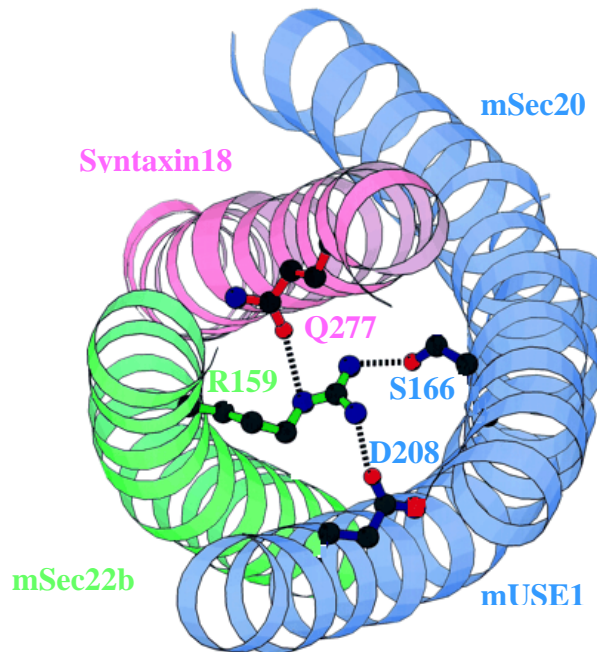


Figure 9: (A) Amino Acids sequence alignment of SNARE-motifs of mammalian SNARE-proteins. Syntaxin1a (Sx1a), SNAP25 (N), SNAP25 (C) and Synaptobrevin2 (Sb2) are involved in the synaptic complex. Syntaxin7 (Sx7), Vti1b, Syntaxin8 (Sx8) and Endobrevin (Eb) compose the early endosomal SNARE complex. Syntaxin5, membrin, mBet1 and mSec22b form a SNARE complex involved in ER-to-Golgi transport. Syntaxin18 (Sx18), mSec20, mUse1 and mSec22b are the candidates for forming a retrograde Golgi-to-ER SNARE complex. The numbers below and above the sequences represent the layers of contacting residues on the inner surface as in figure 8. The red and blue letters represent the amino acid of the zero layer and of the other layers

Results

respectively. The letters in green show the amino acids involved in salt-bridge formation. **(B)** This scheme represents a hypothetical structural view of the zero layer of the putative Golgi-to-ER complex by homology with the synaptic complex crystal structure [82].

5.2. Purity of the proteins and of the antibodies produced and used in this study

To produce antibodies, all proteins were expressed and purified as described in the methods part and samples run on SDS-gel (12%).

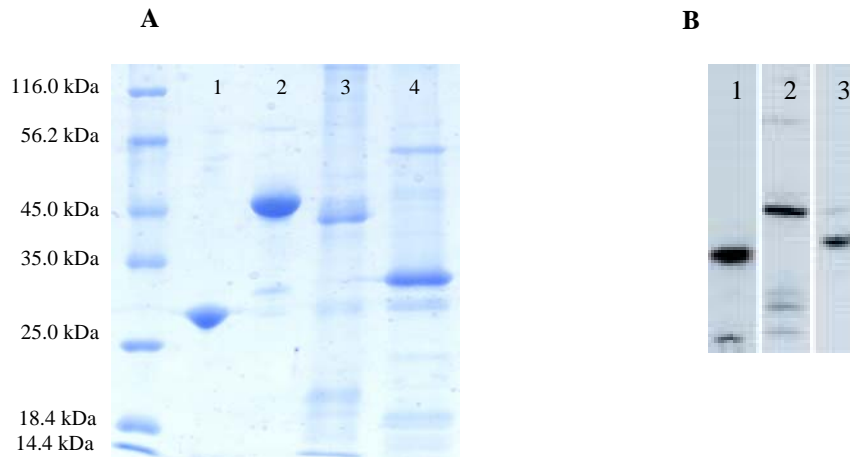


Figure 10: Coomassie stained SDS gel showing purified recombinant proteins **(A)**. Lane 1: GST, lane 2: GST-mSec22b(ΔTM), lane 3: His₆-Syntaxin18(ΔTM), lane 4: His₆-mUse1(ΔTM). Nitrocellulose membrane showing the specificity of affinity-purified antibodies **(B)** raised against mSec22b (lane 1), mUse1 (lane 2) and mSec20 (lane 3).

The GST tag, GST-mSec22b(ΔTM), His₆-Syntaxin18(ΔTM) and His₆-mUse1(ΔTM) run at approximately 27 kDa, 46 kDa (GST 27kDa + mSec22b 22kDa – TM 2.2kDa), 44 kDa (His₆ 1kDa + Syntaxin18 45kDa – TM 2kDa) and 30 kDa (His₆ 1kDa + mUse1 31kDa – TM 2.5kDa), respectively. GST-mSec22b(ΔTM) and His₆-mUse1(ΔTM) were used for rabbit immunisation. The rabbit polyclonal antibodies were produced and purified by affinity chromatography as described in the methods part and tested for their specificity on rat liver crude microsomal preparations (Fig.10b) by western-blotting. For all antibodies, one main band which was detected at around 22 kDa for mSec22b (lane 1), 31kDa for mUse1 (lane 2) and 25kDa for mSec20 (lane 3).

5.3. Expression level and localization of endogenous proteins and various overexpressed GFP-fusion proteins expressed in Vero cells.

To determine whether the GFP fusion retrograde Golgi-ER SNARE-proteins were properly localized, they were overexpressed in Vero cells and their localization as compared to that of the corresponding endogenous proteins. When Sec22, Sec20 and Use1 are N-terminally fused to a GFP variant they show the same steady-state distribution as the endogenous WT-proteins. Indeed, YFP-Use1 and YFP-mSec20 exhibit the same ER-localization as the endogenous WT-proteins and the majority of YFP-mSec22b is found in the Golgi as is the endogenous mSec22b (figure11). However, the distribution of YFP-syntaxin18 varied between different experiments and did not show the same reticular distribution as the endogenous syntaxin18, especially when co-expressed with other GFP variant fusion SNARE protein. Therefore, we omitted experiments with syntaxin18 GFP fusion protein in the following FRET studies.

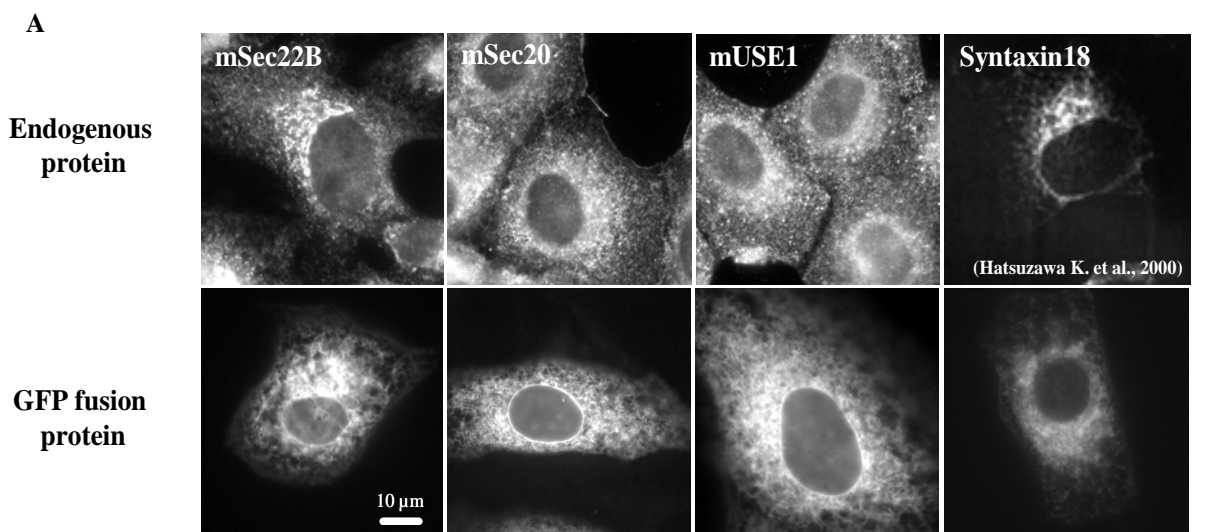
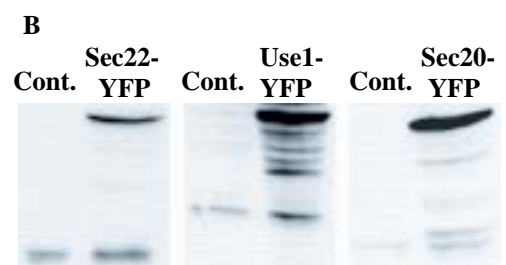


Figure 11. Endogenous and YFP fusion SNARE proteins expressed in Vero cells. Vero cells were transfected (lower panel) or not (upper panel) to express YFP fusion SNARE-proteins. Untransfected cells were immunostained for the indicated SNARE-proteins and transfected cells were observed

10 to 12 hours after transfection by microscopy (A). The localization of the fusion proteins is similar to that of the endogenous proteins. Untransfected (Cont.) and transfected (Sec22-YFP, Use1-YFP or Sec20-YFP) cell lysates were also analysed by western-blotting (B).



Results

The degree of overexpression was roughly estimated by western blotting comparing the amount of overexpressed and endogenous proteins in transfected Vero cells. The expression level of the endogenous proteins was corrected considering the transfection efficiency which was estimated to be 65%. mSec22b-YFP was about 2 times more abundant than the endogenously expressed mSec22b in Vero cells whereas the amount of mUse1-YFP and mSec20-YFP was about 14 times higher than that of their respective endogenous protein. For Use1-YFP, the bands observed below the highest band (representing Use1-YFP) on the membrane are most probably degradation products from the fusion protein meaning that the overexpression factor calculated above is in reality slightly higher than 14.

The localisation of the endogenous proteins was further studied using specific markers for ER (calnexin), ERGIC (ERGIC53) and Golgi (2-OST).

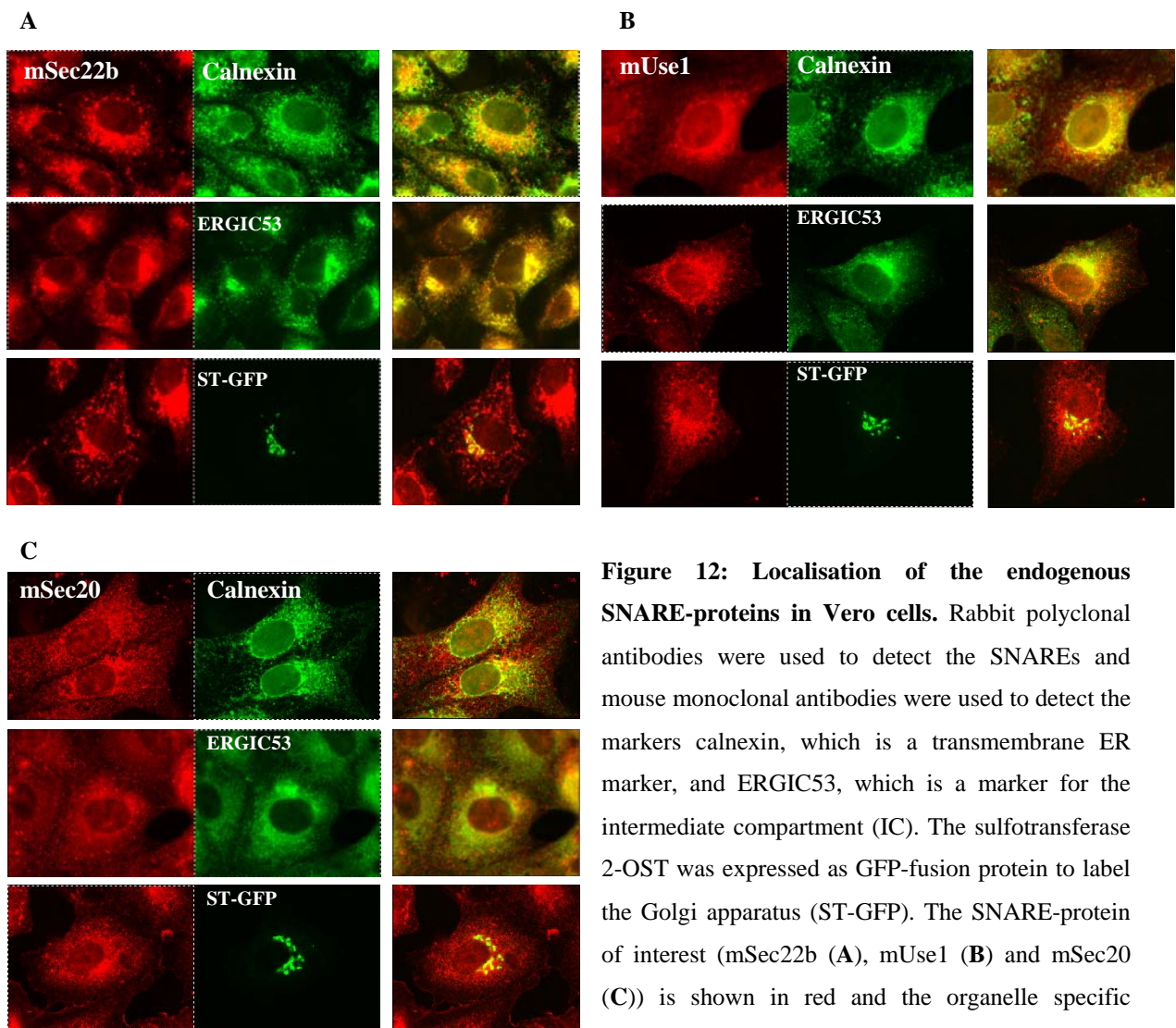


Figure 12: Localisation of the endogenous SNARE-proteins in Vero cells. Rabbit polyclonal antibodies were used to detect the SNAREs and mouse monoclonal antibodies were used to detect the markers calnexin, which is a transmembrane ER marker, and ERGIC53, which is a marker for the intermediate compartment (IC). The sulfotransferase 2-OST was expressed as GFP-fusion protein to label the Golgi apparatus (ST-GFP). The SNARE-protein of interest (mSec22b (A), mUse1 (B) and mSec20 (C)) is shown in red and the organelle specific marker in green. Both pictures were then overlaid

(right column). Co-localisation of both proteins resulted in yellow colour on the picture.

Interestingly, the distribution of mSec22b is very similar to that of ERGIC53, it shows significant overlap with the Golgi marker 2-OST but only very little with the ER marker calnexin. mUse1 co-localises only partially with ERGIC53 but significantly with calnexin. No or very little mUse1 protein was found in the Golgi. A low concentration of mSec20 seems to be evenly distributed between the ER and the Golgi, but does not appear to be present in the ERGIC eventhough it is difficult to estimate as when ERGIC53 antibodies were used with mSec20 antibodies the ERGIC staining was not typical. The staining for mSec20 shows punctuated structures which are dispersed throughout the cell and need to be further characterized.

5.4. Detection of interactions between Sec22, Sec20 and Use1 with live cell FRET spectroscopy.

The Golgi-to-ER yeast SNARE proteins Sec22p, Use1p, Ufe1p and Sec20p were shown to form a SNARE complex [91] by co-immunoprecipitation. In order to know whether interactions between the mammalian homologues of these SNARE proteins occur in living mammalian cells we performed live cell FRET experiments. FRET allows to measure short distances between two molecules. The distances must be comprised between 1 and 7 nm and indicate interaction (if stochastic FRET signals can be excluded). One advantage of GFP-based FRET is its ability to study protein-protein interactions in a physiological environment [271, 272]. It provides the potential to measure the interaction of molecular species in intact living cells where the donor and acceptor fluorophores are actually part of the molecules themselves.

Reliable positive and negative controls are essential for the accurate quantification of FRET. For negative controls, Vero cells were transfected to co-express either the donor GFP₂ together with the acceptor VenusYFP or two markers localised in two distinct organelles and fused one to GFP₂ and the other to venusYFP. As positive control, a protein composed of the two fluorescent protein moieties separated by a short spacer (14 amino acids) was expressed in Vero cells. After 10 to 12 hours, the measurements were performed and the results analysed as described in the methods.

In experiments involving GFP fusion proteins, overexpression of the recombinant proteins may result in nonspecific interaction between the donor and the acceptor. Purified GFP has been shown to dimerize at extremely high concentrations (> 4 μ M) in vitro [273]. In our current system, however, only negligible FRET signals were measured due to nonspecific

Results

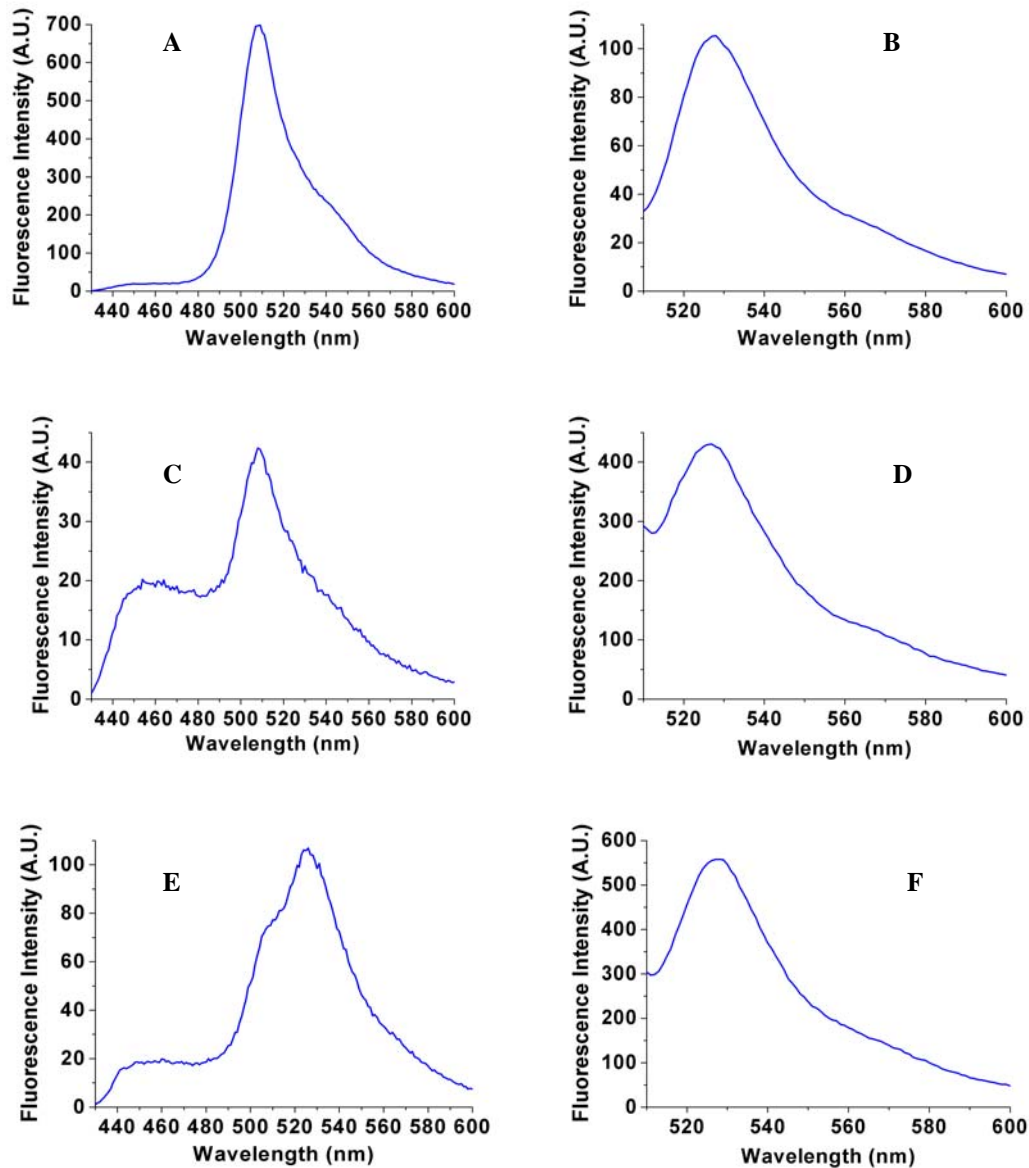


Figure 13a: Spectra obtained for the negative and positive FRET controls. Vero cells were co-expressing GFP₂ and venusYFP (upper panel: A and B, respectively) or ST-GFP₂ and CD63-VenusYFP (middle panel: C and D, respectively) and used as negative controls. ST is a medial-cis Golgi marker and CD63 is a lysosomal / endosomal membrane protein. Vero cells expressing the construct GFP₂-14AA-vYFP (lower panel: E and F) were used as positive control. Suspensions of transfected cells were excited (left column: A, C and E) at $\lambda_{ex}=390$ nm and subsequently (right column: B, D and F) at $\lambda_{ex}=498$ nm and emission spectra were acquired (blue line). The spectra obtained were analyzed according to the equation given in the Methods part.

interactions between GFP₂ and venusYFP (Fig.13a upper panel). The same holds for cells co-expressing the medial-cis Golgi marker [274] 2-OST fused to GFP₂ (ST-GFP₂) and the lysosomal / endosomal transmembrane protein CD63 fused to VenusYFP (CD63-vY) (Fig.13b middle panel). Indeed, in both cases, the spectrum did not show a FRET peak at 526 nm (Fig. 13a, A and C), and the normalized FRET values (N_{FRET} , see methods) obtained for the two samples were equal to 0.040 ± 0.002 and 0.02 ± 0.018 , respectively, corresponding to

Results

approximately 8 % of the mean value obtained for the cells expressing GFP₂-14AA-vYFP ($N_{\text{FRET}} = 0.36 \pm 0.02$) (Fig.13 C). The latter is taken as the maximum FRET value which can be obtained in our system as high intensity emission peak at $\lambda=526$ nm (Fig. 13a E).

Vero cells were then transfected to express GFP₂- and VenusYFP-SNARE proteins pairwise (Use1-GFP₂ and Sec22-vYFP, Use1-GFP₂ and Sec20-vYFP or Sec22-GFP₂ and Sec20-vYFP).

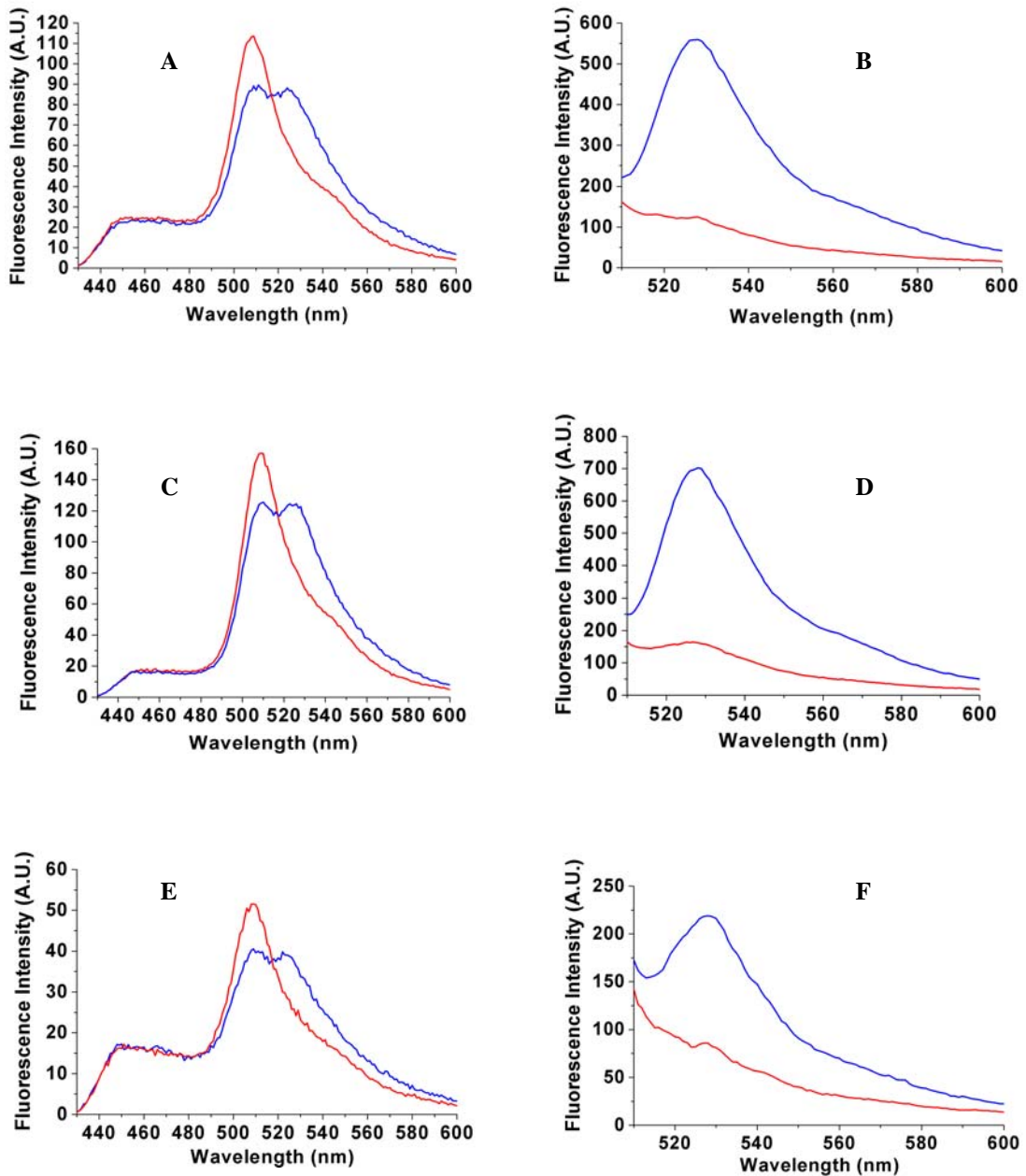


Figure 13b: Spectra obtained for different pairs of SNARE-fusion proteins. Suspensions of cells co-expressing Use1-GFP₂ and Sec22-vYFP (upper panel: A and B), Use1-GFP₂ and Sec20-vYFP (middle panel: C and D) or Sec22-GFP₂ and Sec20-vYFP (lower panel E and F) were excited at 390 nm (left panel: A, C and E) and subsequently at 498 nm (right panel: B, D and F), the excitation wavelengths for GFP₂ and venusYFP

Results

respectively. Emission spectra were acquired before (blue line) and after (red line) acceptor photobleaching. The spectra obtained were analyzed according to the equation given in the Methods part.

Under steady-state conditions, the spectra measured for the different SNARE-pairs using the excitation wavelength $\lambda=390$ nm showed a significantly elevated intensity peak at 526nm (Fig. 13b, A, C and E; blue line). After acceptor bleaching (shown in Figs. 13b, B, D and F), this peak disappeared, but donor fluorescence measured at $\lambda=510$ nm increased (Fig. 13b, A, C and E; red line). Thus, the peak observed at 526 nm before acceptor bleaching was the result of an energy transfer between the two fluorescent proteins due to the interaction or close proximity of the SNARE-proteins. The normalized FRET values calculated for the three SNARE-pairings (GFP₂-mUse1 and VenusYFP-mSec22b, GFP₂-mUse1 and VenusYFP-mSec20, and GFP₂-mSec22 and VenusYFP-mSec20) amounted to around 0.22. These values are significantly higher (~ 7 times) than the FRET values obtained for the negative controls and represent approximately 60% of the maximum FRET value obtained with the G2-14AA-vY control construct (Fig. 13c). The KDEL-receptors (Erd2) which are present in the Golgi-ER system are known to oligomerise depending on the degree of overexpression and occupancy by KDEL-proteins. As a second positive control, Vero cells were transfected to co-express Erd2-vYFP and Erd2-GFP₂ and the samples were used for FRET measurements (Fig. 13c).

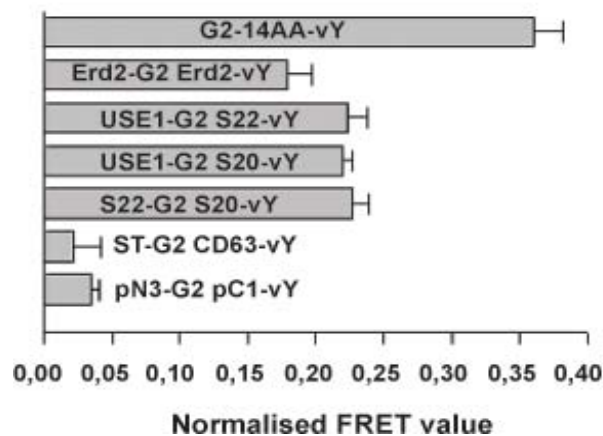


Figure 13c: Graph representing the normalized FRET values obtained by spectrofluorimetry for various partners. G2 and vY are the donor (GFP₂) and the acceptor (venusYFP), respectively. G2-14AA-vY is a control construct localized in the nucleus and the cytoplasm. Erd2 is the KDEL receptor; S22, S20 and Use1 are the SNARE candidates; ST stands for 2-O-sulfotransferase which is a medial-cis Golgi marker; CD63 is a lysosomal/ endosomal membrane protein. pN3G2 and pC1vY are the plasmids coding for each fluorophore. The normalized FRET values were obtained as described in the Methods part. The values given are mean values \pm standard deviation of at least 5 independent transfections.

5.5. Localization of the specific interactions between Sec22, Sec20 and using with live cell FRET and BiFC imaging.

5.5.1. Single live cell FRET microscopy.

To estimate the intracellular distribution of the FRET-signals, we performed FRET-measurements in single living cells. For this type of experiment, an inverted fluorescence microscope with three filter-sets was used: one to measure the donor fluorescence, one to measure the acceptor fluorescence and one to measure the FRET signal. Important cross-talks were observed when using the FRET pair GFP₂ / venusYFP. In this case, the most commonly used FRET pair CFP/YFP showed less cross-talk and thus was used for this system. As negative control, Vero cells were transfected to co-express the donor CFP together with the acceptor YFP and as positive control, Vero cells expressed the construct CFP-15AA-YFP in which the two fluorescent protein moieties are separated by 15 amino acids. Ten to twelve hours after transfection, the measurements were performed, and the results were analysed as described in the Methods part.

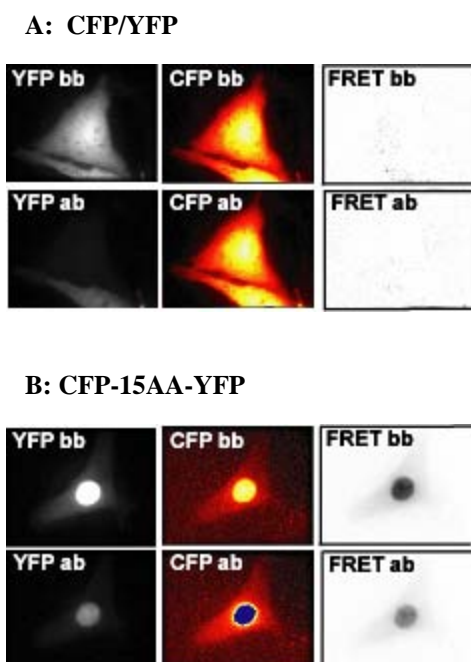


Figure 14a: Images obtained for the negative and positive FRET controls. Vero cells were co-expressing CFP and YFP (A) and used as negative controls. Vero cells expressing the construct CFP-15AA-YFP (B) were used as positive controls. Images were acquired in the YFP channel (left column), in the CFP channel (middle column) and in the FRET channel (right column), before (bb, upper panels) and after (ab, lower panels) acceptor photobleaching. The pictures obtained were analyzed as given in the Methods section and N_{FRET} was calculated using equation 1 (see Methods part). The intensity of the pictures taken in the CFP channel is represented by a false colour scale (red-orange-yellow). The blue colour indicates that fluorescence intensity at or above saturation.

In single cell experiments, very low FRET signals could be observed resulting from nonspecific interactions between CFP and YFP (Fig.14a, A). Indeed, the normalized FRET value (N_{FRET} , see Methods) calculated was 0.015 ± 0.018 , corresponding to approximately 3,5 % of the value obtained for the cells expressing the control construct CFP-15AA-YFP

Results

(Fig.14a, B; $N_{\text{FRET}} = 0.447 \pm 0.055$). As in the spectrofluorimetry experiments, this N_{FRET} value was taken as the maximum FRET value obtainable in our system (Fig. 14b D). The fact that the FRET signals obtained represent true sensitised emission is supported by the increase of donor (CFP) fluorescence intensity (picture CFPab, panel B) after acceptor (YFP) photobleaching (YFPab, panel B).

Vero cells co-expressing SNARE-pairs (mUse1-CFP/mSec22b-YFP (A), mUse1-CFP/mSec20-YFP (B) and mSec22b-CFP/mSec20-YFP (C)) were also analysed by single-cell FRET microscopy. In all cases, the overall FRET-values obtained were significantly higher than the one obtained for the negative control pair CFP/YFP. Moreover, in each sample, YFP photobleaching led to an increase of CFP intensity (picture CFPab, panels A, B and C) confirming that energy transfer had occurred between the two proteins. Interestingly, the N_{FRET} values measured in the periphery of the cells were always higher than in the perinuclear area (Fig.14b), which could indicate an increased interaction between the SNARE-proteins when they are close to, or in, the ER. Except for the pair mSec22b/mSec20, the N_{FRET} values in the perinuclear region were close to the negative control suggesting that Use1 interacts with mSec22b and mSec20 almost exclusively in the cell periphery. This would fit with the localisation of the endogenous SNARE-proteins reported above (see chapter 5.3., Fig. 12).

Results

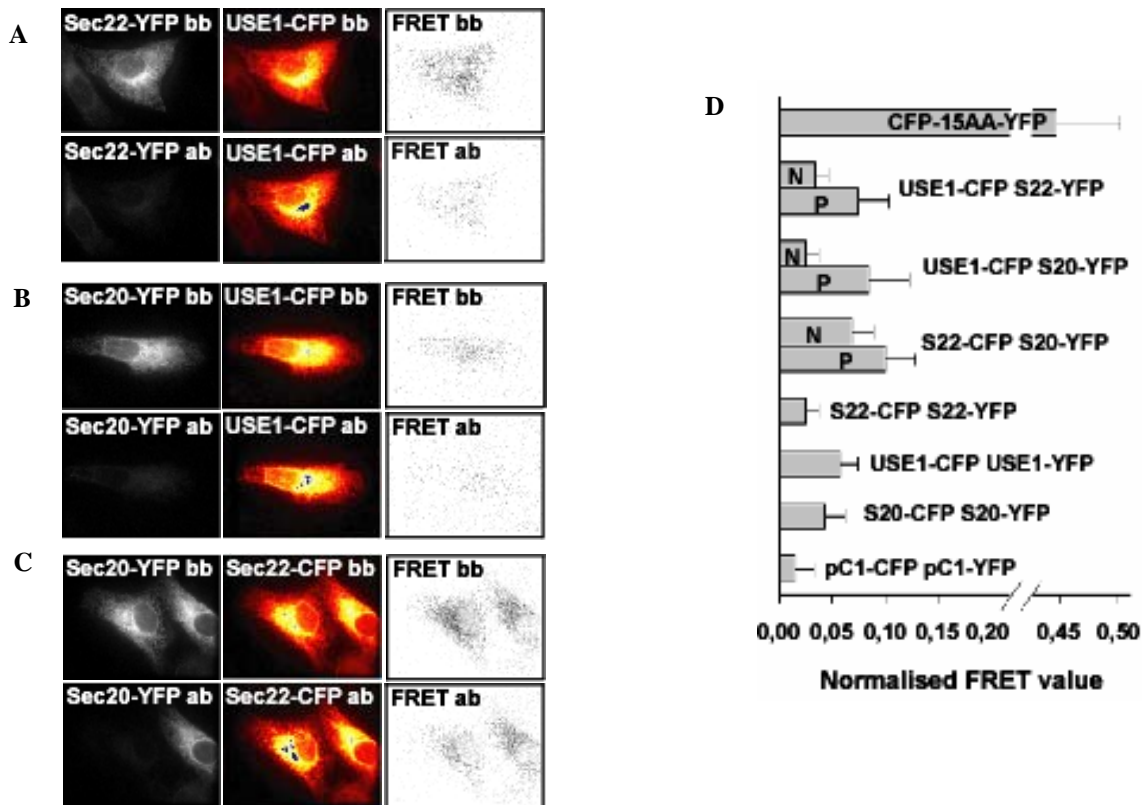


Figure 14b: Vero cells co-expressing USE1-CFP and Sec22-YFP (**A**), USE1-CFP and Sec20-YFP (**B**), or Sec22-CFP and Sec20-YFP (**C**) were grown on coverslips. Images were acquired in the YFP channel (left column), in the CFP channel (middle column) and in the FRET channel (right column), before (bb, upper row) and after (ab, lower row) acceptor photobleaching. The intensity of the pictures taken in the CFP channel is represented using an artificial colour scale (red-orange-yellow). The blue colour appears when the fluorescence intensity was at or above saturation. (**D**) Graph showing the normalized FRET values obtained (see Materials and Methods) for the hetero SNARE pairs and homo SNARE pairs (Sec22-CFP/Sec22-YFP, USE1-CFP/USE1-YFP and Sec20-CFP/Sec20-YFP), for the positive control (CFP-15AA-YFP) and for the negative control (pC1-CFP/ pC1-YFP). Note that for the hetero-SNARE pairs a perinuclear ER FRET signal (N) and a peripheral FRET signal (P) could be distinguished within each cell. The values given are mean values \pm standard deviation of three independent experiments, each analyzing at least 10 cells.

To ensure that the FRET signal observed is not due to ER membrane crowding resulting simply from overexpression, CFP- and YFP-fusions of the same SNARE-protein were co-expressed in Vero cells. Co-expression of mSec22b-CFP and mSec22b-YFP led to a weak FRET signal comparable to the one obtained from co-expressed soluble CFP and YFP indicating that there is little homotypic interaction between mSec22b proteins (Fig.14a). However, co-expression of mUse1-CFP and mUse1-YFP as well as co-expression of mSec20-CFP and mSec20-YFP resulted in a significant FRET signal (Fig.14b, 0.058 ± 0.016 and 0.043 ± 0.019 , respectively). This suggests that these Q-SNAREs partially homo-oligomerize. Interestingly, in those cases, the distribution of the FRET signal was homogenous throughout

the ER. Surprisingly, for the pair mSec20-CFP/mSec20-YFP 30% of the measured cells did not show any FRET signal. To further investigate the nature of the homo-oligomerisation, mUse1-CFP was co-expressed with mUse1 Δ (184-234)-YFP (deleted for the SNARE motif) in Vero cells. The N_{FRET} mean value ($0,054 \pm 0.029$) obtained in this case was almost equal to the one obtained for the wild-type pair indicating that mUse1 does not homo-oligomerise via the SNARE-motif. For mSec20, the co-transfection of plasmids coding for mSec20-CFP and mSec20 Δ (1-194)-YFP led to cells which expressed much more of mutant than of wild-type protein, making it difficult to properly perform FRET measurement.

5.5.2. Bimolecular Fluorescence Complementation (BiFC).

The most widely used approach for the visualization of protein interactions in living cells is FRET. As an alternative, Hu and Kerppola [263] recently developed an approach called Bimolecular Fluorescence Complementation (BiFC, described in the Methods section). In this method, a fluorescent signal is observed only when a complex between two proteins is formed (for illustration see the methods section). One of the advantages is that BiFC analysis allows direct visualization of protein interactions in their normal cellular environment without requiring complex data processing. To apply this method to this study, Vero cells were transfected to co-express CFP with either the pair Sec22-YN/Sec20-YC, USE1-YN/Sec20-YC or USE1-YN/Sec22-YC. These vectors encode for Sec22-, Sec20- and USE1-fusion proteins which carry either the N-terminal part of YFP (-YN) or the C-terminal part of YFP (-YC). When mSec22b linked to the N-terminal YFP fragment (Sec22-YN) was co-expressed together with mSec20 linked to the C-terminal YFP fragment (Sec20-YC), reconstituted YFP fluorescence was detected in the cells, most likely in the endoplasmic reticulum (Fig.15a, A). The same holds for the corresponding co-expression of mUse1-YN/mSec20-YC (Fig.15a, B) and mUse1-YN/mSec22b-YC (Fig.15a, C). Importantly, Vero cells expressing only one of these YFP-fragment fusion proteins did not show any YFP-fluorescence. Moreover, assembly of the YN- and YC-fragments alone resulted only in negligible YFP fluorescence. Thus, the occurrence of YFP fluorescence demonstrates a specific interaction between the SNAREs studied.

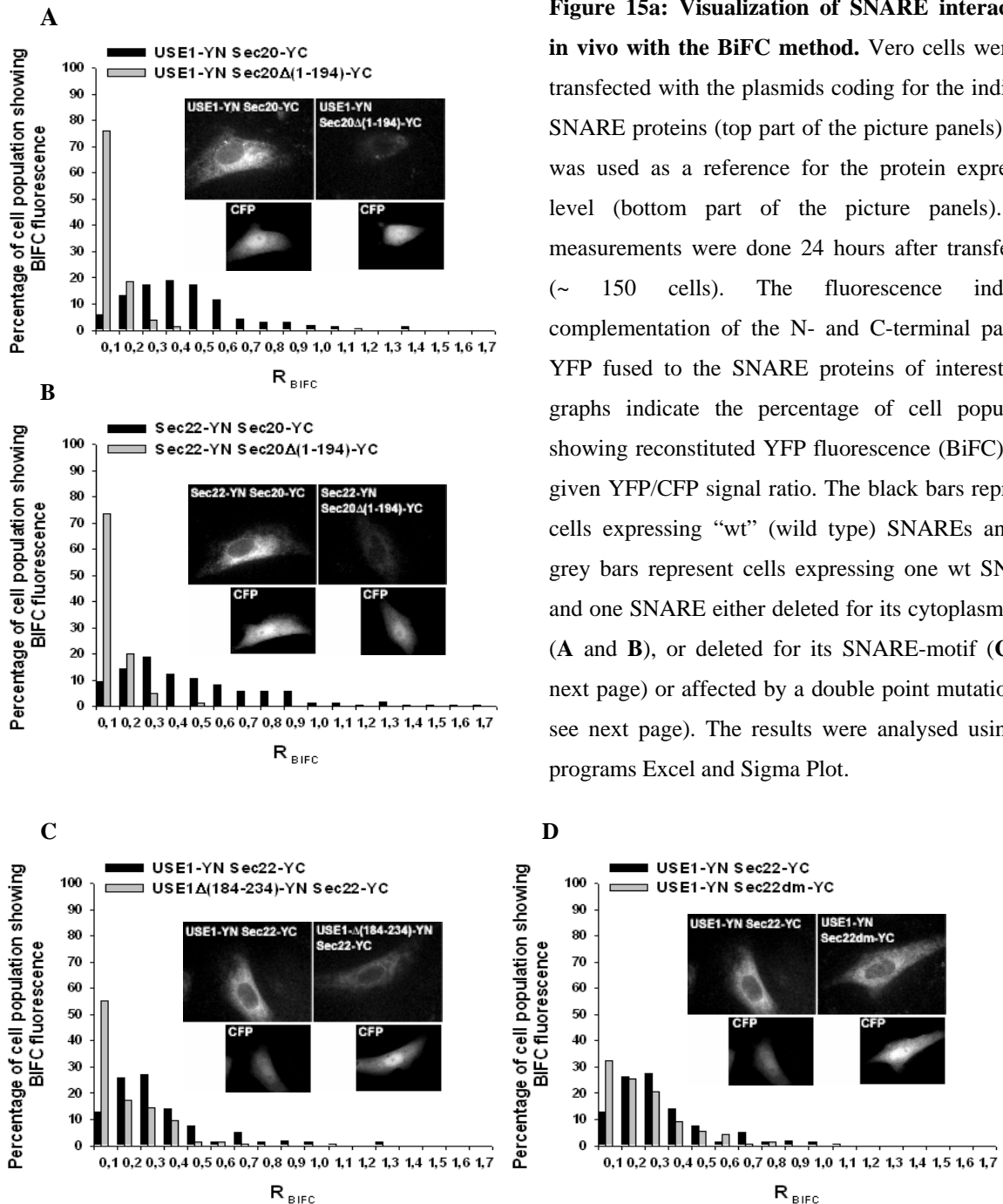


Figure 15a: Visualization of SNARE interactions in vivo with the BiFC method. Vero cells were co-transfected with the plasmids coding for the indicated SNARE proteins (top part of the picture panels). CFP was used as a reference for the protein expression level (bottom part of the picture panels). The measurements were done 24 hours after transfection (~ 150 cells). The fluorescence indicates complementation of the N- and C-terminal parts of YFP fused to the SNARE proteins of interest. The graphs indicate the percentage of cell population showing reconstituted YFP fluorescence (BiFC) for a given YFP/CFP signal ratio. The black bars represent cells expressing “wt” (wild type) SNAREs and the grey bars represent cells expressing one wt SNARE and one SNARE either deleted for its cytoplasmic tail (A and B), or deleted for its SNARE-motif (C, see next page) or affected by a double point mutation (D, see next page). The results were analysed using the programs Excel and Sigma Plot.

The specificity of these interactions was further emphasized by the results of mutation experiments. When mSec22b or mUse1 linked to the N-terminal fragment of YFP were co-expressed with the C-terminal YFP-fragment linked to the C-terminus (last 36 amino acids) of mSec20, the histograms of the fluorescence ratios showed a strong left shift, indicating an almost complete loss of interaction (figure 15a, A and B). Similarly, when the N-terminal YFP-fragment was expressed as a fusion protein with mUse1 lacking the SNARE motif (amino acids 184 – 234) together with the C-terminal YFP-fragment linked to mSec22b, fluorescence complementation was almost completely abolished (figure 15a, C).

Results

The formation of salt-bridges between the C terminal SNARE motif of SNAP25 and synaptobrevin (Sb2) has been shown to be essential for the synaptic SNARE complex formation implying the residues SNAP25-R₁₆₁/Sb2-E₄₁ and SNAP25-D₁₈₆ /Sb2-R₆₆ [82]. By homology, Joglekar et al. [107] reported that the interaction between the ER-Golgi anterograde SNAREs mBet1 and mSec22b might involve salt bridge formation between mBet1-K₄₇ and mSec22b-D₁₄₄, and mBet1-D₇₂ and mSec22b-K₁₆₉. According to the alignment of SNARE motif sequences, lysine₁₉₅ and aspartate₂₂₀ exist in the SNARE-motif of mUse1 in similar positions to the corresponding amino acids in the SNARE-motif of mBet1 (Fig. 9A). We, therefore, considered that a similar salt bridge formation might be involved in the interaction between mSec22b and mUse1. Therefore, we co-expressed the N-terminal fragment of YFP fused to a doubly mutated mSec22b (D169A, K144D) with WT-mUse1 fused to the C-terminal fragment of YFP. These mutations in mSec22b were sufficient to induce a clear left shift in the histogram (Fig.15a D) indicating a decreased interaction between the two SNARE proteins. The Mann and Whitney test (performed by Matthias Willmann) applied on these results gave a very high probability ($p < 0.0001$) for the results not to be accidental.

As the truncations and deletions applied here could have affected the intracellular localisation of the corresponding SNARE proteins, we have expressed these mutants as fusion proteins with full length YFP and analysed their localisation in comparison to the corresponding wt-SNARE. This was done 24 hours after transfection as for the BiFC experiments. Deletion of the N-terminal 194 amino acids (which includes the SNARE-motif) did not affect the ER-localisation of mSec20 (Fig.15b, A). In contrast, truncation of the N-terminal portion (including the SNARE-motif) of mUse1 abolished its retention in the ER. Instead the truncated protein appeared in the Golgi 8 hours after transfection and finally in the plasma membrane 24 hours after transfection (Fig.15b, B). This does not result from the loss of the SNARE motif as deletion of the SNARE motif alone did not change the steady-state distribution of mUse1 in comparison to that of WT-mUse1 (Fig.15b, B right picture). Thus, retention of mSec20 in the ER requires mainly, if not exclusively its transmembrane domain, whereas in case of mUse1 the N-terminal portion upstream of the SNARE-motif is required for proper localisation.

Results

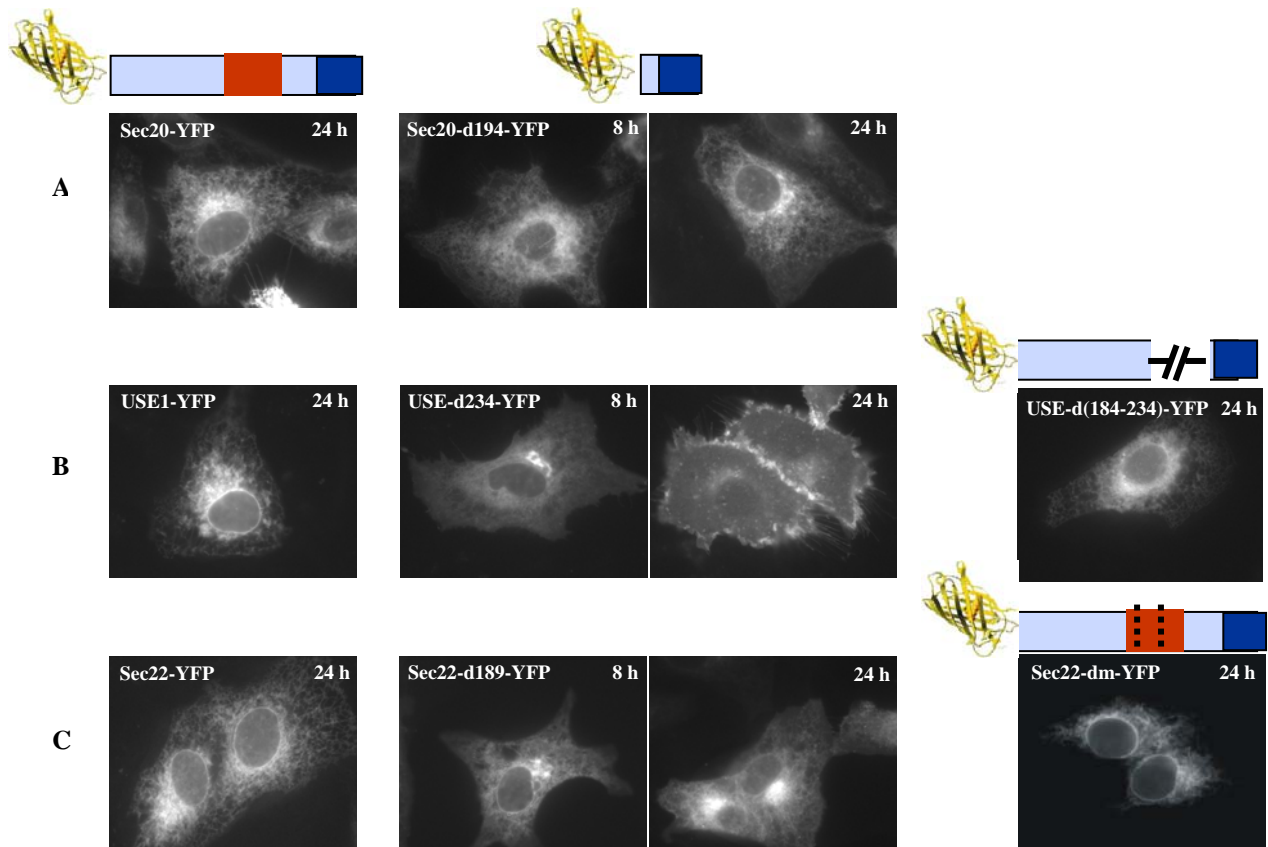


Figure 15b: Effect of various mutations on the intracellular localisation of SNARE-proteins. The drawings depict the different constructs expressed in Vero cells: the yellow part represents YFP, the light blue part the protein sequence, the red rectangle is the SNARE motif and the blue rectangle the transmembrane domain. The pictures show the expression pattern of the indicated proteins (wt and corresponding mutants) after expression for 8 or 24 hours (A: mSec20; B: mUse1 and C: mSec22b).

For mSec22b, truncation of its N-terminal 189 amino acids (including the SNARE-motif) changed the distribution of YFP-mSec22b in comparison to the wt-fusion protein (Fig.15b, C): 8 hours after transfection, an accumulation of the protein in the Golgi was observed and this effect was even stronger 16 hours later. In this case, the transmembrane domain seems to play a role in the retention of mSec22b in the Golgi-ER system. When the amino acids assumed to be involved in the salt-bridge formation were mutated in the SNARE-motif of mSec22b (D169A, K144D), its localisation was not affected (Fig.15b, C right picture).

In summary, when most of the cytoplasmic tail was deleted, the distribution of Sec20 remained unchanged, mSec22b accumulated in the Golgi, and finally Use1 reached the plasma membrane. This would be consistent with the finding that increasing the length of the transmembrane domain of several Golgi- and ER-proteins results in their movement to the

plasma membrane [193, 275-277]. Indeed, Use1 transmembrane domain (23AA) is longer than that of mSec22b (20AA) which is longer than the transmembrane domain of mSec20 (17AA).

5.6. Immunoprecipitation of the native retrograde SNARE complex.

To determine whether the four putative retrograde Golgi-ER SNAREs could form a complex, rat liver microsomal membranes were extracted with a Triton X-100 containing buffer, and appropriate aliquots were used for immunoprecipitation using affinity-purified antibodies directed against mUse1, mSec22b, or mSec20, or corresponding pre-immune sera.

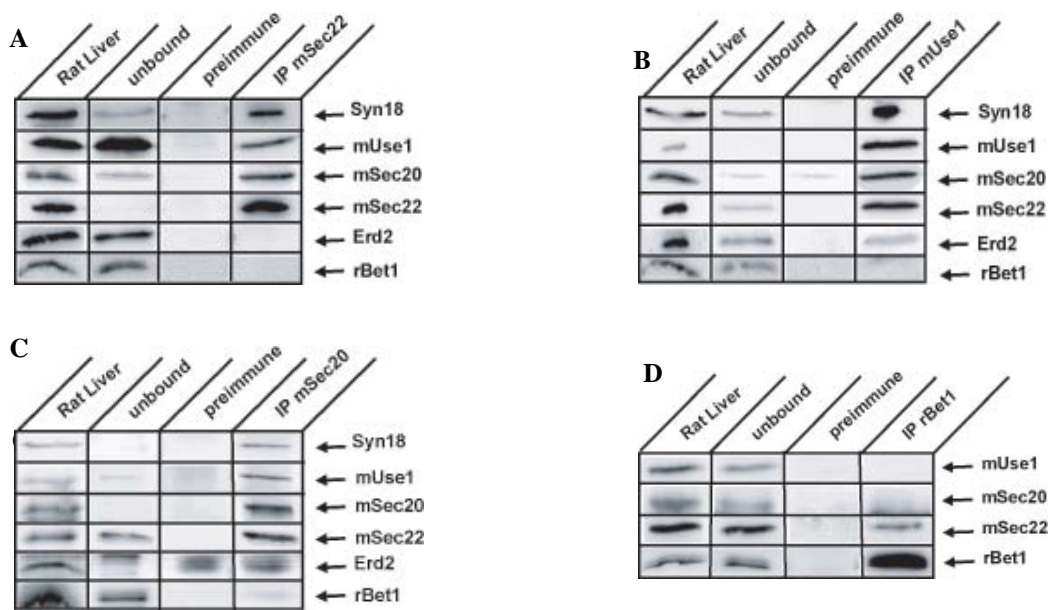


Figure 16: Syntaxin 18, mUse1, mSec20 and mSec22b form a specific SNARE complex. Affinity-purified antibodies directed against mSec22b (A), mUse1 (B), mSec20 (C) and rBet1 (D) were used for co-immunoprecipitations. Detergent extracts from rat liver microsomal membranes were incubated with antibodies against the indicated SNARE-protein or with preimmune serum and thereafter with protein A-Sepharose. Unbound fractions were separated from the immunoprecipitates (IP and preimmune). Fractions were separated by 12% SDS-PAGE and analyzed by immunoblotting using antibodies against Syntaxin18 (Syn 18), mUse1, mSec20, mSec22b, Erd2 and rBet1. Starting samples (Rat Liver) correspond to 5% of the precipitated material. The unbound loaded fraction corresponds to 4% of the total unbound proteins. No unspecific binding to pre-immune serum was observed. Note that the band obtained for Erd2 after immunoprecipitation with mSec20 antibodies is unspecific as it was also found in the preimmune serum precipitate.

All 3 antibodies precipitated not only the authentic antigen, but also the other 3 SNARE proteins of the postulated SNARE-complex (Fig.16a A, B and C), whereas the preimmune sera gave only negative results. In no case, the anterograde ER-Golgi SNARE rBet1 was co-precipitated although one might have expected rBet1 to become coprecipitated

Results

together with mSec22b as they both participate in the formation of the anterograde ER-Golgi SNARE-complex (Fig.16a A). The specificity of the formation of the retrograde SNARE-complex is further underlined by the observation, that immunoprecipitation with anti-rBet1 antibodies co-precipitated some mSec22b, but no mSec20, mUse1, or Syntaxin18 (Fig.16 D). Moreover only weak FRET signal ($N_{\text{FRET}} = 0,043 \pm 0,019$) was measured at the Golgi region between rBet1-CFP and mUse1-YFP. The observation that anti-rBet1 co-precipitates mSec22b although anti-mSec22b does not coprecipitate rBet1 was also reported by Hay et al. when studying the anterograde ER-Golgi SNARE-complex [278].

To exclude that the SNARE co-immunoprecipitations had arisen from complexes that only form after detergent solubilisation and to ensure that the majority of the retrograde complex exists in the intact membrane, [^{35}S]-methionine labelled mSec20 (synthesized in a cell-free system) was added to the membranes and the usual extraction and immunoprecipitation procedures were performed, using anti-mUse1 antibodies.

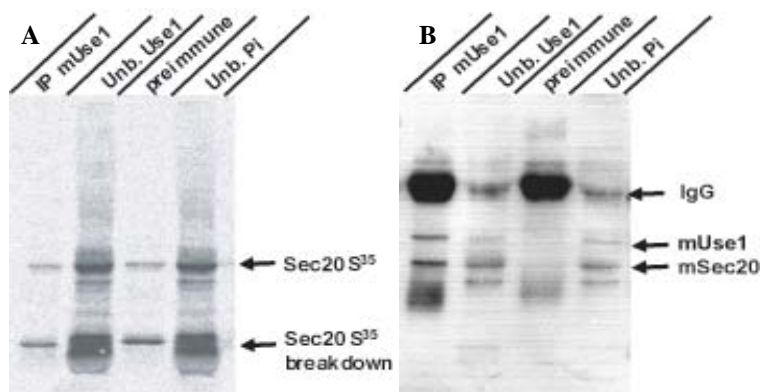


Fig. 17: The SNARE-complex formed by Syntaxin18, mUse1, mSec20 and mSec22b exists in intact membranes. Rat liver microsomal membranes were incubated with [^{35}S]-methionine labelled mSec20 and solubilised with Triton X, simultaneously. Affinity-purified antibodies against

mUse1 or preimmune serum were used for coimmunoprecipitation and the same procedure as described in Fig.16 was followed. The nitrocellulose membrane was analysed by autoradiography (A) and subsequently by immuno-blot (B).

Only traces of labelled mSec20 coprecipitated with the non-labeled SNAREs and this amount did not exceed the amount precipitated with the preimmune serum (Fig.17 A). In these experiments the portion of mSec20 precipitated amounted to 4 % of the total mSec20 in the membrane extract (Fig.17 B). These data show that the retrograde SNARE-complex demonstrated by co-immunoprecipitation exists before membrane extraction and does not form only after membrane solubilisation.

The role of NSF and α -SNAP is to disassemble some, if not all, SNARE-complexes in an ATP-dependent manner, leading to free-SNAREs release. To test their ability to disassemble the putational retrograde SNARE-complex, the membrane extracts were

Results

incubated with both proteins for 1 h under the conditions given in Fig.18. Immunoprecipitation was performed with anti-mUse1 antibodies.

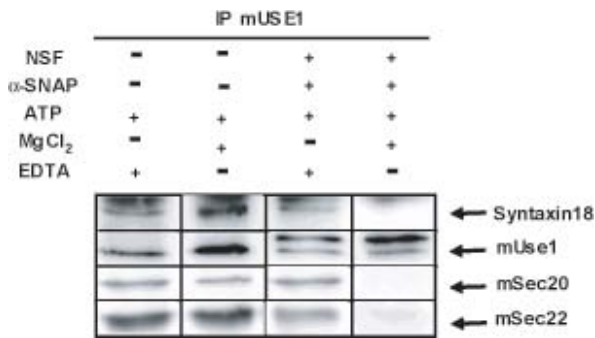


Figure 18: The SNARE-complex formed by Syntaxin18, mUse1, mSec20 and mSec22b is disassembled by NSF and α -SNAP. Antibodies directed against mUse1 were used for co-immunoprecipitation performed as described in Fig.16. The membrane extracts were incubated for 1 h at 16°C in the presence (+) or absence (-) of the indicated

components: NSF (50nM), α -SNAP (2 μ M), ATP (5mM), MgCl₂ (8mM) and EDTA (2mM). Note that the protein concentration given for NSF includes active and inactive NSF. The NSF activity was previously tested (by Ulrike Winter) with an in vitro assay following the kinetic of disassembly of the synaptic SNARE-complex and found to be active.

When both NSF and α -SNAP are absent from the incubation, Syntaxin18, mSec20 and mSec22 were co-immunoprecipitated with mUse1 as observed previously (Fig. 16a B). When NSF and α -SNAP are added in presence of EDTA without MgCl₂, the same result was obtained since EDTA inhibits NSF ATPase activity by chelating divalent cations. In contrast, in the presence of ATP and MgCl₂ (absence of EDTA), only mUse1 became precipitated indicating that the complex had been dissociated by NSF and α -SNAP (Fig. 18).

5.7. Interaction of the SNARE-proteins mUse1, mSec20 and mSec22b with the KDEL-receptor Erd2.

ERD2 binds in the Golgi ER-resident proteins which possess a C-terminal KDEL (-XXEL) motif when they have escaped from the ER, and allows for their back-transport to the ER. This required that the occupied KDEL-receptor is sorted into budding retrograde vesicles or tubules. Therefore, we have examined whether components of the retrograde SNARE complex might interact with Erd2 in single living cells. Vero cells co-expressing Erd2-YFP and one of the retrograde SNAREs fused to CFP (mSec22b-CFP (A), mUse1-CFP (B) and mSec20-CFP(C)) were analysed by single-cell FRET microscopy (Fig.19).

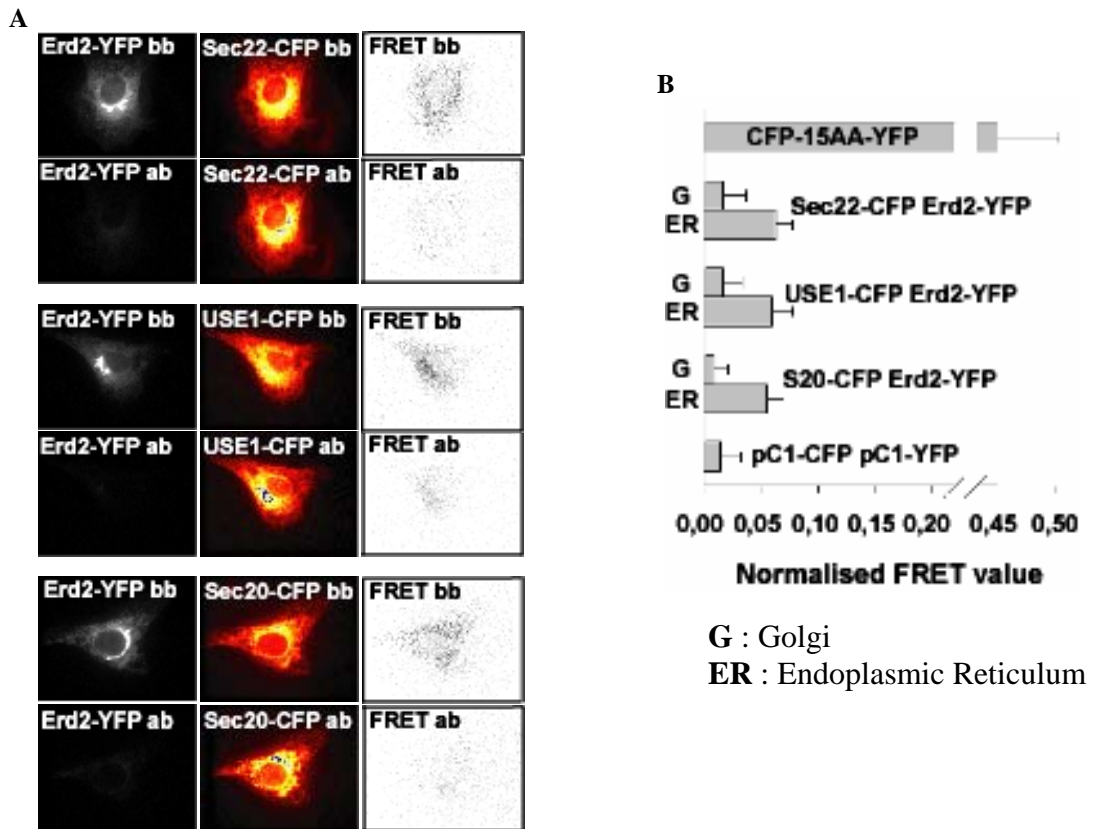


Figure 19: interaction with the KDEL-receptor or Erd2. (A) FRET measurements in Vero cells co-expressing Erd2-YFP (KDEL-receptor fused to YFP) and the indicated SNARE-proteins fused to CFP. The measurements were performed in single-cells by fluorescence microscopy as described in the Methods part. Cells co-expressing Erd2-YFP with either Sec22-CFP, or USE1-CFP, or Sec20-CFP were grown on coverslips. Images were acquired in the YFP channel (left column), in the CFP channel (middle column), and in the FRET channel (right column), before (bb) and after (ab) acceptor photobleaching. The intensity of the pictures taken in the CFP channel is represented using an artificial colour scale (red-orange-yellow). The blue colour appeared when the fluorescence intensity was at or above saturation. (B) Graph showing the normalized FRET values (N_{FRET}) obtained (see Materials and Methods) for the indicated protein pairs, for the positive control (CFP-15AA-YFP) and for the negative control (pC1-CFP pC1-YFP). Note that the FRET signal reflecting the interaction between Erd2 and each of the SNARE proteins was mainly detected in the peripheral area of the cell, most likely the ER (ER) whereas only negligible signals were obtained in the perinuclear region (G). The values given are mean values \pm standard deviation of three independent experiments, each analyzing at least 10 cells.

When co-expressing mSec22b-CFP and Erd2-YFP, a moderate, but significant FRET signal ($N_{\text{FRET}} = 0,060 \pm 0,017$) could be registered in the peripheral parts of the cells most likely the ER (Fig.19 A, upper panel). In the perinuclear area (here arbitrarily called “Golgi”) no significant FRET signal was measured (Fig19 B). The same was observed when Erd2-YFP was co-expressed together with mUse1-CFP or mSec20-CFP (Fig.19 A, middle panel and lower panel). The increase of CFP fluorescence (picture CFPab) after acceptor photobleaching was observed for all the pairs supporting that the KDEL-receptor interacts

indeed with the different SNAREs of interest. Moreover, in immunoprecipitation experiments with rat liver microsomal membranes, antibodies directed against mUse1 co-precipitated Erd2 (Fig.16 B).

5.8. Presence of the SNARE-proteins in COPI vesicles.

It is generally assumed that COPI-coated transport intermediates, believed to be either vesicles or tubules, mediate intra-Golgi and Golgi-to-ER retrograde transport. COPI-dependent retrograde transport has in particular been described to be followed by the occupied KDEL-receptors and membrane proteins containing a cytoplasmic C-terminal KKXX motif. These reports together with the co-immunoprecipitation experiments and FRET data reported here which indicate interactions between Erd2 and the different retrograde SNARE candidates suggest that mSec22b, mUse1, mSec20 and Syntaxin18 could be involved in a COPI-dependent transport from the Golgi to the ERGIC and/or to the ER. To study this issue, Golgi stacks were isolated from rat liver and incubated under conditions which allow for vesicle release under the indicated conditions (Fig.20 A). Thereafter, the vesicles were isolated and their compositions were analysed by western-blotting (Fig.20 A) and by immuno-electron microscopy (Fig.20 B).

β' -COP, one of the subunits of the COPI coat, was present in all the Golgi (G1,G2 and G3) and vesicles (V1, V2 and V3) fractions after incubation. It was found in a larger amount in the G2 fraction. Indeed, as GTP γ S prevents COPI coat disassembly, the coatomer tended to accumulate at the Golgi membrane, whereas for the G3 fraction in presence of GTP the coat can be disassembled and released from the vesicles. In case of incubation condition1, neither the disassembly nor the assembly of COPI coatomer was stimulated, therefore, most of the β' -COP subunits stayed in the supernatant (S1, Fig.20 B) as compared to S2 and S3 supernatants. Low amounts of ERGIC53 and syntaxin18 were found consistently in the V2 and V3 fractions. Thus, the IC did not seem to be present in any of the isolated Golgi or vesicles fractions. As syntaxin18 was shown to be localized principally in the ER [222], the signal observed in the vesicles V2 and V3 fractions can come either from an ER contamination during the preparation or a few molecules of syntaxin18 which escaped from the ER and are recycled back. KDEL-receptors resided mostly in the Golgi fractions but were also clearly present in the vesicle fractions (Fig.20 A).

Results

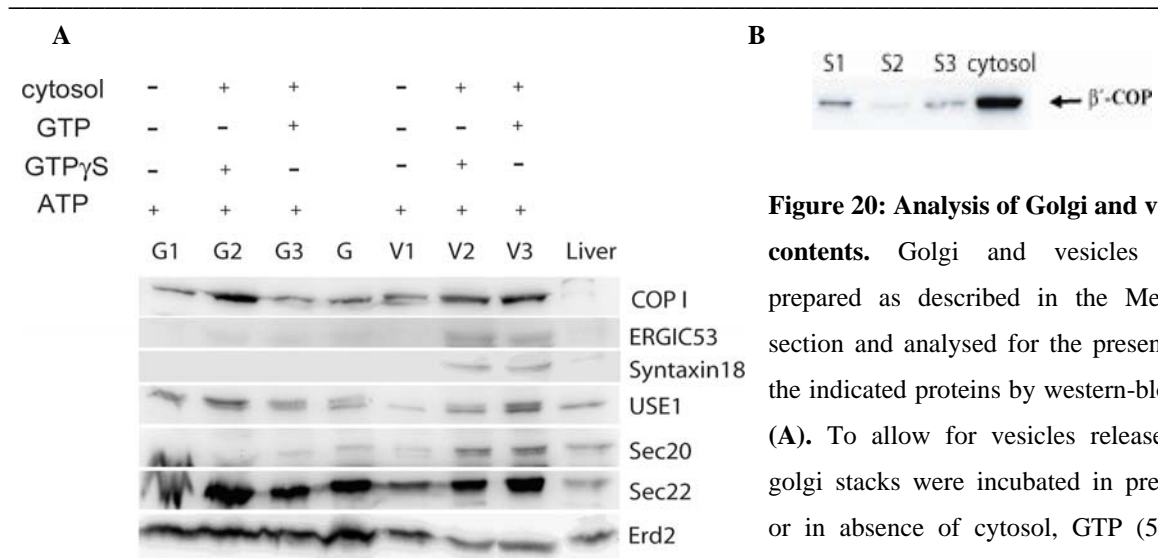
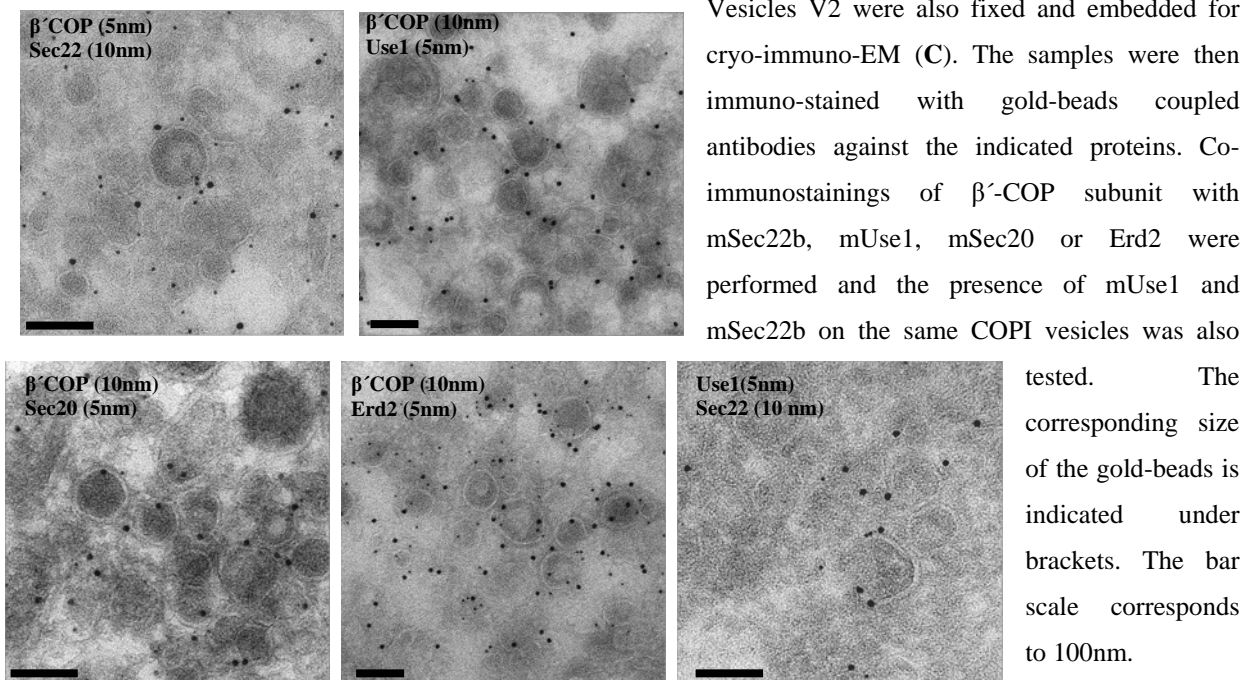


Figure 20: Analysis of Golgi and vesicle contents. Golgi and vesicles were prepared as described in the Methods section and analysed for the presence of the indicated proteins by western-blotting (A). To allow for vesicles release, the golgi stacks were incubated in presence or in absence of cytosol, GTP (5mM), GTP γ S (100 μ M) and ATP (5mM). The

cytosol used for Golgi incubation and the supernatants obtained after isolation of vesicles were also analysed for the presence of cytosolic β' -COP protein (B). The same amounts of total proteins were loaded on a 15% SDS-gel for the Golgi fractions G1, G2, G3 and G, for the Liver sample (100 μ g) as well as for the samples containing vesicles V1, V2 and V3 (50 μ g) (A). For the supernatant fractions S1, S2, S3 and cytosol the same volumes were loaded on a 12% SDS-gel (B). The fractions contents were analysed for the indicated proteins.

C



Interestingly, mSec22b appeared at high concentration in the vesicle V2 and V3-fraction but still remained in large amounts in the Golgi suggesting an important sorting of mSec22b into the Golgi-derived vesicles. The novel mammalian SNAREs mUse1 and mSec20 were found both in the vesicle-fractions while mUse1 was also present in the Golgi, mSec20 was almost absent from this compartment. Since these SNARE-proteins seem to exist

Results

in a relatively small amount as compare to mSec22b (Fig.20 A and C), they could be sorted into Golgi vesicles (most likely retrograde Golgi-ER COPI vesicles) which contain mSec22b.

The vesicle population obtained after incubation of the Golgi for vesicle release is most likely highly heterogeneous meaning that only a small part correspond to Golgi-ER retrograde COPI vesicles. Indeed, intra-Golgi COPI vesicles as well as uncoated vesicles or undefined coated vesicles can also be found in the fractions. Therefore, the presence of the different SNARE-proteins of interest on COPI vesicles was further analysed by immuno-EM (Fig.20, C). The existence of mSec22b, mUse1 and mSec20 on COPI vesicles was confirmed even though the staining for mSec20 (Fig.20, C) was weak which is in line with the immunoblotting experiment (Fig.20, A). Importantly, mSec22b and mUse1 were found on the same vesicles, which are most probably COPI vesicles as seen by the specific pattern (thick coat) around the vesicles. As expected, KDEL-receptors were quite abundant in COPI-vesicles.

Since mUse1 and mSec22b are found within small membrane-enclosed COPI vesicles, the possibility that they interact with one of the subunits constituting the COPI coat was tested by co-immunoprecipitation using from detergent-extracts V2 and V3 vesicles.

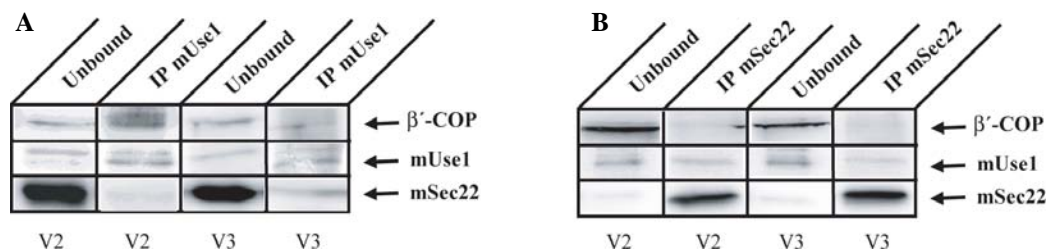


Figure 21: Interaction of mUse1 with COPI coatomers. Antibodies directed against mUse1 (A) and mSec22b (B) were used for co-immunoprecipitation detergent extracts of from V2- and V3- Golgi-derived vesicles and experiments were performed as described in the legend to Fig.16. V2 and V3 are vesicles obtained from the Golgi as described in the legend to Fig.20. Fractions were separated by 12% SDS-PAGE and analyzed by immunoblotting using antibodies against β' -COP, mUse1 and mSec22b. The unbound loaded fraction corresponds to 5% of the total unbound proteins.

When mUse1 was used as target protein, a significant amount of β' -COP was detected in the V2-precipitate but only traces in the V3-precipitate. No coprecipitation of mSec22b was found in extracts from V2-vesicles and only a very weak signal for mSec22b was obtained in the V3-vesicle precipitate. mSec22b antibodies did not precipitate β' -COP but some mUse1 could be detected in precipitates from V2- and V3-fractions. All together these data suggest

that mUse1 interacts with components of the coat in COPI coated vesicles whereas mSec22b does not, even when the coatomers are abundant on the vesicles (V2 sample). As anti-mUse1 antibodies coprecipitated β' -COP under conditions where almost no mSec22b was coprecipitated, it appears that the free mUse1, rather than mUSE1 present in SNARE-complexes, was interacting with β' -COP.

5.9. Effects of down-regulation of mSec22b, mUse1, or mSec20.

If these SNAREs are involved in Golgi-ER retrograde transport, one should expect that down-regulation of their expression might impair cargo translocation from the Golgi to the ER, although one has to consider the possibility that structurally related SNARE-proteins mainly involved in other transport steps could functionally compensate for the loss. Cholera toxin is a retrograde cargo which is, via the interaction of its B-subunits with the plasma membrane ganglioside, endocytosed and transported to the Golgi, where its A-subunit, which possesses a C-terminal KDEL-signal, interacts with the KDEL-receptor Erd2 and becomes translocated by retrograde transport to the ER. Therefore, mSec22b was down-regulated in Vero cells by transfection with an appropriate siRNA for 72 h and cholera toxin was subsequently applied to the cells.

The amount of Sec22 protein in sham-transfected cells (siRNA GL2) and in the siRNA Sec22 transfected cells was estimated by western-blotting (Fig. 22a, A). 72 hours after transfection about 90% of the endogenous mSec22b has disappeared in the siRNA Sec22 transfected cells whereas no effect was observed in sham treated-cells. In both cases, no effect on Use1 expression was observed.

In sham-transfected cells, CTX-A had accumulated in the ER 120 min after start of CTX uptake (Fig.22a, B left panel). In mSec22b-downregulated cells, the toxin did not reach the ER but instead accumulated in perinuclear punctuated structures (Fig.22a, B right panel). This suggests that the CTX transport is disturbed when mSec22b becomes quasi depleted from the cells.

Downregulation of mSec20 or mUse1 did not give meaningful results as far as retrograde transport of CTX is concerned, as in both cases, down-regulation was associated with severe disturbances of intracellular membrane organization (Fig.22b, A and B), which in the case of mSec20 down regulation was frequently associated with cell death. A similar observation has recently reported by Nakajima et al. [226] for down-regulation of the human mSec20 ortholog.

Results

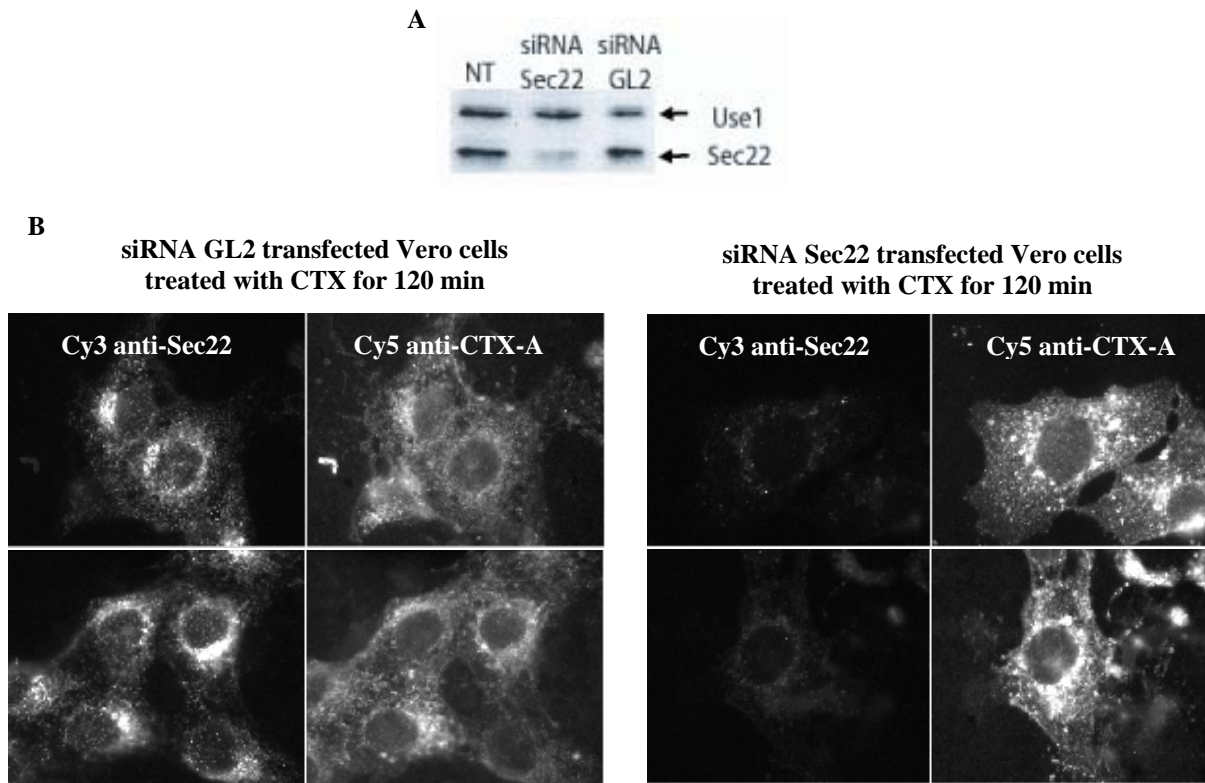


Figure 22a: Down-regulation of mSec22b affects CTX transport. Vero cells were transfected with siRNA GL2 (sham-cells) or with siRNA to down-regulate mSec22b. Cells were either collected and the lysates analysed by western blotting for the indicated proteins (**A**) or cells were treated with cholera toxin (CTX) for 120 min and immunostained to detect mSec22b (Cy3) and CTX-A (Cy5) as described in the Methods part (**B**). Note that the distribution of CTX-A in sham-cells (left panel) is diffuse in a ER-like structure whereas in the siRNA Sec22 transfected cells it is localized in perinuclear punctuated structures. For western-blotting (**A**), non-transfected Vero cells (NT) were used as control and the same amounts of total proteins were loaded on the SDS-gel for the different samples. Use1 was used as a control for the specificity of the siRNA for Sec22.

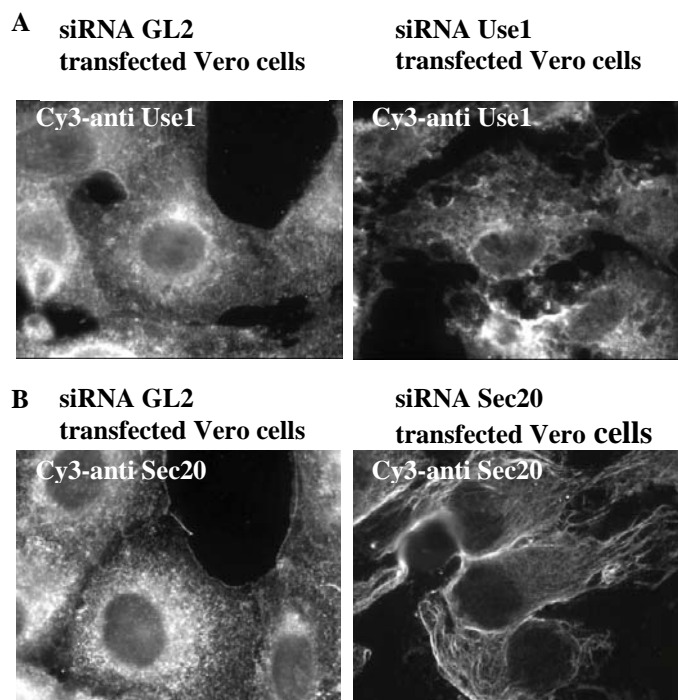


Figure 22b: down-regulations of mUse1 and mSec20 affect the morphology of the cell. Vero cells were transfected with siRNA GL2 (sham-cells) or with siRNA to down-regulate mUse1 (**A**) or mSec20 (**B**). 72 hours after transfection, cells were immunostained for the indicated protein.

6. DISCUSSION

In this work, I have shown that in mammalian cells mSec22b and Syntaxin18 can form a SNARE-complex with the novel SNARE-proteins mSec20 and mUse1, which is most likely involved in retrograde Golgi-(ERGIC)-ER transport. Live cell FRET and BiFC measurements as well as co-immunoprecipitation indicated that these SNARE-proteins interact with each other and with components of the retrograde transport machinery. The function of mSec22b, mSec20, and mUse1 was further demonstrated in cells where their expression was down-regulated using siRNA.

6.1. Characterisation of a new mammalian SNARE-complex

According to the alignment of SNARE motif sequences (Fig. 9A), the zero layer of the new mammalian SNARE-complex described here is composed of one arginine, one glutamine, one serine, and one aspartate (1R-1Q-1S-1D). This differs from most other known SNARE-complexes where the zero layer is composed of one arginine and three glutamines (1R-3Q). Other SNARE-complexes also possess a zero layer where one of the “Q-SNAREs” is a serine or an aspartate instead of a glutamate [83-85]. The presence of both serine and aspartate residues in the zero layer should not induce strong changes in the complex structure as both are polar residues and can form hydrogen bonds with the side chain of the R-SNARE mSec22b (Fig. 9B). When taking a closer look at the novel mammalian SNARE-protein mSec20, its SNARE motif sequence is only weakly related to that of other known mammalian SNAREs; also, it shows only 15% homology (8% identity) with its yeast homolog Sec20p. Even though this retrograde Golgi-ER SNARE-complex does not follow the “1R-3Q rule” previously defined for other SNARE-complexes, its formation depends on the presence of the SNARE-motif as shown by the results of the BiFC experiments (Fig. 15a). Here, deletion of the mUse1 SNARE motif revealed that the SNARE motif is essential for SNARE pairing. This had previously been observed in yeast for Sec22p where the SNARE motif deletion mutants failed to assemble into SNARE complexes [279]. Even the mutation of only two amino acids within the mSec22b SNARE motif already induced a decrease of its interaction with mUse1 (Fig.15a, D). Similar to other SNARE-complexes, the retrograde SNARE-complex described here can be disassembled by NSF and α -SNAP (Fig.18). Altogether, these observations both show that the four proteins studied in this work form a new SNARE-complex which has similar and different features to classical synaptic SNARE-complex. It would be interesting to perform structural studies with the individual proteins

mUse1 and mSec20 since they appear to be unusual SNAREs. It would also be of interest to know more about the biochemical and structural features of the complex they form with mSec22b and Syntaxin18.

6.2. Distribution of the retrograde Golgi-ER SNARE-proteins

The steady state distribution of the four retrograde Golgi-ER SNARE-proteins is different throughout the cell. The R-SNARE mSec22b is mainly present in the Golgi and in the ERGIC, but can also be found at lower concentrations in the ER. The Q-SNAREs (mUse1, mSec20 and Syntaxin18) are differently distributed between these three compartments. mUse1 is mostly found in the ER, the same holds for Syntaxin18 [222]. Nevertheless, mUse1 was also consistently found in the ERGIC and in lower concentrations in the Golgi. Interestingly, mSec20 was evenly distributed between the Golgi and the ER but was also found in the ERGIC at a very low concentration. The dispersed punctuated structures observed for mSec20 may correspond to the ER exit sites. This could be further studied using proper antibodies against Sec13 or Sec31. According to the distribution of the different individual SNAREs, the most probable scenario is that mSec22b is the v-SNARE present on the vesicle which buds from the Golgi or from the ERGIC. The vesicle is then transported to the ER where mSec22b can form a SNARE complex with three ER-t-SNAREs, which could be mUse1, mSec20 and Syntaxin18. mSec22b being the R-SNARE in both anterograde and retrograde transport, the retrograde complex could be disassembled by NSF/ α -SNAP and the free mSec22b could be recycled to the ERGIC or the Golgi where it could either become part of the anterograde SNARE-complex with Syntaxin5, membrin and rBet1 or be involved in another retrograde transport fusion event. mSec22b could also play the role of a v-SNARE for Golgi-to-ERGIC transport and form a SNARE-complex with mUse1 and two other Q-SNAREs which would be localized in the ERGIC. It has to be further analysed whether one of these Q-SNAREs could be syntaxin18. Alternatively, the v-SNARE for the retrograde transport could also be mUse1 as it is significantly expressed in the ERGIC (also suggested in the review [80]). Moreover, anti-mUse1 antibodies precipitate β' -COP even though mUse1 is only present at a low concentration in the Golgi (Figures 12 and 20; see below). Finally, one cannot exclude the existence of unknown SNARE-proteins and, therefore, of other SNARE complexes in the Golgi-ERGIC-ER system.

According to the results obtained with the cell-free Golgi budding assay, mSec22b and mUse1 were strongly enriched in the Golgi-derived vesicles, while mSec20, which is weakly

present in the Golgi, was almost completely sorted into the vesicles (Fig.20, A and C). Moreover, the majority of the vesicle populations must have been released from the Golgi stacks, as ERGIC was not present in the Golgi fractions (Fig. 20A). These data suggest that mSec22b and mUse1 are actively sorted from the Golgi into vesicles and that mSec20 and syntaxin18 escaped from the ER and cycle between the ER, the ERGIC and the Golgi and need to be retrieved back to the ER probably in the same vesicles which contain both, mSec22b and mUse1 (Fig. 20C).

FRET data obtained in live single cells showed interactions between the fluorescent fusion proteins of mSec22b, mSec20 and mUse1 (Fig.14b). So far, similar experiments using syntaxin 18 with the fluorophore linked to its N-terminus did not give reliable results, so that the demonstration of a participation of syntaxin18 in the Golgi-ER SNARE-complex in intact mammalian cells needs further experimentation. The BiFC experiments confirm the results of the FRET-experiments. Moreover, BiFC experiments using mSec20 deleted for its SNARE motif underline the specificity of the interactions of mSec20 with mUse1 and mSec22b, and exclude that the interactions involve mainly transmembrane domains or are simply stochastic phenomena resulting from “membrane crowding” (Fig.15a). Additionally, FRET results showed that the interactions between the different SNAREs occur mainly at the periphery of the cell, which most likely represents the ER and ER exit sites, and perhaps includes parts of the ERGIC (Fig.14d, D).

This observation is in line with the localisation of mSec22b, mSec20 and mUse1 (Fig.12) and with the previous suggestions concerning a role for the studied SNARE-complex in ERGIC to ER retrograde transport. One should point out that the distinction between regions in the cell where the proteins interact or not can only be made if the FRET raw data are normalized by the expression levels of the SNARE-fusion proteins. The method of calculations of N_{FRET} (see methods) allows for such a distinction.

The only SNARE-pair for which a FRET signal could be measured in the perinuclear region is mSec22b-mSec20 (Fig.14d, D). This region includes most likely the Golgi and partially the ERGIC. These data are in agreement with the intracellular localisation of the two SNAREs and suggest that, since mSec20 is in the Golgi and not in the ERGIC (Fig.12), mSec20 could interact with mSec22b to form a “binary SNARE-complex” which would be transported directly to the ER where it could form a quaternary SNARE-complex with Syntaxin 18 and mUse1 or other SNAREs. mSec22b would additionally be guided to the ERGIC in vesicles containing mUse1 as observed with immuno-EM (Fig. 20). In this context, it would be interesting to see whether the different combinations (1R-3Q, 1R1Q-2Q...) can

form a SNARE-complex by using the approach of a reconstituted proteoliposome fusion assay [280].

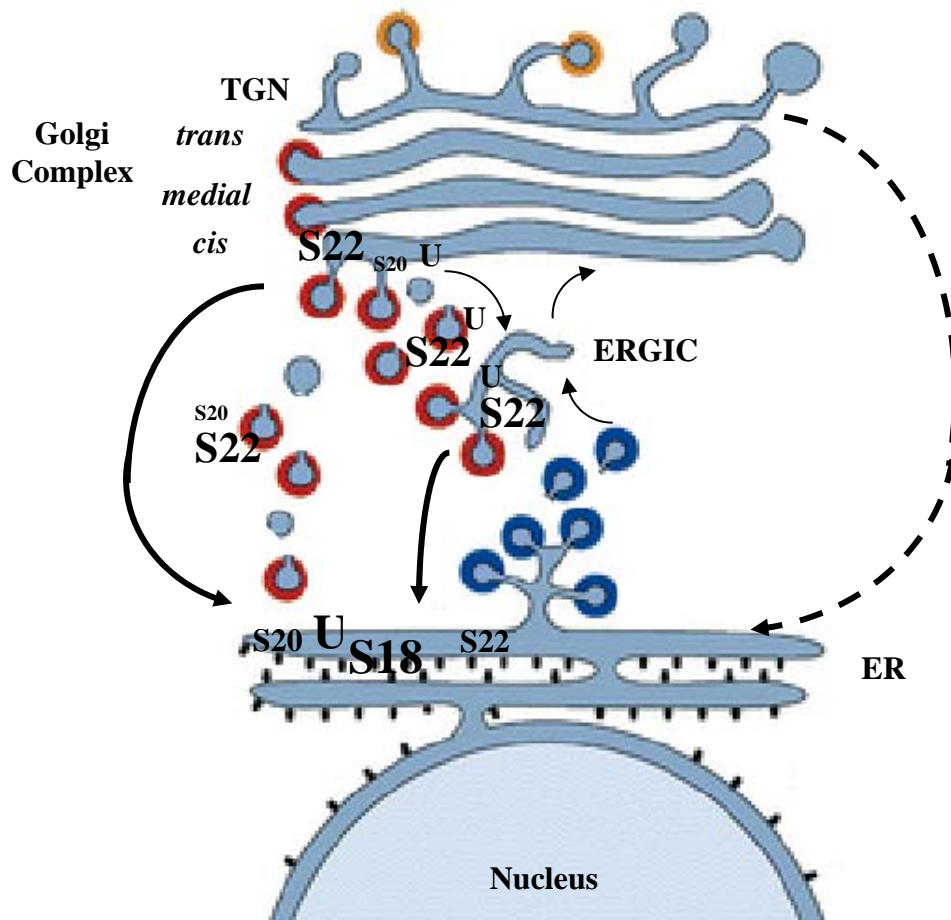


Figure 23: Distribution of the retrograde Golgi-ER SNARE-proteins within the Golgi-ERGIC-ER system.

The scheme depicts the Golgi, the ERGIC and the ER. Arrows indicate retrograde and anterograde transport steps and the dashed arrow indicates the putative COPI-independent pathway between the TGN and the ER. Colors show coatomers: Clathrin (orange), COPII (blue) and COPI (red). The concentration of the SNARE-proteins differ between the three organelles. This is shown by the font size (small, medium and large) used to indicate the name of the different SNAREs mSec22b (S22), mUse1 (U), mSec20 (S20) and syntaxin18 (S18).

6.3. Role of the Golgi-ER retrograde SNARE-proteins in the COPI-dependent pathway

Coimmunoprecipitations of detergent extracts from Golgi-derived vesicles show that β' COP can be co-precipitated with mUse1 but not with mSec22b. Moreover, in the same experiment, antibodies against mUse1 which co-precipitated the β' -COP subunit did not co-precipitate mSec22b, while mSec22b antibodies which did not co-precipitate β' -COP co-

precipitated mUse1. Interestingly, Mossessova et al. [111] have recently described a set of interactions between COPII and ER–Golgi SNAREs, involving discrete peptide sequences of 10–15 residues which could function as signals for ER export. COPII discriminated between the free and the complexed forms of Bet1 by binding a motif (LxxLE) buried in the N-terminal region of the v-/t-SNARE helical bundle and only available in the unstructured free v-SNARE. The authors designate this mechanism of coat selectivity as “v-SNARE conduction”, to convey the notion that this specific recognition process causes the sorting of the v-SNARE from the donor membrane into the vesicles. Miller et al. [110] and Liu et al. [279] demonstrated that in yeast at least two separate sites were necessary for optimal packaging of Sec22p into COPII vesicles : (1) the N-terminal domain, (2) the 10 amino acid residues between the -4 and -1 layers of the SNARE motif. Liu et al suggested that these anterograde SNARE proteins (*i.e.* Bos1p, Sed5p, and Bet1p) were transported individually [92], although this result does not rule out the possibility that Bos1p, Sed5p, and Bet1p exit the ER in a ternary SNARE complex. As far as the mammalian ER/Golgi SNARE proteins are concerned, heteromeric SNARE interactions are not required at any step in rbet1 targeting or transport dynamics [107]. Moreover, antibodies against the mammalian ER/Golgi SNARE proteins (*i.e.* syntaxin5, membrin, mSec22b, and rbet1) blocked the recruitment of these individual SNARE proteins into COPII vesicles without any effect on the packaging of the other SNARE proteins [107, 181]. Therefore, the trafficking of ER/Golgi SNARE proteins from the ER in unassembled states seems to represent a general mechanism conserved from yeast to mammals. According to our results obtained with Golgi-derived vesicles *in vitro*, mUse1 could be the v-SNARE which interacts with the COPI coat. mSec22b, via its interaction with mUse1, would be directed into COPI vesicles and retrieved back to the ER where the quaternary SNARE-fusion complex could be formed with mSec20 and Syntaxin18. Nevertheless, more information concerning interactions between retrograde SNAREs and COPI subunits is needed. Moreover, we cannot exclude the possibility that the anti-mSec22b antibodies used in our experiments do not allow β' COP binding to mSec22b. It would be interesting to know whether other COPI subunits ($\alpha, \beta, \gamma, \delta, \epsilon$ and ζ) can also be precipitated with these antibodies. It has been described that COPII selectivity involves conformation as well as sequence determinants on Sed5 [279]. This could also hold for syntaxin18 in view of the well-documented conformational switching of syntaxin SNAREs (for review see [281]). Interestingly, Sec22p may exit the ER as part of the t-SNARE complex or as a monomer interacting with Sec23/24 [111]. This implies that the ER-to-Golgi SNARE-complex does not need to be disassembled by NSF/ α -SNAP in order to provide mSec22b for the retrograde

Golgi-to-ER SNARE-complex. mSec22b, which arrives as monomer in the Golgi, could be used directly for retrograde transport and the pool of mSec22b which was involved in the anterograde complex can be recycled back from the cis-golgi or from the ERGIC to the ER using COPI dependent or independent pathways. In the ER, it can either form a SNARE complex with the other three retrograde Golgi-ER SNARE-proteins or form a “new” t-SNARE complex with Bos1 (membrin) and Sed5p (syntaxin5). This could also explain the steady state distribution of mSec22b in the Golgi.

Mossessova et al. [111] proposed that the directionality imposed by the coat assembly/disassembly cycle may control fusion of vesicles moving anterogradely, while preventing fusion of COPII vesicles back to the ER (because COPII binds fusogenic SNAREs at the originating membrane). This view cannot be directly applied to COPI vesicles, as COPI coated vesicles are known to be involved in Golgi-ER and intra-Golgi retrograde transport as well as in forward intra-Golgi transport steps. Other additional factors must be involved to direct the COPI vesicles and their contents in one or the other direction. The mechanisms which regulate whether a COPI-coated transport vesicle moves forward or backward are unknown at present. Several scenarios could be considered such as the existence of distinct but related populations of coatomers: one for anterograde, the other for retrograde transport. Another possibility is that coatomers might only be involved in vesicle-mediated transport only in the retrograde direction. Two alternative mechanisms have been proposed for anterograde intra-Golgi transport: first, the existence of a set of still unknown coat proteins and second, the formation of tubular extensions that emanate from one Golgi cisternae and fuse with an adjacent cisternae [214]. In this concept anterograde transport would be mediated by tubules rather than by vesicles. An alternative could be that the direction depends on the nature of SNARE-proteins present on the vesicle. Clathrin-coated vesicles also move along different pathways (Fig.1). This is regulated by the existence of different types of coats mainly due to the different adaptor proteins AP1, AP2, and AP3. In the same way, COPI-coated vesicles might contain some proteins which could play a role as guides for the vesicles; the SNARE-proteins are good candidates for such a role. Indeed, their localization throughout the cell is specific for one or two compartments between which they circulate. Interestingly, Lanoix et al. [53] have previously described the existence of more than one population of COPI vesicle involved in the intra-Golgi transport; at least one containing Mann II/GS28 (a *medial-trans* Golgi enzyme and a Golgi SNARE-protein) and another one in which the four p24 proteins, α_2 , β_1 , δ_1 , and γ_3 , were found. None of them contained significant amounts of anterograde cargo. This is in favour of a two-step intra-Golgi pathway, the first for the CGN

to *cis* cisterna, the second for the later *medial* and *trans* Golgi compartments. Recently, Malsam et al.[213] also described the presence of 2 distinct subpopulations of COPI vesicles: one having a role in intra-Golgi transport containing Golgi enzymes, and the other containing the proteins of the transport machinery retrieving them back to the ER. They suggest a two-step retrograde pathway for the Golgi enzymes, the first step mediated by intra-Golgi COPI transport to the *cis*-Golgi Network (CGN), the second by a COPI-independent pathway to the ER. All these observations show the diversity of COPI vesicles which could be classified depending on their contents. It would be interesting to study whether these COPI vesicles can also be distinguished with respect to their composition of SNARE-proteins. Although we could observe by EM that most of the Golgi-derived vesicles are COPI-coated, we cannot exclude the presence of other vesicles. Indeed, a COPI-independent pathway has been suggested for the retrograde Golgi-ER transport [210]. In case these vesicles would contain some of our SNAREs, this would favour the idea that a certain set of SNARE-proteins is specific for one direction of transport between two compartments in a cell rather than specific for only one type of coat.

Despite the conserved structure and function of the SNARE domain, the N-terminal domain of distinct SNARE proteins appears to be divergent in both structure and function. This is also true for the newly characterised Golgi-ER retrograde SNARE-proteins. Indeed, the truncation of the N-terminal portion (including the SNARE motif) of mUse1 led to its transport to the plasma membrane, whereas in case of mSec20 a N-terminal truncation did not affect the ER localisation of the protein (Fig. 15b). Moreover, when only the SNARE motif was deleted in mUse1, its localisation remained unchanged as compared to the wt-protein. N-terminal regions in mUse1 and other SNARE proteins [132, 133, 282, 283] are required for their proper intracellular targeting. It seems probable that signals within these regions will interact with specific coat protein complexes. Such interactions are likely to govern intracellular location and therefore contribute to the fidelity of membrane fusion reactions. Indeed, SNARE protein localization may play a significant role in specifying membrane fusion partners.

In my experiments, antibodies against rBet1 precipitated mSec22b but not mUse1 or mSec20. Moreover, none of the antibodies raised against the three retrograde SNARE-proteins precipitated rBet1. This suggests that rBet1 is involved only in the anterograde transport but not in the Golgi to ER retrograde transport and underlines further the existence of two distinct pathways with opposite directions between the two compartments, involving at

least partially specific SNARE proteins. Nevertheless, rBet1 must slowly recycle back to the ER, which would explain why a weak FRET signal could be measured between mUse1-YFP and rBet1-CFP in the Golgi region (see page 75).

In the Golgi-ER retrograde pathway, sorting of membrane proteins occurs through the interaction of their cytoplasmic domains with coat proteins. Such membrane proteins typically bear ER retrieval signal such as a dilysine (KKXX) motif at their C-terminus. Although the KDEL receptor lacks such a signal, it is well established that it is transported from the Golgi complex to the ER in COPI coated transport intermediates [158, 206, 210]. Therefore, other factors different from the classic dilysine retrieval motif must be responsible for the interaction of the C-terminal domain of the KDEL receptor with coatomeer proteins. Cabrera et al. [208] suggest that phosphorylation of serine 209 promotes the interaction of the KDEL receptor with both coatomeer proteins and ARF-GAP. Interestingly, I observed that the KDEL receptor interacts with mUse1 (Fig.16). This underlines our findings concerning the binding of mUse1 to the COPI coat. The interaction occurring between the KDEL-receptor and retrograde Golgi-ER SNARE- proteins was further confirmed by live cell microscopy data which showed that mUse1-CFP but also mSec22b-CFP and mSec20-CFP interact with Erd2-YFP in the cell periphery. This indicates that SNARE proteins may be involved in the formation of a sorting/budding complex at the donor compartment. According to the localization of the measured FRET signal between Erd2 and the different SNAREs of interest, this compartment would most likely correspond to the ERGIC as no significant FRET signal was measured in the perinuclear region of the cell.

Down-regulation of mSec22b blocked the accumulation of CTX in the ER but led to the accumulation of CTX in punctuated structures which need to be further characterized. Their perinuclear distribution suggests that these structures could be partially Golgi and/or ERGIC. We cannot exclude that the down-regulation of mSec22b also affects the ER-Golgi anterograde transport. This could lead to a lack of transport from ER to Golgi of the components of the retrograde transport machinery and, therefore, affect also CTX transport. To study the anterograde transport in the mSec22b depleted cells, VSVG-GFP could be used as a marker for the secretory pathway. The other possibility would be that down-regulation of mSec22b induces up-regulation of another R-SNARE such as the partially soluble Ykt6 which could compensate for the transport defect. Indeed, the multicomponent character of the coated-vesicle-based pathways frequently allows compensation sometimes to the extent that

only a weak cellular phenotype becomes manifest, even in a multiple knockout. Ykt6p is partially soluble and this may enable it to substitute for other R-SNAREs in multiple fusion reactions. This could explain why deletions of several yeast R-SNAREs have surprisingly mild phenotypes [92]. The same could hold for mammalian cells, as in the experiments reported here down-regulation of mSec22b did not lead to such dramatic changes in the cellular state as observed for the Q-SNAREs mSec20 and mUse1. This compensation of a low mSec22b expression level by Ykt6 could affect the anterograde ER-to-Golgi COPII and the intra-Golgi COPI pathways selectively. It was previously shown in yeast that when the level of the Golgi/endosomal SNARE protein Ykt6p is elevated on COPII vesicles in the absence of Sec22p, it assembles into an ER/Golgi SNARE complex and can function with non-cognate SNAREs in the fusion of ER-derived vesicles with the Golgi complex [92]. Moreover, Ykt6 is known to be part of the forward intra-golgi SNARE-complex. It could be that Ykt6 does not or only partially compensate for mSec22b in its role in the retrograde SNARE-complex. This would explain why the morphology of the cell is not affected when mSec22b is down-regulated (Fig.22b) while CTX transport is perturbed as indicated by its retention in punctuated structures and by the lack of further transport into the ER.

Down-regulation of mSec20 or mUse1 in Vero cells led to morphological changes of the cell and to a defect in growth/proliferation. These changes could result from the loss of functions which may not be related to SNARE-complex formation and fusion. Indeed, beside its role as a SNARE-protein, mSec20 belongs to the family of BH3-only proteins which are involved in the regulation of apoptosis. This might explain the dramatic effects of its down-regulation.

6.4. Golgi-to-ER retrograde pathways

Several independent lines of evidence indicate that retrograde transport from the Golgi apparatus to the ER may be mediated by COP-I-coated vesicles. COP-I interacts with retrieval motifs of membrane proteins that are known to recycle between the ER and the Golgi apparatus [48]. In yeast strains in which COP-I is mutated and unable to bind retrieval motifs, reporter proteins containing such motifs escape the secretory pathway to the plasma membrane [149, 284]. Furthermore, antibodies to COP-I block the relocation of Golgi enzymes to the ER in the presence of brefeldin A (BFA) [285], which disrupts the Golgi, and transport of cholera toxin from the Golgi to the ER requires COP-I function [206].

Girod et al. [210] demonstrated the existence of at least one Golgi-to-ER recycling pathway that is COP-I independent and appears to be regulated by the small GTPase Rab6. This transport was shown to be followed by labelled Shiga toxin B-fragment (The shiga toxin belongs to the AB₅-toxin family as the cholera toxin) and the Golgi-resident glycosylation enzyme GalNAc-T2. Thus, there are at least two general transport pathways from Golgi to ER. One requires binding to the KDEL-receptor ERD2 in the Golgi apparatus and follow the COPI-dependent pathway and the other would follow the COPI-independent pathway.

The COP-I-independent recycling pathway described by Girod et al. could work at the level of the *cis*-Golgi network, where it would help to return molecules back to the ER alongside the COPI-dependent Golgi-to-ER recycling pathway. An alternative would be that the COPI-independent transport emanates from the TGN and reaches the ER directly. Indeed, a modified version of the Shiga toxin B-fragment engineered to contain a site for modification by *N*-linked oligosaccharides, a site for tyrosine sulphation and a KDEL signal showed that sulphation precedes addition of *N*-linked core glycosylation [286]. As sulphation occurs in the TGN and *N*-linked core glycosylation takes place exclusively in the ER, the Shiga toxin B-fragment must reach the TGN but does not need to pursue its route to the medial and *cis* cisternae before reaching the ER. In this context, it would be useful to apply live cell 4Pi microscopy, a high resolution light microscope which allows to distinguish between the different Golgi cisternae (Verrier, S. et al., work in progress) and follow the Shiga toxin route using appropriate Golgi markers.

Girod et al. suggested that the main function of the observed COP-I-independent recycling pathway might be to recycle lipids. A portion of the lipids which reaches the TGN are predicted to move forward via vesicles to the plasma membrane or into the endocytic pathway, but a significant proportion would remain. Recycling of these remaining lipids back to the ER would then ensure the overall balance of the pathway. This would be in accordance with both of the highly discussed models: the cisternal maturation model and the vesicular transport model. The first one predicts that anterograde cargo remains in Golgi cisternal membranes and that cisternae mature in a *cis*-to-*trans* direction, whereas resident proteins move in the opposite direction via COPI vesicles and in the second one, each cisternae instead constitutes a stable compartment, and anterograde cargo move via COPI anterograde vesicles from cisterna to cisterna in a *cis*-to-*trans* direction.

The mechanisms of retrograde trafficking are likely to be highly regulated [12, 134, 287] and to involve lipid partitioning to segregate recycling components from forward moving cargo [193]. Indeed, certain lipids (e.g., glycosphingolipids and cholesterol) may help to

partition proteins into specific membrane domains [288] while others (e.g., phosphoinositides) can regulate the membrane recruitment of clathrin coats and of other trafficking components [289, 290]. This may hold as well for the COPI recruitment at the Golgi and ERGIC membranes. Other factors are likely to be identified, such as motor molecules and their regulators that could be recruited to the membrane-microtubule interface to guide the retrograde transport carriers (as proposed by Duran et al.[291]).

6.5. Perspectives for a better understanding of intracellular trafficking

Upon arrival at the cis-Golgi, anterograde cargo must physically segregate from retrograde cargo in order to be delivered for further transit through the secretory pathway, whereas retrograde cargo must be returned back to the ER. The mechanism by which this is achieved cannot yet be revealed by time-lapse microscopy of GFP-tagged markers, due to the lack of appropriate retrograde transport markers and the limits of resolution of light microscopy. The best characterized transport intermediates are indeed small, spherical coated vesicles. But emerging evidence from mammalian cells points to an additional form of transport by large pleiomorphic intermediates[42]. A well-documented example of such a transport intermediate are the COPI-containing VTCs that move from ER exit sites to the Golgi complex [165, 292, 293]. Using current light microscopy techniques, small 60-80 nm vesicles cannot be seen in living cells. Many of the structures observed so far could represent vesicle populations, which might even be tethered one to another and, therefore appear as a pleiomorphic transport complex. Correlated analyses using light and electron microscopy on the same cell [38] could be one way to resolve these questions. Perhaps one limitation is that usually the GFP-tagged molecule is ectopically expressed in a system already containing a background of the untagged endogenous protein. Ideally one would like to examine these GFP-tagged markers by using regulated expression systems in a null background. It seems likely that the availability of further spectral variants of GFP, together with developments in light microscopy [274, 294]Klar et al., 2000), will facilitate the greater use of light microscopy in the analysis of intracellular membrane traffic. Fast-acquisition systems would also much improve our ability to analyse the dynamics of vesicular traffic inside living cells. The new technical developments mentioned in combination with FRET or BiFC measurements will certainly enhance our understanding of the mechanisms involved in different pathways.

7. REFERENCE

1. Palade, G. (1975). Intracellular aspects of the process of protein synthesis. *Science* 189, 347-358.
2. Pelham, H.R., and Rothman, J.E. (2000). The debate about transport in the Golgi--two sides of the same coin? *Cell* 102, 713-719.
3. Kirchhausen, T., Bonifacino, J.S., and Riezman, H. (1997). Linking cargo to vesicle formation: receptor tail interactions with coat proteins. *Curr Opin Cell Biol* 9, 488-495.
4. Kuehn, M.J., and Schekman, R. (1997). COPII and secretory cargo capture into transport vesicles. *Curr Opin Cell Biol* 9, 477-483.
5. Hay, J.C., and Scheller, R.H. (1997). SNAREs and NSF in targeted membrane fusion. *Curr Opin Cell Biol* 9, 505-512.
6. Rothman, J.E., and Sollner, T.H. (1997). Throttles and dampers: controlling the engine of membrane fusion [see comments]. *Science* 276, 1212-1213.
7. Rothman, J.E. (1994). Mechanisms of intracellular protein transport. *Nature* 372, 55-63.
8. Pevsner, J. (1996). The role of Sec1p-related proteins in vesicle trafficking in the nerve terminal. *J Neurosci Res* 45, 89-95.
9. Lupashin, V.V., and Waters, M.G. (1997). t-SNARE activation through transient interaction with a rab-like guanosine triphosphatase [see comments]. *Science* 276, 1255-1258.
10. Clary, D.O., Griff, I.C., and Rothman, J.E. (1990). SNAPs, a family of NSF attachment proteins involved in intracellular membrane fusion in animals and yeast. *Cell* 61, 709-721.
11. Bonifacino, J.S., and Glick, B.S. (2004). The mechanisms of vesicle budding and fusion. *Cell* 116, 153-166.
12. Pelham, H.R. (1991). Recycling of proteins between the endoplasmic reticulum and Golgi complex. *Curr Opin Cell Biol* 3, 585-591.
13. Stinchcombe, J.C., Nomoto, H., Cutler, D.F., and Hopkins, C.R. (1995). Anterograde and retrograde traffic between the rough endoplasmic reticulum and the Golgi complex. *J Cell Biol* 131, 1387-1401.
14. Wilson, D.W., Wilcox, C.A., Flynn, G.C., Chen, E., Kuang, W.J., Henzel, W.J., Block, M.R., Ullrich, A., and Rothman, J.E. (1989). A fusion protein required for vesicle-mediated transport in both mammalian cells and yeast. *Nature* 339, 355-359.
15. Griff, I.C., Schekman, R., Rothman, J.E., and Kaiser, C.A. (1992). The yeast SEC17 gene product is functionally equivalent to mammalian alpha-SNAP protein. *J. Biol. Chem.* 267, 12106-12115.
16. Barlowe, C., Orci, L., Yeung, T., Hosobuchi, M., Hamamoto, S., Salama, N., Rexach, M.F., Ravazzola, M., Amherdt, M., and Schekman, R. (1994). COPII: a membrane coat formed by Sec proteins that drive vesicle budding from the endoplasmic reticulum. *Cell* 77, 895-907.
17. Bannykh, S.I., Rowe, T., and Balch, W.E. (1996). The organization of endoplasmic reticulum export complexes. *J Cell Biol* 135, 19-35.
18. Hermo, L., and Smith, C.E. (1998). The structure of the Golgi apparatus: a sperm's eye view in principal epithelial cells of the rat epididymis. *Histochem Cell Biol* 109, 431-447.
19. Balch, W.E., and Keller, D.S. (1986). ATP-coupled transport of vesicular stomatitis virus G protein. Functional boundaries of secretory compartments. *J Biol Chem* 261, 14690-14696.

Reference

20. Verde, C., Pascale, M.C., Martire, G., Lotti, L.V., Torrisi, M.R., Helenius, A., and Bonatti, S. (1995). Effect of ATP depletion and DTT on the transport of membrane proteins from the endoplasmic reticulum and the intermediate compartment to the Golgi complex. *Eur J Cell Biol* 67, 267-274.
21. Rothman, J.E., and Wieland, F.T. (1996). Protein sorting by transport vesicles. *Science* 272, 227-234.
22. Tanaka, K., Mitsushima, A., Fukudome, H., and Kashima, Y. (1986). Three-dimensional architecture of the Golgi complex observed by high resolution scanning electron microscopy. *J Submicrosc Cytol* 18, 1-9.
23. Sesso, A., Azimovas, S.R., and Ferreira, M.A. (1994). Freeze-fracture and thin section study of the rough ER-Golgi interface in the pancreatic acinar cell. Resemblance between the intramembranal architecture of the outermost Golgi cisterna and the post-rough ER vesicular and tubular elements. *Biol Cell* 81, 165-176.
24. Rambourg, A., Clermont, Y., and Hermo, L. (1979). Three-dimensional architecture of the golgi apparatus in Sertoli cells of the rat. *Am J Anat* 154, 455-476.
25. Clermont, Y., Rambourg, A., and Hermo, L. (1995). Trans-Golgi network (TGN) of different cell types: three-dimensional structural characteristics and variability. *Anat Rec* 242, 289-301.
26. Cluett, E.B., Wood, S.A., Banta, M., and Brown, W.J. (1993). Tubulation of Golgi membranes in vivo and in vitro in the absence of brefeldin A. *J Cell Biol* 120, 15-24.
27. Cooper, M.S., Cornell-Bell, A.H., Chernjavsky, A., Dani, J.W., and Smith, S.J. (1990). Tubulovesicular processes emerge from trans-Golgi cisternae, extend along microtubules, and interlink adjacent trans-golgi elements into a reticulum. *Cell* 61, 135-145.
28. Fujiwara, T., Oda, K., Yokota, S., Takatsuki, A., and Ikehara, Y. (1988). Brefeldin A causes disassembly of the Golgi complex and accumulation of secretory proteins in the endoplasmic reticulum. *J Biol Chem* 263, 18545-18552.
29. Doms, R.W., Russ, G., and Yewdell, J.W. (1989). Brefeldin A redistributes resident and itinerant Golgi proteins to the endoplasmic reticulum. *J Cell Biol* 109, 61-72.
30. Donaldson, J.G., Lippincott-Schwartz, J., and Klausner, R.D. (1991). Guanine nucleotides modulate the effects of brefeldin A in semipermeable cells: regulation of the association of a 110-kD peripheral membrane protein with the Golgi apparatus. *J Cell Biol* 112, 579-588.
31. Orci, L., Tagaya, M., Amherdt, M., Perrelet, A., Donaldson, J.G., Lippincott-Schwartz, J., Klausner, R.D., and Rothman, J.E. (1991). Brefeldin A, a drug that blocks secretion, prevents the assembly of non-clathrin-coated buds on Golgi cisternae. *Cell* 64, 1183-1195.
32. Helms, J.B., and Rothman, J.E. (1992). Inhibition by brefeldin A of a Golgi membrane enzyme that catalyses exchange of guanine nucleotide bound to ARF. *Nature* 360, 352-354.
33. Lippincott-Schwartz, J., Donaldson, J.G., Schweizer, A., Berger, E.G., Hauri, H.P., Yuan, L.C., and Klausner, R.D. (1990). Microtubule-dependent retrograde transport of proteins into the ER in the presence of brefeldin A suggests an ER recycling pathway. *Cell* 60, 821-836.
34. Anderson, R.G. (1998). The caveolae membrane system. *Annu Rev Biochem* 67, 199-225.
35. Hirschberg, K., Miller, C.M., Ellenberg, J., Presley, J.F., Siggia, E.D., Phair, R.D., and Lippincott-Schwartz, J. (1998). Kinetic analysis of secretory protein traffic and characterization of golgi to plasma membrane transport intermediates in living cells. *J Cell Biol* 143, 1485-1503.

Reference

36. Presley, J.F., Smith, C., Hirschberg, K., Miller, C., Cole, N.B., Zaal, K.J., and Lippincott-Schwartz, J. (1998). Golgi membrane dynamics. *Mol Biol Cell* 9, 1617-1626.
37. Gruenberg, J., and Maxfield, F.R. (1995). Membrane transport in the endocytic pathway. *Curr Opin Cell Biol* 7, 552-563.
38. Polishchuk, R.S., Polishchuk, E.V., Marra, P., Alberti, S., Buccione, R., Luini, A., and Mironov, A.A. (2000). Correlative light-electron microscopy reveals the tubular-saccular ultrastructure of carriers operating between Golgi apparatus and plasma membrane. *J Cell Biol* 148, 45-58.
39. Volchuk, A., Amherdt, M., Ravazzola, M., Brugger, B., Rivera, V.M., Clackson, T., Perrelet, A., Sollner, T.H., Rothman, J.E., and Orci, L. (2000). Megavesicles implicated in the rapid transport of intracisternal aggregates across the Golgi stack. *Cell* 102, 335-348.
40. Luini, A., Ragnini-Wilson, A., Polishchuk, R.S., and De Matteis, M.A. (2005). Large pleiomorphic traffic intermediates in the secretory pathway. *Curr Opin Cell Biol* 17, 353-361.
41. Kirchhausen, T. (2000). Three ways to make a vesicle. *Nat Rev Mol Cell Biol* 1, 187-198.
42. Bonifacino, J.S., and Lippincott-Schwartz, J. (2003). Coat proteins: shaping membrane transport. *Nat Rev Mol Cell Biol* 4, 409-414.
43. Pearse, B.M. (1976). Clathrin: a unique protein associated with intracellular transfer of membrane by coated vesicles. *Proc Natl Acad Sci U S A* 73, 1255-1259.
44. Waters, M.G., Serafini, T., and Rothman, J.E. (1991). 'Coatomer': a cytosolic protein complex containing subunits of non-clathrin-coated Golgi transport vesicles. *Nature* 349, 248-251.
45. Oprins, A., Duden, R., Kreis, T.E., Geuze, H.J., and Slot, J.W. (1993). Beta-COP localizes mainly to the cis-Golgi side in exocrine pancreas. *J Cell Biol* 121, 49-59.
46. Griffiths, G., Pepperkok, R., Locker, J.K., and Kreis, T.E. (1995). Immunocytochemical localization of beta-COP to the ER-Golgi boundary and the TGN. *J Cell Sci* 108 (Pt 8), 2839-2856.
47. Hara-Kuge, S., Kuge, O., Orci, L., Amherdt, M., Ravazzola, M., Wieland, F.T., and Rothman, J.E. (1994). En bloc incorporation of coatomer subunits during the assembly of COP-coated vesicles [published erratum appears in *J Cell Biol* 1994 Jul;126(2):589]. *Journal of Cell Biology* 124, 883-892.
48. Cosson, P., and Letourneur, F. (1994). Coatomer interaction with di-lysine endoplasmic reticulum retention motifs. *Science* 263, 1629-1631.
49. Bremser, M., Nickel, W., Schweikert, M., Ravazzola, M., Amherdt, M., Hughes, C.A., Sollner, T.H., Rothman, J.E., and Wieland, F.T. (1999). Coupling of coat assembly and vesicle budding to packaging of putative cargo receptors. *Cell* 96, 495-506.
50. Harter, C., Pavel, J., Coccia, F., Draken, E., Wegehingel, S., Tschochner, H., and Wieland, F. (1996). Nonclathrin coat protein gamma, a subunit of coatomer, binds to the cytoplasmic dilysine motif of membrane proteins of the early secretory pathway. *Proc Natl Acad Sci U S A* 93, 1902-1906.
51. Kaiser, C. (2000). Thinking about p24 proteins and how transport vesicles select their cargo. *Proc Natl Acad Sci U S A* 97, 3783-3785.
52. Cukierman, E., Huber, I., Rotman, M., and Cassel, D. (1995). The ARF1 GTPase-activating protein: zinc finger motif and Golgi complex localization. *Science* 270, 1999-2002.
53. Lanoix, J., Ouwendijk, J., Stark, A., Szafer, E., Cassel, D., Dejgaard, K., Weiss, M., and Nilsson, T. (2001). Sorting of Golgi resident proteins into different subpopulations of COPI vesicles: a role for ArfGAP1. *J Cell Biol* 155, 1199-1212.

Reference

54. Yang, J.S., Lee, S.Y., Gao, M., Bourgoïn, S., Randazzo, P.A., Premont, R.T., and Hsu, V.W. (2002). ARFGAP1 promotes the formation of COPI vesicles, suggesting function as a component of the coat. *J Cell Biol* 159, 69-78.
55. Donaldson, J.G., Cassel, D., Kahn, R.A., and Klausner, R.D. (1992). ADP-ribosylation factor, a small GTP-binding protein, is required for binding of the coatomer protein beta-COP to Golgi membranes. *Proc Natl Acad Sci U S A* 89, 6408-6412.
56. Nie, Z., Hirsch, D.S., and Randazzo, P.A. (2003). Arf and its many interactors. *Curr Opin Cell Biol* 15, 396-404.
57. Franco, M., Boretto, J., Robineau, S., Monier, S., Goud, B., Chardin, P., and Chavrier, P. (1998). ARNO3, a Sec7-domain guanine nucleotide exchange factor for ADP ribosylation factor 1, is involved in the control of Golgi structure and function. *Proc Natl Acad Sci U S A* 95, 9926-9931.
58. Zhao, L., Helms, J.B., Brunner, J., and Wieland, F.T. (1999). GTP-dependent binding of ADP-ribosylation factor to coatomer in close proximity to the binding site for dilysine retrieval motifs and p23. *J Biol Chem* 274, 14198-14203.
59. Goldberg, J. (1999). Structural and functional analysis of the ARF1-ARFGAP complex reveals a role for coatomer in GTP hydrolysis. *Cell* 96, 893-902.
60. Goldberg, J. (2000). Decoding of sorting signals by coatomer through a GTPase switch in the COPI coat complex. *Cell* 100, 671-679.
61. Sollner, T., Whiteheart, S.W., Brunner, M., Erdjument-Bromage, H., Geromanos, S., Tempst, P., and Rothman, J.E. (1993). SNAP receptors implicated in vesicle targeting and fusion. *Nature* 362, 318-324.
62. Glick, B.S., and Rothman, J.E. (1987). Possible role for fatty acyl-coenzyme A in intracellular protein transport. *Nature* 326, 309-312.
63. Malhotra, V., Orci, L., Glick, B.S., Block, M.R., and Rothman, J.E. (1988). Role of an N-ethylmaleimide-sensitive transport component in promoting fusion of transport vesicles with cisternae of the Golgi stack. *Cell* 54, 221-227.
64. Eakle, K.A., Bernstein, M., and Emr, S.D. (1988). Characterization of a component of the yeast secretion machinery: identification of the SEC18 gene product. *Mol Cell Biol* 8, 4098-4109.
65. Beckers, C.J., Block, M.R., Glick, B.S., Rothman, J.E., and Balch, W.E. (1989). Vesicular transport between the endoplasmic reticulum and the Golgi stack requires the NEM-sensitive fusion protein. *Nature* 339, 397-398.
66. Diaz, R., Mayorga, L.S., Weidman, P.J., Rothman, J.E., and Stahl, P.D. (1989). Vesicle fusion following receptor-mediated endocytosis requires a protein active in Golgi transport. *Nature* 339, 398-400.
67. Whiteheart, S.W., Schraw, T., and Matveeva, E.A. (2001). N-ethylmaleimide sensitive factor (NSF) structure and function. *Int Rev Cytol* 207, 71-112.
68. Lupas, A.N., and Martin, J. (2002). AAA proteins. *Curr Opin Struct Biol* 12, 746-753.
69. Walch-Solimena, C., Jahn, R., and Südhof, T.C. (1993). Synaptic vesicle proteins in exocytosis: what do we know? *Curr. Opin. Neurobiol.* 3, 329-336.
70. Hanson, P.I., Heuser, J.E., and Jahn, R. (1997). Neurotransmitter release - four years of SNARE complexes. *Curr. Opin. Neurobiol.* 7, 310-315.
71. Rizo, J., and Südhof, T.C. (1998). Mechanics of membrane fusion. *Nat Struct Biol* 5, 839-842.
72. Weimbs, T., Low, S.H., Chapin, S.J., Mostov, K.E., Bucher, P., and Hofmann, K. (1997). A conserved domain is present in different families of vesicular fusion proteins: a new superfamily. *Proc Natl Acad Sci U S A* 94, 3046-3051.

Reference

73. Fasshauer, D., Sutton, R.B., Brünger, A.T., and Jahn, R. (1998). Conserved structural features of the synaptic fusion complex: SNARE proteins reclassified as Q- and R-SNAREs. *Proc. Natl. Acad. Sci. U S A* *95*, 15781-15786.
74. Chen, Y.A., Scales, S.J., Duvvuri, V., Murthy, M., Patel, S.M., Schulman, H., and Scheller, R.H. (2001). Calcium regulation of exocytosis in PC12 cells. *J Biol Chem* *276*, 26680-26687.
75. Jahn, R., and Sudhof, T.C. (1999). Membrane fusion and exocytosis. *Annu Rev Biochem* *68*, 863-911.
76. Fukasawa, M., Varlamov, O., Eng, W.S., Sollner, T.H., and Rothman, J.E. (2004). Localization and activity of the SNARE Ykt6 determined by its regulatory domain and palmitoylation. *Proc Natl Acad Sci U S A* *101*, 4815-4820.
77. Veit, M., Soellner, T.H., and Rothman, J.E. (1996). Multiple palmitoylation of synaptotagmin and the t-SNARE SNAP-25. *FEBS Lett.* *385*, 119-123.
78. Prekeris, R., Klumperman, J., and Scheller, R.H. (2000). Syntaxin 11 is an atypical SNARE abundant in the immune system. *Eur J Cell Biol* *79*, 771-780.
79. Vogel, K., Cabaniols, J.P., and Roche, P.A. (2000). Targeting of SNAP-25 to membranes is mediated by its association with the target SNARE syntaxin. *J Biol Chem* *275*, 2959-2965.
80. Hong, W. (2005). SNAREs and traffic. *Biochim Biophys Acta* *1744*, 493-517.
81. Katz, L., Hanson, P.I., Heuser, J.E., and Brennwald, P. (1998). Genetic and morphological analyses reveal a critical interaction between the C-termini of two SNARE proteins and a parallel four helical arrangement for the exocytic SNARE complex. *Embo J* *17*, 6200-6209.
82. Sutton, R.B., Fasshauer, D., Jahn, R., and Brunger, A.T. (1998). Crystal structure of a SNARE complex involved in synaptic exocytosis at 2.4 Å resolution. *Nature* *395*, 347-353.
83. Antonin, W., Fasshauer, D., Becker, S., Jahn, R., and Schneider, T.R. (2002). Crystal structure of the endosomal SNARE complex reveals common structural principles of all SNAREs. *Nat Struct Biol* *9*, 107-111.
84. Parlati, F., McNew, J.A., Fukuda, R., Miller, R., Sollner, T.H., and Rothman, J.E. (2000). Topological restriction of SNARE-dependent membrane fusion. *Nature* *407*, 194-198.
85. Dilcher, M., Veith, B., Chidambaram, S., Hartmann, E., Schmitt, H.D., and Fischer von Mollard, G. (2003). Use1p is a yeast SNARE protein required for retrograde traffic to the ER. *Embo J* *22*, 3664-3674.
86. Chen, Y.A., and Scheller, R.H. (2001). SNARE-mediated membrane fusion. *Nat Rev Mol Cell Biol* *2*, 98-106.
87. Hay, J.C. (2001). SNARE complex structure and function. *Exp Cell Res* *271*, 10-21.
88. Pelham, H.R. (2001). SNAREs and the specificity of membrane fusion. *Trends Cell Biol* *11*, 99-101.
89. Lewis, M.J., and Pelham, H.R. (2002). A new yeast endosomal SNARE related to mammalian syntaxin 8. *Traffic* *3*, 922-929.
90. Brickner, J.H., Blanchette, J.M., Sipos, G., and Fuller, R.S. (2001). The Tlg SNARE complex is required for TGN homotypic fusion. *J Cell Biol* *155*, 969-978.
91. Dilcher, M., Kohler, B., and von Mollard, G.F. (2001). Genetic interactions with the yeast Q-SNARE VTI1 reveal novel functions for the R-SNARE YKT6. *J Biol Chem* *276*, 34537-34544.
92. Liu, Y., and Barlowe, C. (2002). Analysis of Sec22p in Endoplasmic Reticulum/Golgi Transport Reveals Cellular Redundancy in SNARE Protein Function. *Mol Biol Cell* *13*, 3314-3324.

Reference

93. Hanson, P.I., Roth, R., Morisaki, H., Jahn, R., and Heuser, J.E. (1997). Structure and conformational changes in NSF and its membrane receptor complexes visualized by quick-freeze/deep-etch electron microscopy. *Cell* 90, 523-535.
94. Lin, R.C., and Scheller, R.H. (1997). Structural organization of the synaptic exocytosis core complex. *Neuron* 19, 1087-1094.
95. Rice, L.M., and Brünger, A.T. (1999). Crystal structure of the vesicular transport protein Sec17: implications for SNAP function in SNARE complex disassembly. *Mol Cell* 4, 85-95.
96. Jahn, R., Lang, T., and Sudhof, T.C. (2003). Membrane fusion. *Cell* 112, 519-533.
97. Sudhof, T.C. (2004). The synaptic vesicle cycle. *Annu Rev Neurosci* 27, 509-547.
98. Hohl, T.M., Parlati, F., Wimmer, C., Rothman, J.E., Söllner, T.H., and Engelhardt, H. (1998). Arrangement of subunits in 20 S particles consisting of NSF, SNAPs, and SNARE complexes. *Mol Cell* 2, 539-548.
99. Brunger, A.T., and DeLaBarre, B. (2003). NSF and p97/VCP: similar at first, different at last. *FEBS Lett* 555, 126-133.
100. Mayer, A., Wickner, W., and Haas, A. (1996). Sec18p (NSF)-driven release of Sec17p (alpha-SNAP) can precede docking and fusion of yeast vacuoles. *Cell* 85, 83-94.
101. Weber, T., Zemelman, B.V., McNew, J.A., Westermann, B., Gmachl, M., Parlati, F., Sollner, T.H., and Rothman, J.E. (1998). SNAREpins: minimal machinery for membrane fusion. *Cell* 92, 759-772.
102. Hu, C., Ahmed, M., Melia, T.J., Sollner, T.H., Mayer, T., and Rothman, J.E. (2003). Fusion of cells by flipped SNAREs. *Science* 300, 1745-1749.
103. McNew, J.A., Parlati, F., Fukuda, R., Johnston, R.J., Paz, K., Paumet, F., Sollner, T.H., and Rothman, J.E. (2000). Compartmental specificity of cellular membrane fusion encoded in SNARE proteins [In Process Citation]. *Nature* 407, 153-159.
104. Bennett, M.K., and Scheller, R.H. (1993). The molecular machinery for secretion is conserved from yeast to neurons. [Review]. *Proceedings of the National Academy of Sciences of the United States of America* 90, 2559-2563.
105. Parlati, F., Varlamov, O., Paz, K., McNew, J.A., Hurtado, D., Sollner, T.H., and Rothman, J.E. (2002). Distinct SNARE complexes mediating membrane fusion in Golgi transport based on combinatorial specificity. *Proc Natl Acad Sci U S A* 99, 5424-5429.
106. Segev, N. (2001). Ypt and Rab GTPases: insight into functions through novel interactions. *Curr Opin Cell Biol* 13, 500-511.
107. Joglekar, A.P., Xu, D., Rigotti, D.J., Fairman, R., and Hay, J.C. (2003). The SNARE Motif Contributes to rbt1 Intracellular Targeting and Dynamics Independently of SNARE Interactions. *J Biol Chem* 278, 14121-14133.
108. Springer, S., and Schekman, R. (1998). Nucleation of COPII vesicular coat complex by endoplasmic reticulum to Golgi vesicle SNAREs. *Science* 281, 698-700.
109. Rein, U., Andag, U., Duden, R., Schmitt, H.D., and Spang, A. (2002). ARF-GAP-mediated interaction between the ER-Golgi v-SNAREs and the COPI coat. *J Cell Biol* 157, 395-404.
110. Miller, E.A., Beilharz, T.H., Malkus, P.N., Lee, M.C., Hamamoto, S., Orci, L., and Schekman, R. (2003). Multiple cargo binding sites on the COPII subunit Sec24p ensure capture of diverse membrane proteins into transport vesicles. *Cell* 114, 497-509.
111. Mossessova, E., Bickford, L.C., and Goldberg, J. (2003). SNARE selectivity of the COPII coat. *Cell* 114, 483-495.
112. Hirst, J., Miller, S.E., Taylor, M.J., von Mollard, G.F., and Robinson, M.S. (2004). EpsinR is an adaptor for the SNARE protein Vti1b. *Mol Biol Cell* 15, 5593-5602.

Reference

113. Deak, F., Schoch, S., Liu, X., Sudhof, T.C., and Kavalali, E.T. (2004). Synaptobrevin is essential for fast synaptic-vesicle endocytosis. *Nat Cell Biol* 6, 1102-1108.
114. Gerst, J.E. (2003). SNARE regulators: matchmakers and matchbreakers. *Biochim Biophys Acta* 1641, 99-110.
115. Elazar, Z., Scherz-Shouval, R., and Shorer, H. (2003). Involvement of LMA1 and GATE-16 family members in intracellular membrane dynamics. *Biochim Biophys Acta* 1641, 145-156.
116. Hinnert, I., Wendler, F., Fei, H., Thomas, L., Thomas, G., and Tooze, S.A. (2003). AP-1 recruitment to VAMP4 is modulated by phosphorylation-dependent binding of PACS-1. *EMBO Rep* 4, 1182-1189.
117. Xu, N.J., Yu, Y.X., Zhu, J.M., Liu, H., Shen, L., Zeng, R., Zhang, X., and Pei, G. (2004). Inhibition of SNAP-25 phosphorylation at Ser187 is involved in chronic morphine-induced down-regulation of SNARE complex formation. *J Biol Chem* 279, 40601-40608.
118. Nagy, G., Reim, K., Matti, U., Brose, N., Binz, T., Rettig, J., Neher, E., and Sorensen, J.B. (2004). Regulation of releasable vesicle pool sizes by protein kinase A-dependent phosphorylation of SNAP-25. *Neuron* 41, 417-429.
119. Polgar, J., Lane, W.S., Chung, S.H., Houg, A.K., and Reed, G.L. (2003). Phosphorylation of SNAP-23 in activated human platelets. *J Biol Chem*.
120. Hasegawa, H., Yang, Z., Olstedal, L., Davanger, S., and Hay, J.C. (2004). Intramolecular protein-protein and protein-lipid interactions control the conformation and subcellular targeting of neuronal Ykt6. *J Cell Sci* 117, 4495-4508.
121. Dietrich, L.E., Boeddinghaus, C., LaGrassa, T.J., and Ungermann, C. (2003). Control of eukaryotic membrane fusion by N-terminal domains of SNARE proteins. *Biochim Biophys Acta* 1641, 111-119.
122. Bai, J., Wang, C.T., Richards, D.A., Jackson, M.B., and Chapman, E.R. (2004). Fusion pore dynamics are regulated by synaptotagmin**t*-SNARE interactions. *Neuron* 41, 929-942.
123. McMahon, H.T., Missler, M., Li, C., and Sudhof, T.C. (1995). Complexins: cytosolic proteins that regulate SNAP receptor function. *Cell* 83, 111-119.
124. Hatsuzawa, K., Lang, T., Fasshauer, D., Bruns, D., and Jahn, R. (2003). The R-SNARE motif of tomosyn forms SNARE core complexes with syntaxin 1 and SNAP-25 and down-regulates exocytosis. *J Biol Chem* 278, 31159-31166.
125. Scales, S.J., Hesser, B.A., Masuda, E.S., and Scheller, R.H. (2002). Amisyn, a Novel Syntaxin-binding Protein That May Regulate SNARE Complex Assembly. *J Biol Chem* 277, 28271-28279.
126. Novick, P., and Schekman, R. (1979). Secretion and cell-surface growth are blocked in a temperature-sensitive mutant of *Saccharomyces cerevisiae*. *Proc Natl Acad Sci U S A* 76, 1858-1862.
127. Toonen, R.F., and Verhage, M. (2003). Vesicle trafficking: pleasure and pain from SM genes. *Trends Cell Biol* 13, 177-186.
128. Misura, K.M., Scheller, R.H., and Weis, W.I. (2000). Three-dimensional structure of the neuronal-Sec1-syntaxin 1a complex. *Nature* 404, 355-362.
129. Suzuki, T., Oiso, N., Gautam, R., Novak, E.K., Panthier, J.J., Suprabha, P.G., Vida, T., Swank, R.T., and Spritz, R.A. (2003). The mouse organellar biogenesis mutant buff results from a mutation in Vps33a, a homologue of yeast vps33 and *Drosophila* carnation. *Proc Natl Acad Sci U S A* 100, 1146-1150.
130. Gissen, P., Johnson, C.A., Morgan, N.V., Stapelbroek, J.M., Forshew, T., Cooper, W.N., McKiernan, P.J., Klomp, L.W., Morris, A.A., Wraith, J.E., McClean, P., Lynch, S.A., Thompson, R.J., Lo, B., Quarrell, O.W., Di Rocco, M., Trembath, R.C., Mandel, H., Wali, S., Karet, F.E., Knisely, A.S., Houwen, R.H., Kelly, D.A., and Maher, E.R.

Reference

- (2004). Mutations in VPS33B, encoding a regulator of SNARE-dependent membrane fusion, cause arthrogyryposis-renal dysfunction-cholestasis (ARC) syndrome. *Nat Genet* 36, 400-404.
131. Gallwitz, D., and Jahn, R. (2003). The riddle of the Sec1/Munc-18 proteins - new twists added to their interactions with SNAREs. *Trends Biochem Sci* 28, 113-116.
132. Dulubova, I., Yamaguchi, T., Gao, Y., Min, S.W., Huryeva, I., Sudhof, T.C., and Rizo, J. (2002). How Tlg2p/syntaxin 16 'snares' Vps45. *Embo J* 21, 3620-3631.
133. Yamaguchi, T., Dulubova, I., Min, S.W., Chen, X., Rizo, J., and Sudhof, T.C. (2002). Sly1 binds to Golgi and ER syntaxins via a conserved N-terminal peptide motif. *Dev Cell* 2, 295-305.
134. Echard, A., Jollivet, F., Martinez, O., Lacapere, J.J., Rousselet, A., Janoueix-Lerosey, I., and Goud, B. (1998). Interaction of a Golgi-associated kinesin-like protein with Rab6. *Science* 279, 580-585.
135. Rybin, V., Ullrich, O., Rubino, M., Alexandrov, K., Simon, I., Seabra, M.C., Goody, R., and Zerial, M. (1996). GTPase activity of Rab5 acts as a timer for endocytic membrane fusion. *Nature* 383, 266-269.
136. Zerial, M., and McBride, H. (2001). Rab proteins as membrane organizers. *Nat Rev Mol Cell Biol* 2, 107-117.
137. Gillingham, A.K., and Munro, S. (2003). Long coiled-coil proteins and membrane traffic. *Biochim Biophys Acta* 1641, 71-85.
138. Whyte, J.R., and Munro, S. (2002). Vesicle tethering complexes in membrane traffic. *J Cell Sci* 115, 2627-2637.
139. Guo, S., Stolz, L.E., Lemrow, S.M., and York, J.D. (1999). SAC1-like domains of yeast SAC1, INP52, and INP53 and of human synaptojanin encode polyphosphoinositide phosphatases. *J Biol Chem* 274, 12990-12995.
140. Schekman, R., and Novick, P. (2004). 23 genes, 23 years later. *Cell* 116, S13-15, 11 p following S19.
141. Ungar, D., Oka, T., Brittle, E.E., Vasile, E., Lupashin, V.V., Chatterton, J.E., Heuser, J.E., Krieger, M., and Waters, M.G. (2002). Characterization of a mammalian Golgi-localized protein complex, COG, that is required for normal Golgi morphology and function. *J Cell Biol* 157, 405-415.
142. Shorter, J., and Warren, G. (2002). Golgi architecture and inheritance. *Annu Rev Cell Dev Biol* 18, 379-420.
143. Muller, J.M., Shorter, J., Newman, R., Deinhardt, K., Sagiv, Y., Elazar, Z., Warren, G., and Shima, D.T. (2002). Sequential SNARE disassembly and GATE-16-GOS-28 complex assembly mediated by distinct NSF activities drives Golgi membrane fusion. *J Cell Biol* 157, 1161-1173.
144. Sun, W., Yan, Q., Vida, T.A., and Bean, A.J. (2003). Hrs regulates early endosome fusion by inhibiting formation of an endosomal SNARE complex. *J Cell Biol* 162, 125-137.
145. Barr, F.A., and Short, B. (2003). Golgins in the structure and dynamics of the Golgi apparatus. *Curr Opin Cell Biol* 15, 405-413.
146. McBride, H.M., Rybin, V., Murphy, C., Giner, A., Teasdale, R., and Zerial, M. (1999). Oligomeric complexes link Rab5 effectors with NSF and drive membrane fusion via interactions between EEA1 and syntaxin 13. *Cell* 98, 377-386.
147. Lewis, M.J., and Pelham, H.R. (1990). A human homologue of the yeast HDEL receptor. *Nature* 348, 162-163.
148. Semenza, J.C., Hardwick, K.G., Dean, N., and Pelham, H.R. (1990). ERD2, a yeast gene required for the receptor-mediated retrieval of luminal ER proteins from the secretory pathway. *Cell* 61, 1349-1357.

Reference

149. Letourneur, F., Gaynor, E.C., Hennecke, S., Demolliere, C., Duden, R., Emr, S.D., Riezman, H., and Cosson, P. (1994). Coatamer is essential for retrieval of dilysine-tagged proteins to the endoplasmic reticulum. *Cell* 79, 1199-1207.
150. Sato, K., Sato, M., and Nakano, A. (1997). Rer1p as common machinery for the endoplasmic reticulum localization of membrane proteins. *Proc Natl Acad Sci U S A* 94, 9693-9698.
151. Schekman, R., and Orci, L. (1996). Coat proteins and vesicle budding. *Science* 271, 1526-1533.
152. McNew, J.A., Sogaard, M., Lampen, N.M., Machida, S., Ye, R.R., Lacomis, L., Tempst, P., Rothman, J.E., and Sollner, T.H. (1997). Ykt6p, a prenylated SNARE essential for endoplasmic reticulum-Golgi transport. *J Biol Chem* 272, 17776-17783.
153. Gaynor, E.C., Graham, T.R., and Emr, S.D. (1998). COPI in ER/Golgi and intra-Golgi transport: do yeast COPI mutants point the way? *Biochim Biophys Acta* 1404, 33-51.
154. Barlowe, C. (1998). COPII and selective export from the endoplasmic reticulum. *Biochim Biophys Acta* 1404, 67-76.
155. Dominguez, M., Dejgaard, K., Fullekrug, J., Dahan, S., Fazel, A., Paccaud, J.P., Thomas, D.Y., Bergeron, J.J., and Nilsson, T. (1998). gp25L/emp24/p24 protein family members of the cis-Golgi network bind both COP I and II coatamer. *J Cell Biol* 140, 751-765.
156. Hauri, H.P., and Schweizer, A. (1992). The endoplasmic reticulum-Golgi intermediate compartment. *Curr Opin Cell Biol* 4, 600-608.
157. Wieland, F., and Harter, C. (1999). Mechanisms of vesicle formation: insights from the COP system. *Curr Opin Cell Biol* 11, 440-446.
158. Orci, L., Starnes, M., Ravazzola, M., Amherdt, M., Perrelet, A., Sollner, T.H., and Rothman, J.E. (1997). Bidirectional transport by distinct populations of COPI-coated vesicles. *Cell* 90, 335-349.
159. Fra, A.M., Fagioli, C., Finazzi, D., Sitia, R., and Alberini, C.M. (1993). Quality control of ER synthesized proteins: an exposed thiol group as a three-way switch mediating assembly, retention and degradation. *Embo J* 12, 4755-4761.
160. Hurlley, S.M., and Helenius, A. (1989). Protein oligomerization in the endoplasmic reticulum. *Annu Rev Cell Biol* 5, 277-307.
161. Klausner, R.D., and Sitia, R. (1990). Protein degradation in the endoplasmic reticulum. *Cell* 62, 611-614.
162. Terasaki, M., Chen, L.B., and Fujiwara, K. (1986). Microtubules and the endoplasmic reticulum are highly interdependent structures. *J Cell Biol* 103, 1557-1568.
163. Mizuno, M., and Singer, S.J. (1993). A soluble secretory protein is first concentrated in the endoplasmic reticulum before transfer to the Golgi apparatus. *Proc Natl Acad Sci U S A* 90, 5732-5736.
164. Balch, W.E., McCaffery, J.M., Plutner, H., and Farquhar, M.G. (1994). Vesicular stomatitis virus glycoprotein is sorted and concentrated during export from the endoplasmic reticulum. *Cell* 76, 841-852.
165. Presley, J.F., Cole, N.B., Schroer, T.A., Hirschberg, K., Zaal, K.J., and Lippincott-Schwartz, J. (1997). ER-to-Golgi transport visualized in living cells. *Nature* 389, 81-85.
166. Schweizer, A., Fransen, J.A., Matter, K., Kreis, T.E., Ginsel, L., and Hauri, H.P. (1990). Identification of an intermediate compartment involved in protein transport from endoplasmic reticulum to Golgi apparatus. *Eur J Cell Biol* 53, 185-196.
167. Saraste, J., and Svensson, K. (1991). Distribution of the intermediate elements operating in ER to Golgi transport. *J Cell Sci* 100 (Pt 3), 415-430.

Reference

168. Clermont, Y., Rambourg, A., and Hermo, L. (1994). Connections between the various elements of the cis- and mid-compartments of the Golgi apparatus of early rat spermatids. *Anat Rec* 240, 469-480.
169. Cole, N.B., Sciaky, N., Marotta, A., Song, J., and Lippincott-Schwartz, J. (1996). Golgi dispersal during microtubule disruption: regeneration of Golgi stacks at peripheral endoplasmic reticulum exit sites. *Mol Biol Cell* 7, 631-650.
170. Farquhar, M.G., and Palade, G.E. (1998). The Golgi apparatus: 100 years of progress and controversy. *Trends Cell Biol* 8, 2-10.
171. Rambourg, A., and Clermont, Y. (1990). Three-dimensional electron microscopy: structure of the Golgi apparatus. *Eur J Cell Biol* 51, 189-200.
172. Kornfeld, R., and Kornfeld, S. (1985). Assembly of asparagine-linked oligosaccharides. *Annu Rev Biochem* 54, 631-664.
173. Mellman, I., and Simons, K. (1992). The Golgi complex: in vitro veritas? *Cell* 68, 829-840.
174. Marsh, B.J., and Howell, K.E. (2002). The mammalian Golgi--complex debates. *Nat Rev Mol Cell Biol* 3, 789-795.
175. Harter, C., and Wieland, F. (1996). The secretory pathway: mechanisms of protein sorting and transport. *Biochim Biophys Acta* 1286, 75-93.
176. Sitia, R., and Meldolesi, J. (1992). Endoplasmic reticulum: a dynamic patchwork of specialized subregions. *Mol Biol Cell* 3, 1067-1072.
177. Pelham, H.R. (1989). Control of protein exit from the endoplasmic reticulum. *Annu Rev Cell Biol* 5, 1-23.
178. Lotti, L.V., Torrisi, M.R., Pascale, M.C., and Bonatti, S. (1992). Immunocytochemical analysis of the transfer of vesicular stomatitis virus G glycoprotein from the intermediate compartment to the Golgi complex. *J Cell Biol* 118, 43-50.
179. Scales, S.J., Pepperkok, R., and Kreis, T.E. (1997). Visualization of ER-to-Golgi transport in living cells reveals a sequential mode of action for COPII and COPI. *Cell* 90, 1137-1148.
180. Tang, B.L., Low, S.H., Hauri, H.P., and Hong, W. (1995). Segregation of ERGIC53 and the mammalian KDEL receptor upon exit from the 15 degrees C compartment. *Eur J Cell Biol* 68, 398-410.
181. Rowe, T., Dascher, C., Bannykh, S., Plutner, H., and Balch, W.E. (1998). Role of vesicle-associated syntaxin 5 in the assembly of pre-Golgi intermediates. *Science* 279, 696-700.
182. Saraste, J., and Kuismanen, E. (1992). Pathways of protein sorting and membrane traffic between the rough endoplasmic reticulum and the Golgi complex. *Semin Cell Biol* 3, 343-355.
183. Lippincott-Schwartz, J. (1993). Bidirectional membrane traffic between the endoplasmic reticulum and Golgi apparatus. *Trends Cell Biol* 3, 81-88.
184. Bannykh, S.I., and Balch, W.E. (1997). Membrane dynamics at the endoplasmic reticulum-Golgi interface. *J Cell Biol* 138, 1-4.
185. Glick, B.S., Elston, T., and Oster, G. (1997). A cisternal maturation mechanism can explain the asymmetry of the Golgi stack. *FEBS Lett* 414, 177-181.
186. Mironov, A.A., Weidman, P., and Luini, A. (1997). Variations on the intracellular transport theme: maturing cisternae and trafficking tubules. *J Cell Biol* 138, 481-484.
187. Pelham, H.R. (1998). Getting through the Golgi complex. *Trends Cell Biol* 8, 45-49.
188. Sato, K., Nishikawa, S., and Nakano, A. (1995). Membrane protein retrieval from the Golgi apparatus to the endoplasmic reticulum (ER): characterization of the RER1 gene product as a component involved in ER localization of Sec12p. *Molecular Biology of the Cell* 6, 1459-1477.

Reference

189. Zhang, T., Wong, S.H., Tang, B.L., Xu, Y., Peter, F., Subramaniam, V.N., and Hong, W. (1997). The mammalian protein (rbet1) homologous to yeast Bet1p is primarily associated with the pre-Golgi intermediate compartment and is involved in vesicular transport from the endoplasmic reticulum to the Golgi apparatus. *J Cell Biol* *139*, 1157-1168.
190. Hammond, C., and Helenius, A. (1994). Quality control in the secretory pathway: retention of a misfolded viral membrane glycoprotein involves cycling between the ER, intermediate compartment, and Golgi apparatus. *J Cell Biol* *126*, 41-52.
191. Vashist, S., Kim, W., Belden, W.J., Spear, E.D., Barlowe, C., and Ng, D.T. (2001). Distinct retrieval and retention mechanisms are required for the quality control of endoplasmic reticulum protein folding. *J Cell Biol* *155*, 355-368.
192. Storrie, B., White, J., Rottger, S., Stelzer, E.H., Sukanuma, T., and Nilsson, T. (1998). Recycling of golgi-resident glycosyltransferases through the ER reveals a novel pathway and provides an explanation for nocodazole-induced Golgi scattering. *J Cell Biol* *143*, 1505-1521.
193. Cole, N.B., Ellenberg, J., Song, J., DiEuliis, D., and Lippincott-Schwartz, J. (1998). Retrograde transport of Golgi-localized proteins to the ER. *J Cell Biol* *140*, 1-15.
194. Lord, J.M., and Roberts, L.M. (1998). Toxin entry: retrograde transport through the secretory pathway. *J Cell Biol* *140*, 733-736.
195. Zaal, K.J., Smith, C.L., Polishchuk, R.S., Altan, N., Cole, N.B., Ellenberg, J., Hirschberg, K., Presley, J.F., Roberts, T.H., Siggia, E., Phair, R.D., and Lippincott-Schwartz, J. (1999). Golgi membranes are absorbed into and reemerge from the ER during mitosis. *Cell* *99*, 589-601.
196. Munro, S., and Pelham, H.R. (1987). A C-terminal signal prevents secretion of luminal ER proteins. *Cell* *48*, 899-907.
197. Pelham, H.R. (1988). Evidence that luminal ER proteins are sorted from secreted proteins in a post-ER compartment. *Embo J* *7*, 913-918.
198. Yamamoto, K., Fujii, R., Toyofuku, Y., Saito, T., Koseki, H., Hsu, V.W., and Aoe, T. (2001). The KDEL receptor mediates a retrieval mechanism that contributes to quality control at the endoplasmic reticulum. *Embo J* *20*, 3082-3091.
199. Jackson, M.R., Nilsson, T., and Peterson, P.A. (1990). Identification of a consensus motif for retention of transmembrane proteins in the endoplasmic reticulum. *Embo J* *9*, 3153-3162.
200. Jackson, M.R., Nilsson, T., and Peterson, P.A. (1993). Retrieval of transmembrane proteins to the endoplasmic reticulum. *J Cell Biol* *121*, 317-333.
201. Wilson, B.S., Palade, G.E., and Farquhar, M.G. (1993). Endoplasmic reticulum-through-Golgi transport assay based on O-glycosylation of native glycophorin in permeabilized erythroleukemia cells: role for Gi3. *Proc Natl Acad Sci U S A* *90*, 1681-1685.
202. Lewis, M.J., and Pelham, H.R. (1992). Sequence of a second human KDEL receptor. *J Mol Biol* *226*, 913-916.
203. Pelham, H.R. (1994). About turn for the COPs? *Cell* *79*, 1125-1127.
204. Sciaky, N., Presley, J., Smith, C., Zaal, K.J., Cole, N., Moreira, J.E., Terasaki, M., Siggia, E., and Lippincott-Schwartz, J. (1997). Golgi tubule traffic and the effects of brefeldin A visualized in living cells. *J Cell Biol* *139*, 1137-1155.
205. Richards, A.A., Stang, E., Pepperkok, R., and Parton, R.G. (2002). Inhibitors of COP-mediated transport and cholera toxin action inhibit simian virus 40 infection. *Mol Biol Cell* *13*, 1750-1764.
206. Majoul, I., Sohn, K., Wieland, F.T., Pepperkok, R., Pizza, M., Hillemann, J., and Soling, H.D. (1998). KDEL receptor (Erd2p)-mediated retrograde transport of the

Reference

- cholera toxin A subunit from the Golgi involves COPI, p23, and the COOH terminus of Erd2p. *J Cell Biol* *143*, 601-612.
207. Aoe, T., Lee, A.J., van Donselaar, E., Peters, P.J., and Hsu, V.W. (1998). Modulation of intracellular transport by transported proteins: insight from regulation of COPI-mediated transport. *Proc Natl Acad Sci U S A* *95*, 1624-1629.
208. Cabrera, M., Muniz, M., Hidalgo, J., Vega, L., Martin, M.E., and Velasco, A. (2003). The retrieval function of the KDEL receptor requires PKA phosphorylation of its C-terminus. *Mol Biol Cell* *14*, 4114-4125.
209. White, J., Johannes, L., Mallard, F., Girod, A., Grill, S., Reinsch, S., Keller, P., Tzschaschel, B., Echard, A., Goud, B., and Stelzer, E.H. (1999). Rab6 coordinates a novel Golgi to ER retrograde transport pathway in live cells. *J Cell Biol* *147*, 743-760.
210. Girod, A., Storrie, B., Simpson, J.C., Johannes, L., Goud, B., Roberts, L.M., Lord, J.M., Nilsson, T., and Pepperkok, R. (1999). Evidence for a COP-I-independent transport route from the Golgi complex to the endoplasmic reticulum. *Nat Cell Biol* *1*, 423-430.
211. Klumperman, J., Schweizer, A., Clausen, H., Tang, B.L., Hong, W., Oorschot, V., and Hauri, H.P. (1998). The recycling pathway of protein ERGIC-53 and dynamics of the ER-Golgi intermediate compartment. *J Cell Sci* *111* (Pt 22), 3411-3425.
212. Lippincott-Schwartz, J., Cole, N.B., and Donaldson, J.G. (1998). Building a secretory apparatus: role of ARF1/COPI in Golgi biogenesis and maintenance. *Histochem Cell Biol* *109*, 449-462.
213. Malsam, J., Satoh, A., Pelletier, L., and Warren, G. (2005). Golgin tethers define subpopulations of COPI vesicles. *Science* *307*, 1095-1098.
214. Trucco, A., Polishchuk, R.S., Martella, O., Di Pentima, A., Fusella, A., Di Giandomenico, D., San Pietro, E., Beznoussenko, G.V., Polishchuk, E.V., Baldassarre, M., Buccione, R., Geerts, W.J., Koster, A.J., Burger, K.N., Mironov, A.A., and Luini, A. (2004). Secretory traffic triggers the formation of tubular continuities across Golgi sub-compartments. *Nat Cell Biol* *6*, 1071-1081.
215. Lowe, M., and Kreis, T.E. (1998). Regulation of membrane traffic in animal cells by COPI. *Biochim Biophys Acta* *1404*, 53-66.
216. Shima, D.T., Scales, S.J., Kreis, T.E., and Pepperkok, R. (1999). Segregation of COPI-rich and anterograde-cargo-rich domains in endoplasmic-reticulum-to-Golgi transport complexes. *Curr Biol* *9*, 821-824.
217. Olgart, C., Gustafsson, L.E., and Wiklund, N.P. (2000). Evidence for nonvesicular nitric oxide release evoked by nerve activation. *Eur J Neurosci* *12*, 1303-1309.
218. Zhang, T., Wong, S.H., Tang, B.L., Xu, Y., and Hong, W. (1999). Morphological and functional association of Sec22b/ERS-24 with the pre- Golgi intermediate compartment. *Mol Biol Cell* *10*, 435-453.
219. Zhang, T., and Hong, W. (2001). Ykt6 forms a SNARE complex with syntaxin 5, GS28 and Bet1 and participates in a late stage in ER-Golgi transport. *J Biol Chem* *275*, 25.
220. Shorter, J., Beard, M.B., Seemann, J., Dirac-Svejstrup, A.B., and Warren, G. (2002). Sequential tethering of Golgins and catalysis of SNAREpin assembly by the vesicle-tethering protein p115. *J Cell Biol* *157*, 45-62.
221. Xu, Y., Martin, S., James, D.E., and Hong, W. (2002). GS15 forms a SNARE complex with syntaxin 5, GS28, and Ykt6 and is implicated in traffic in the early cisternae of the Golgi apparatus. *Mol Biol Cell* *13*, 3493-3507.
222. Hatsuzawa, K., Hirose, H., Tani, K., Yamamoto, A., Scheller, R.H., and Tagaya, M. (2000). Syntaxin 18, a SNAP receptor that functions in the endoplasmic reticulum, intermediate compartment, and cis-Golgi vesicle trafficking. *J Biol Chem* *275*, 13713-13720.

Reference

-
223. Lewis, M.J., Rayner, J.C., and Pelham, H.R. (1997). A novel SNARE complex implicated in vesicle fusion with the endoplasmic reticulum. *Embo J* 16, 3017-3024.
224. Burri, L., Varlamov, O., Doege, C.A., Hofmann, K., Beilharz, T., Rothman, J.E., Sollner, T.H., and Lithgow, T. (2003). A SNARE required for retrograde transport to the endoplasmic reticulum. *Proc Natl Acad Sci U S A* 100, 9873-9877.
225. Sweet, D.J., and Pelham, H.R. (1993). The TIP1 gene of *Saccharomyces cerevisiae* encodes an 80 kDa cytoplasmic protein that interacts with the cytoplasmic domain of Sec20p. *Embo J* 12, 2831-2840.
226. Nakajima, K., Hirose, H., Taniguchi, M., Kurashina, H., Arasaki, K., Nagahama, M., Tani, K., Yamamoto, A., and Tagaya, M. (2004). Involvement of BNIP1 in apoptosis and endoplasmic reticulum membrane fusion. *Embo J* 23, 3216-3226.
227. Hirose, H., Arasaki, K., Dohmae, N., Takio, K., Hatsuzawa, K., Nagahama, M., Tani, K., Yamamoto, A., Tohyama, M., and Tagaya, M. (2004). Implication of ZW10 in membrane trafficking between the endoplasmic reticulum and Golgi. *Embo J* 23, 1267-1278.
228. Gonzalez, L.C., Jr., Weis, W.I., and Scheller, R.H. (2001). A novel snare N-terminal domain revealed by the crystal structure of Sec22b. *J Biol Chem* 276, 24203-24211.
229. Tochio, H., Tsui, M.M., Banfield, D.K., and Zhang, M. (2001). An autoinhibitory mechanism for nonsyntaxin SNARE proteins revealed by the structure of Ykt6p. *Science* 293, 698-702.
230. Jang, S.B., Kim, Y.G., Cho, Y.S., Suh, P.G., Kim, K.H., and Oh, B.H. (2002). Crystal structure of SEDL and its implications for a genetic disease spondyloepiphyseal dysplasia tarda. *J Biol Chem* 277, 49863-49869.
231. Gill, D.M. (1976). The arrangement of subunits in cholera toxin. *Biochemistry* 15, 1242-1248.
232. Spangler, B.D. (1992). Structure and function of cholera toxin and the related *Escherichia coli* heat-labile enterotoxin. *Microbiol Rev* 56, 622-647.
233. Simons, K., and Ikonen, E. (1997). Functional rafts in cell membranes. *Nature* 387, 569-572.
234. London, E., and Brown, D.A. (2000). Insolubility of lipids in triton X-100: physical origin and relationship to sphingolipid/cholesterol membrane domains (rafts). *Biochim Biophys Acta* 1508, 182-195.
235. Wolf, A.A., Fujinaga, Y., and Lencer, W.I. (2002). Uncoupling of the cholera toxin-G(M1) ganglioside receptor complex from endocytosis, retrograde Golgi trafficking, and downstream signal transduction by depletion of membrane cholesterol. *J Biol Chem* 277, 16249-16256.
236. Orlandi, P.A., and Fishman, P.H. (1998). Filipin-dependent inhibition of cholera toxin: evidence for toxin internalization and activation through caveolae-like domains. *J Cell Biol* 141, 905-915.
237. Cuatrecasas, P. (1973). Gangliosides and membrane receptors for cholera toxin. *Biochemistry* 12, 3558-3566.
238. Montesano, R., Roth, J., Robert, A., and Orci, L. (1982). Non-coated membrane invaginations are involved in binding and internalization of cholera and tetanus toxins. *Nature* 296, 651-653.
239. Majoul, I.V., Bastiaens, P.I., and Soling, H.D. (1996). Transport of an external Lys-Asp-Glu-Leu (KDEL) protein from the plasma membrane to the endoplasmic reticulum: studies with cholera toxin in Vero cells. *J Cell Biol* 133, 777-789.
240. Fujinaga, Y., Wolf, A.A., Rodighiero, C., Wheeler, H., Tsai, B., Allen, L., Jobling, M.G., Rapoport, T., Holmes, R.K., and Lencer, W.I. (2003). Gangliosides that associate with lipid rafts mediate transport of cholera and related toxins from the plasma membrane to endoplasmic reticulum. *Mol Biol Cell* 14, 4783-4793.

Reference

241. Lencer, W.I., Constable, C., Moe, S., Jobling, M.G., Webb, H.M., Ruston, S., Madara, J.L., Hirst, T.R., and Holmes, R.K. (1995). Targeting of cholera toxin and Escherichia coli heat labile toxin in polarized epithelia: role of COOH-terminal KDEL. *J Cell Biol* 131, 951-962.
242. Tsai, B., Ye, Y., and Rapoport, T.A. (2002). Retro-translocation of proteins from the endoplasmic reticulum into the cytosol. *Nat Rev Mol Cell Biol* 3, 246-255.
243. Gill, D.M., and Meren, R. (1978). ADP-ribosylation of membrane proteins catalyzed by cholera toxin: basis of the activation of adenylate cyclase. *Proc Natl Acad Sci U S A* 75, 3050-3054.
244. Katada, T., Oinuma, M., and Ui, M. (1986). Mechanisms for inhibition of the catalytic activity of adenylate cyclase by the guanine nucleotide-binding proteins serving as the substrate of islet-activating protein, pertussis toxin. *J Biol Chem* 261, 5215-5221.
245. Bachmann, B.J. (1987). Linkage map of Escherichia coli K12. In: *Escherichia coli and Salmonella typhimurium* (Washington D.C., USA: American Society for Microbiology).
246. Chester, N., and Marshak, D.R. (1993). Dimethyl sulfoxide-mediated primer Tm reduction: a method for analyzing the role of renaturation temperature in the polymerase chain reaction. *Anal Biochem* 209, 284-290.
247. Inoue, H., Nojima, H., and Okayama, H. (1990). High efficiency transformation of Escherichia coli with plasmids. *Gene* 96, 23-28.
248. Bradford, M.M. (1976). A rapid and sensitive method for the quantitation of microgram quantities of protein utilizing the principle of protein-dye binding. *Anal Biochem* 72, 248-254.
249. Odgen, R.C., and Adams, D.A. (1987). Electrophoresis in agarose and acrylamide gels. *Methods Enzymol.* 152, 61-87.
250. Weber, K., and Osborn, M. (1969). The reliability of molecular weight determinations by dodecyl sulfate-polyacrylamide gel electrophoresis. *J Biol Chem* 244, 4406-4412.
251. Laemmli, U.K. (1970). Cleavage of structural proteins during the assembly of the head of bacteriophage T4. *Nature* 227, 680-685.
252. Vaux, D., Tooze, J., and Fuller, S. (1990). Identification by anti-idiotypic antibodies of an intracellular membrane protein that recognizes a mammalian endoplasmic reticulum retention signal. *Nature* 345, 495-502.
253. Elbashir, S.M., Harborth, J., Weber, K., and Tuschl, T. (2002). Analysis of gene function in somatic mammalian cells using small interfering RNAs. *Methods* 26, 199-213.
254. Wessel, D., and Flugge, U.I. (1984). A method for the quantitative recovery of protein in dilute solution in the presence of detergents and lipids. *Anal Biochem* 138, 141-143.
255. Pelham, H.R., and Jackson, R.J. (1976). An efficient mRNA-dependent translation system from reticulocyte lysates. *Eur J Biochem* 67, 247-256.
256. Anderson, C.W., Straus, J.W., and Dudock, B.S. (1983). Preparation of a cell-free protein-synthesizing system from wheat germ. *Methods Enzymol* 101, 635-644.
257. Förster, T. (1948). Intermolecular energy migration and fluorescence. *Ann.Phys.* 2, 55-75.
258. Zimmermann, T., Rietdorf, J., Girod, A., Georget, V., and Pepperkok, R. (2002). Spectral imaging and linear un-mixing enables improved FRET efficiency with a novel GFP2-YFP FRET pair. *FEBS Lett* 531, 245-249.
259. Nagai, T., Ibata, K., Park, E.S., Kubota, M., Mikoshiba, K., and Miyawaki, A. (2002). A variant of yellow fluorescent protein with fast and efficient maturation for cell-biological applications. *Nat Biotechnol* 20, 87-90.
260. Patterson, G., Day, R.N., and Piston, D. (2001). Fluorescent protein spectra. *J Cell Sci* 114, 837-838.

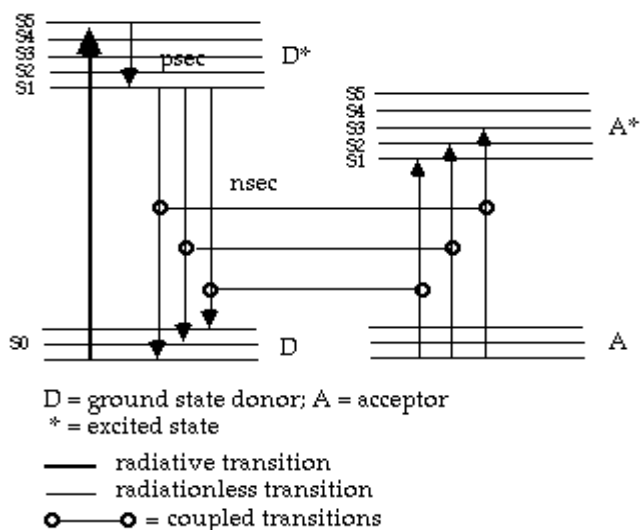
Reference

261. Gordon, G.W., Berry, G., Liang, X.H., Levine, B., and Herman, B. (1998). Quantitative fluorescence resonance energy transfer measurements using fluorescence microscopy. *Biophys J* 74, 2702-2713.
262. Xia, Z., and Liu, Y. (2001). Reliable and global measurement of fluorescence resonance energy transfer using fluorescence microscopes. *Biophys J* 81, 2395-2402.
263. Hu, C.D., Chinenov, Y., and Kerppola, T.K. (2002). Visualization of interactions among bZIP and Rel family proteins in living cells using bimolecular fluorescence complementation. *Mol Cell* 9, 789-798.
264. Hui, N., Nakamura, N., Slusarewicz, P., and Warren, G. (1998). Purification of Rat Liver Golgi Stacks, Volume 2, second edition Edition (Aarhus, Denmark: Academic Press).
265. Hay, J.C., Hirling, H., and Scheller, R.H. (1996). Mammalian vesicle trafficking proteins of the endoplasmic reticulum and Golgi apparatus. *J Biol Chem* 271, 5671-5679.
266. Bracher, A., and Weissenhorn, W. (2002). Structural basis for the Golgi membrane recruitment of Sly1p by Sed5p. *Embo J* 21, 6114-6124.
267. Dulubova, I., Yamaguchi, T., Arac, D., Li, H., Huryeva, I., Min, S.W., Rizo, J., and Sudhof, T.C. (2003). Convergence and divergence in the mechanism of SNARE binding by Sec1/Munc18-like proteins. *Proc Natl Acad Sci U S A* 100, 32-37.
268. Filippini, F., Rossi, V., Galli, T., Budillon, A., D'Urso, M., and D'Esposito, M. (2001). Longins: a new evolutionary conserved VAMP family sharing a novel SNARE domain. *Trends Biochem Sci* 26, 407-409.
269. Rossi, V., Banfield, D.K., Vacca, M., Dietrich, L.E., Ungermann, C., D'Esposito, M., Galli, T., and Filippini, F. (2004). Longins and their longin domains: regulated SNAREs and multifunctional SNARE regulators. *Trends Biochem Sci* 29, 682-688.
270. Gonzalez, L.C., Jr., Weis, W.I., and Scheller, R.H. (2001). A novel SNARE N-terminal domain revealed by the crystal structure of Sec22b. *J Biol Chem* 276, 17.
271. Tsien, R.Y., and Miyawaki, A. (1998). Seeing the machinery of live cells. *Science* 280, 1954-1955.
272. Pollok, B.A., and Heim, R. (1999). Using GFP in FRET-based applications. *Trends Cell Biol* 9, 57-60.
273. Heim, R. (1999). Green fluorescent protein forms for energy transfer. *Methods Enzymol* 302, 408-423.
274. Egner, A., Verrier, S., Goroshkov, A., Soling, H.D., and Hell, S.W. (2004). 4Pi-microscopy of the Golgi apparatus in live mammalian cells. *J Struct Biol* 147, 70-76.
275. Munro, S. (1995). A comparison of the transmembrane domains of Golgi and plasma membrane proteins. *Biochem Soc Trans* 23, 527-530.
276. Colley, K.J. (1997). Golgi localization of glycosyltransferases: more questions than answers. *Glycobiology* 7, 1-13.
277. Yang, M., Ellenberg, J., Bonifacino, J.S., and Weissman, A.M. (1997). The transmembrane domain of a carboxyl-terminal anchored protein determines localization to the endoplasmic reticulum. *J Biol Chem* 272, 1970-1975.
278. Hay, J.C., Chao, D.S., Kuo, C.S., and Scheller, R.H. (1997). Protein interactions regulating vesicle transport between the endoplasmic reticulum and Golgi apparatus in mammalian cells. *Cell* 89, 149-158.
279. Liu, Y., Flanagan, J.J., and Barlowe, C. (2004). Sec22p export from the endoplasmic reticulum is independent of SNARE pairing. *J Biol Chem* 279, 27225-27232.
280. Schuette, C.G., Hatsuzawa, K., Margittai, M., Stein, A., Riedel, D., Kuster, P., Konig, M., Seidel, C., and Jahn, R. (2004). Determinants of liposome fusion mediated by synaptic SNARE proteins. *Proc Natl Acad Sci U S A* 101, 2858-2863.

Reference

281. Waters, M.G., and Hughson, F.M. (2000). Membrane tethering and fusion in the secretory and endocytic pathways. *Traffic* 1, 588-597.
282. Fernandez, I., Ubach, J., Dulubova, I., Zhang, X., Südhof, T.C., and Rizo, J. (1998). Three-dimensional structure of an evolutionarily conserved N-terminal domain of syntaxin 1A. *Cell* 94, 841-849.
283. Munson, M., and Hughson, F.M. (2002). Conformational regulation of SNARE assembly and disassembly in vivo. *J Biol Chem* 277, 9375-9381.
284. Gaynor, E.C., te Heesen, S., Graham, T.R., Aebi, M., and Emr, S.D. (1994). Signal-mediated retrieval of a membrane protein from the Golgi to the ER in yeast. *J Cell Biol* 127, 653-665.
285. Scheel, J., Pepperkok, R., Lowe, M., Griffiths, G., and Kreis, T.E. (1997). Dissociation of coatamer from membranes is required for brefeldin A-induced transfer of Golgi enzymes to the endoplasmic reticulum. *J Cell Biol* 137, 319-333.
286. Johannes, L., Tenza, D., Antony, C., and Goud, B. (1997). Retrograde transport of KDEL-bearing B-fragment of Shiga toxin. *J Biol Chem* 272, 19554-19561.
287. Hsu, V.W., Shah, N., and Klausner, R.D. (1992). A brefeldin A-like phenotype is induced by the overexpression of a human ERD-2-like protein, ELP-1. *Cell* 69, 625-635.
288. Munro, S. (2003). Lipid rafts: elusive or illusive? *Cell* 115, 377-388.
289. De Matteis, M., Godi, A., and Corda, D. (2002). Phosphoinositides and the golgi complex. *Curr Opin Cell Biol* 14, 434-447.
290. Wang, Y.J., Wang, J., Sun, H.Q., Martinez, M., Sun, Y.X., Macia, E., Kirchhausen, T., Albanesi, J.P., Roth, M.G., and Yin, H.L. (2003). Phosphatidylinositol 4 phosphate regulates targeting of clathrin adaptor AP-1 complexes to the Golgi. *Cell* 114, 299-310.
291. Duran, J.M., Valderrama, F., Castel, S., Magdalena, J., Tomas, M., Hosoya, H., Renau-Piqueras, J., Malhotra, V., and Egea, G. (2003). Myosin motors and not actin comets are mediators of the actin-based Golgi-to-endoplasmic reticulum protein transport. *Mol Biol Cell* 14, 445-459.
292. Aridor, M., Bannykh, S.I., Rowe, T., and Balch, W.E. (1995). Sequential coupling between COPII and COPI vesicle coats in endoplasmic reticulum to Golgi transport. *J Cell Biol* 131, 875-893.
293. Mironov, A.A., Mironov, A.A., Jr., Beznoussenko, G.V., Trucco, A., Lupetti, P., Smith, J.D., Geerts, W.J., Koster, A.J., Burger, K.N., Martone, M.E., Deerinck, T.J., Ellisman, M.H., and Luini, A. (2003). ER-to-Golgi carriers arise through direct en bloc protrusion and multistage maturation of specialized ER exit domains. *Dev Cell* 5, 583-594.
294. Klar, T.A., Jakobs, S., Dyba, M., Egner, A., and Hell, S.W. (2000). Fluorescence microscopy with diffraction resolution barrier broken by stimulated emission. *Proc Natl Acad Sci U S A* 97, 8206-8210.

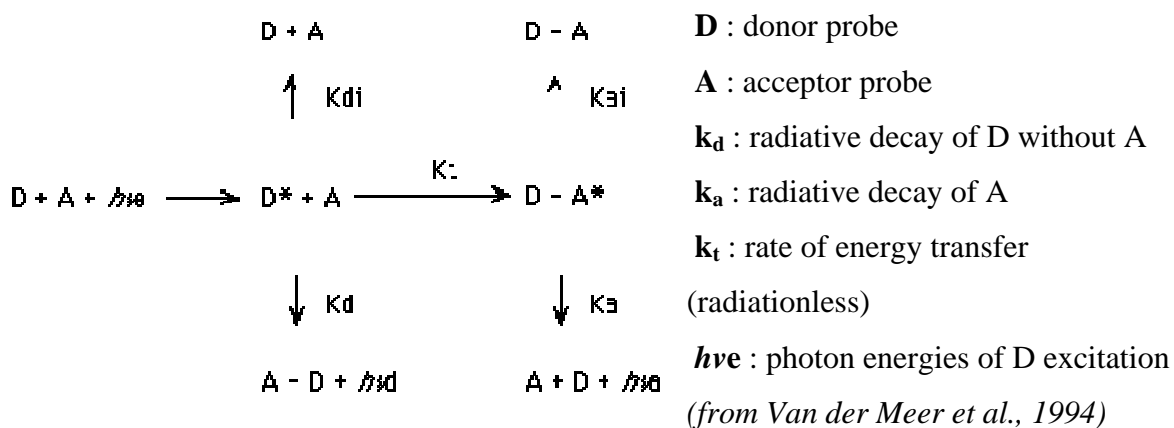
ANNEX I: Principle of FRET



The donor probe D is a fluorescent molecule. When light excites D at an appropriate wavelength (250-500 nm) its electrons jump from the ground state (S0) to a higher vibrational level (S1, S2, S3, etc). Within picoseconds these electrons decay to the lowest of these vibrational levels (S1) and then decay more slowly (nsec) to one of the S0 states and a photon is emitted

whose wavelength is longer than the exciting wavelength.

When the conditions are favorable for energy transfer to occur and the donor probe is excited at the appropriate wavelength, decay of donor fluorescence and energy transfer to the acceptor will compete for the decay of the excitation energy and can be described by the following scheme:



$h\nu_D$: photon energies of the D fluorescence

$h\nu_A$: photon energies of A fluorescence

k_{di} and k_{ai} are radiationless decay constants.

The transfer rate k_t varies inversely with the 6th power of the donor-acceptor separation (r^6) over the range of 1-7 nm, such distances are relevant for most biomolecules or their constituent domains engaged in complex formation and conformational transition.

The transfer rate also depends on J , the overlap integral of the donor emission and acceptor absorption spectra, k^2 , the relative orientation of the donor absorption and acceptor transitions moments (range 0-4); and n , the refractive index (range 1,3-1,6).

Donor quantum yield (Q) is defined as the ratio of the number of photons emitted to the number of photons absorbed, a parameter which depends on the immediate environment of the probe. In the presence of transfer (**Qda**) and in the absence of transfer (**Qd**) we have:

$$Q_{da} = \frac{K_d}{K_t + K_d + K_{di}} \quad Q_d = \frac{K_d}{K_d + K_{di}}$$

FRET efficiency (E) can be obtained by measuring the fluorescence intensities of the donor with acceptor (**Qda**) and without acceptor (**Qd**)

$$E = \frac{K_t}{K_t + K_d + K_{di}} = 1 - \frac{Q_{da}}{Q_d}$$

It can also be measured using the **lifetime** of the donor in presence (**Tda**) and absence of the acceptor probe (**Td**)

$$E = 1 - \frac{T_{da}}{T_d} \quad \text{where} \quad T_{da} = \frac{1}{K_t + K_d + K_{di}} \quad \text{and} \quad T_d = \frac{1}{K_d + K_{di}}$$

Förster distance

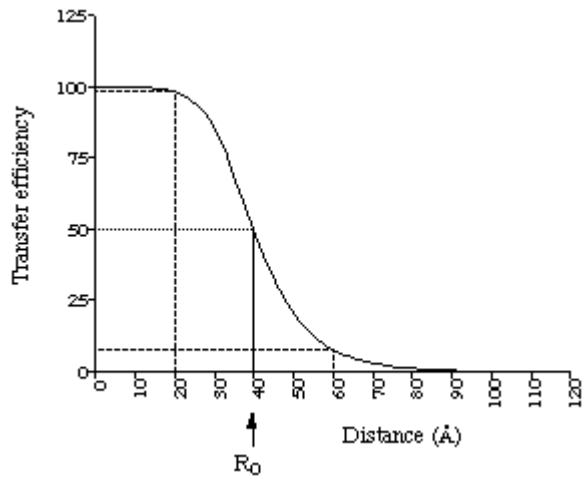
The relationship between the transfer efficiency (**E**) and the distance between the two probes (**R**) is given by the equation:

$$E = \frac{R_0^6}{R_0^6 + R^6}$$

R₀ is the Förster distance between the donor and acceptor probe at which **E** is 50%.

There is a limited range of D-A distances which can be probed by any donor-acceptor pair.

$$R_0 = \left\{ \frac{9000 (\ln 10) K^2 Q_d J}{128 \pi^5 n^4 N_{av}} \right\}^{\frac{1}{6}} = 9.78 \times 10^3 \{Q_d K^2 n^{-4} J\}^{\frac{1}{6}} \text{ \AA}$$



Qd: quantum yield of D,

n: medium refractive index

(Range 1.33-1.6)

N_{av}: Avogadro's number ($N_{av} = 6.02 \times 10^{23}$ per mole),

κ: orientation factor

J: overlap integral

(from Van der Meer et al., 1994).

The **overlap integral J** represents the degree of overlap between the donor fluorescence spectrum and the acceptor absorption spectrum and is given by

$$J = \int_0^{\infty} f_D(\lambda) \epsilon_A(\lambda) \lambda^4 d\lambda$$

λ : wavelength of the light

$\epsilon_A(\lambda)$: molar extinction coefficient of A at λ

$f_D(\lambda)$: fluorescence spectrum of D normalized on the wavelength scale.

$$f_D(\lambda) = \frac{F_{D\lambda}(\lambda)}{\int_0^{\infty} F_{D\lambda}(\lambda) d\lambda}$$

where $F_{D\lambda}(\lambda)$ is the D fluorescence per unit wavelength interval

Kappa square, the orientation factor is defined as

$$\kappa^2 = (\cos \theta_T - 3 \cos \theta_D \cos \theta_A)^2$$

θ_T : angle between the donor emission transition moment and the acceptor absorption transition moment

θ_D and θ_A : angles between the donor-acceptor connection line and the donor emission and the acceptor absorption transition moments, respectively

κ^2 varies between 0 and 4. It assumes a numerical value of 2/3 provided that both probes can undergo unrestricted isotropic motion.

ANNEX II: FRET corrections

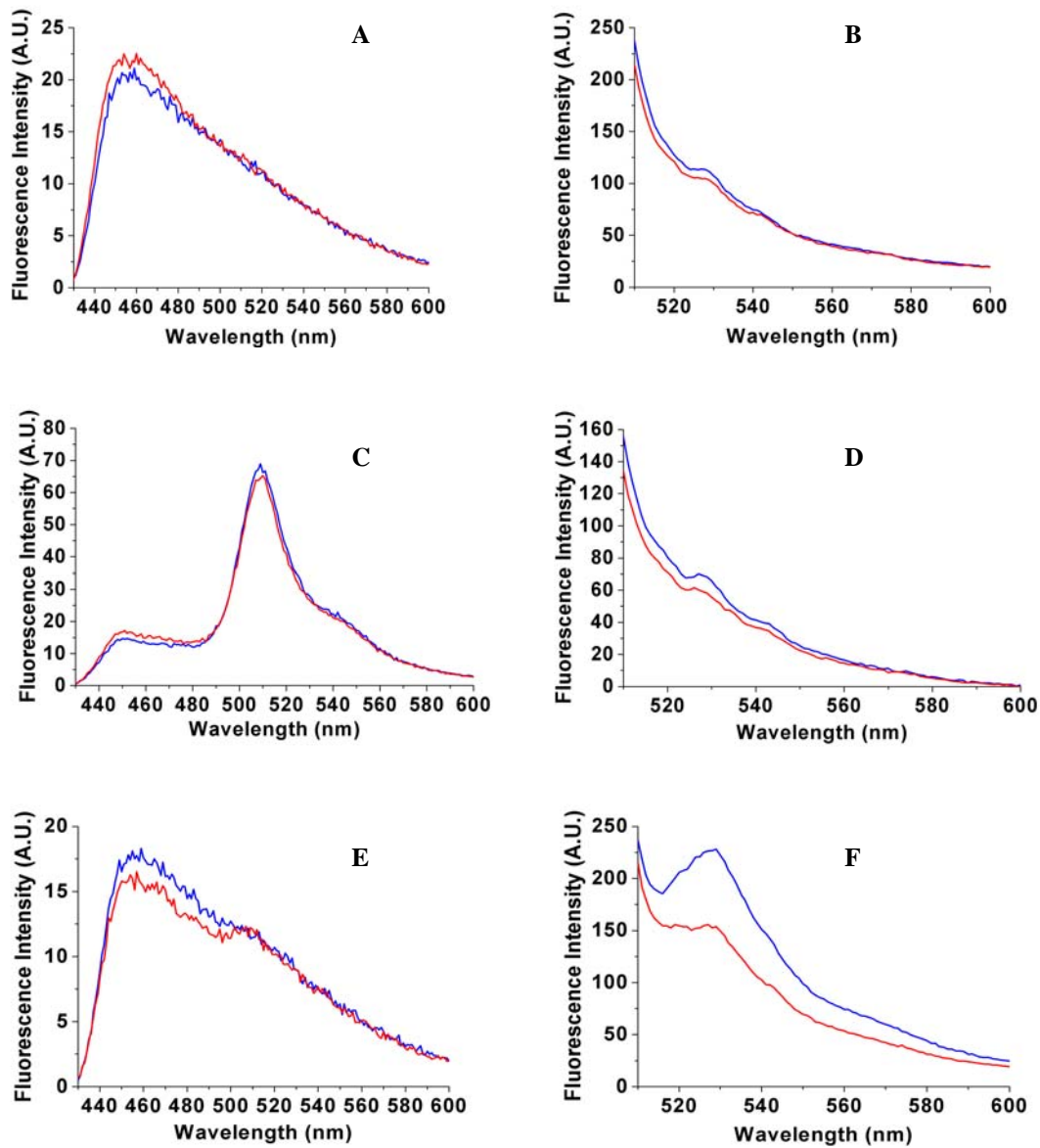
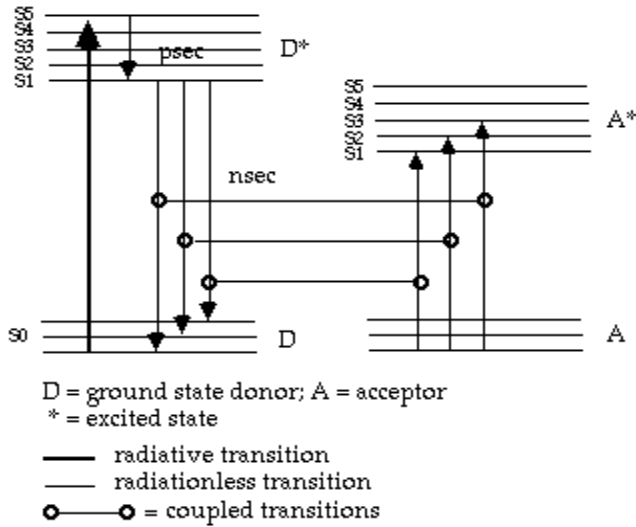


Figure Annex II: Spectra used for background and bleedthrough corrections. Suspensions of non transfected Vero cells (A and B) or Vero cells expressing either GFP₂ (C and D) or venusYFP (E and F) were excited at 390 nm (left panel: A, C and E) and subsequently at 498 nm (right panel: B, D and F), the excitation wavelengths for GFP₂ and venusYFP respectively. Emission spectra were acquired before (blue line) and after (red line) acceptor photobleaching. The spectra obtained were used to calculate the background and the bleedthrough with the programs Origin and Excel.

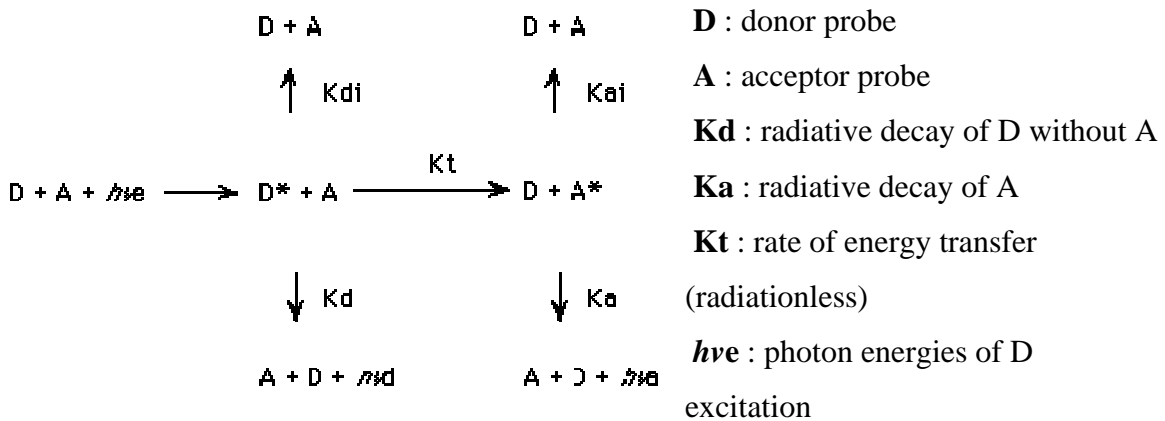
Annex I : Principle of FRET



The donor probe D is a fluorescent molecule. When light excites D at an appropriate wavelength (250-500 nm) its electrons jump from the ground state (S0) to a higher vibrational level (S1, S2, S3, etc). Within picoseconds these electrons decay to the lowest of these vibrational levels (S1) and then decay more slowly

(nsec) to one of the S0 states and a photon of light is emitted whose wavelength is longer than the exciting wavelength.

When the conditions are favorable for energy transfer to occur and the donor probe is excited at the appropriate wavelength, decay of donor fluorescence and energy transfer to the acceptor will compete for the decay of the excitation energy and can be described by the following scheme:



(from Van der Meer et al., 1994)

hν_d : photon energies of the D fluorescence

hν_a : photon energies of A fluorescence

K_{di} and **K_{ai}** are radiationless decay constants.

The transfer rate k_t varies inversely with the 6th power of the donor-acceptor separation (r^6) over the range of 1-7 nm, such distances are relevant for most biomolecules or their constituent domains engaged in complex formation and conformational transition.

The transfer rate also depends on J , the overlap integral of the donor emission and acceptor absorption spectra, k^2 , the relative orientation of the donor absorption and acceptor transitions moments (range 0-4); and n , the refractive index (range 1,3-1,6).

Donor quantum yield (Q) is defined as the ratio of the number of photons emitted to the number absorbed a parameter which depends on the immediate environment of the probe. In the presence of transfer (**Q_{da}**) and in the absence of transfer (**Q_d**) we have:

$$Q_{da} = \frac{k_d}{k_t + k_d + k_{di}} \quad Q_d = \frac{k_d}{k_d + k_{di}}$$

FRET efficiency (E) can be obtained by measuring the fluorescence intensities of the donor with acceptor (**Q_{da}**) and without acceptor (**Q_d**)

$$E = \frac{k_t}{k_t + k_d + k_{di}} = 1 - \frac{Q_{da}}{Q_d}$$

It can also be measured using the **lifetime** of the donor in presence (**T_{da}**) and absence of the acceptor probe (**T_d**)

$$E = 1 - \frac{T_{da}}{T_d} \quad \text{where} \quad T_{da} = \frac{1}{k_t + k_d + k_{di}} \quad \text{and} \quad T_d = \frac{1}{k_d + k_{di}}$$

Förster distance

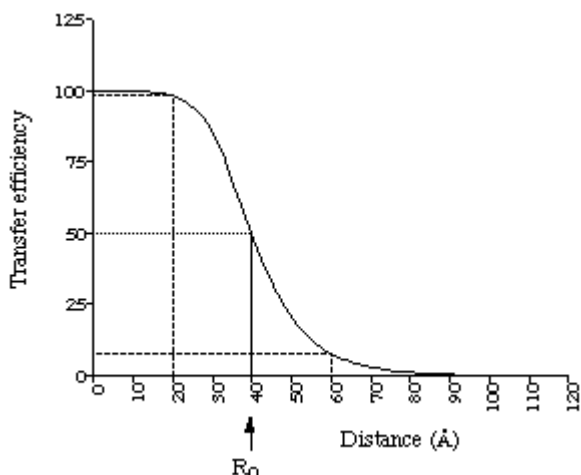
The relationship between the transfer efficiency (**E**) and the distance between the two probes (**R**) is given by the equation:

$$E = \frac{R_0^6}{R_0^6 + R^6}$$

R₀ is the Förster distance between the donor and acceptor probe at which **E** is 50%.

There is a limited range of D-A distances which can be probed by any donor-acceptor pair.

$$R_0 = \left\{ \frac{9000 (\ln 10) K^2 Q_d J}{128 \pi^5 n^4 N_{av}} \right\}^{\frac{1}{6}} = 9.78 \times 10^3 \{Q_d K^2 n^{-4} J\}^{\frac{1}{6}} \text{ \AA}$$



Q_d: quantum yield of D,

n: medium refractive index

(Range 1.33-1.6)

N_{av}: Avogadro's number ($N_{av} = 6.02 \times 10$ per mole),

K: orientation factor

J: overlap integral

(from Van der Meer et al., 1994).

The overlap integral **J** represents the degree of overlap between the donor fluorescence spectrum and the acceptor absorption spectrum and is given by

$$J = \int_0^{\infty} f_D(\lambda) \epsilon_A(\lambda) \lambda^4 d\lambda$$

λ : wavelength of the light

$\epsilon_A(\lambda)$: molar extinction coefficient of A at λ

$f_D(\lambda)$: fluorescence spectrum of D normalized on the wavelength scale.

$$f_D(\lambda) = \frac{F_{D\lambda}(\lambda)}{\int_0^{\infty} F_{D\lambda}(\lambda) d\lambda}$$

where $F_{D\lambda}(\lambda)$ is the D fluorescence per unit wavelength interval

Kappa square, the orientation factor is defined as

$$K^2 = (\cos \theta_T - 3 \cos \theta_D \cos \theta_A)^2$$

θ_T : angle between the donor emission transition moment and the acceptor absorption transition moment

θ_D and θ_A : angles between the donor-acceptor connection line and the donor emission and the acceptor absorption transition moments, respectively

K^2 varies between 0 and 4. It assumes a numerical value of 2/3 provided that both probes can undergo unrestricted isotropic motion.

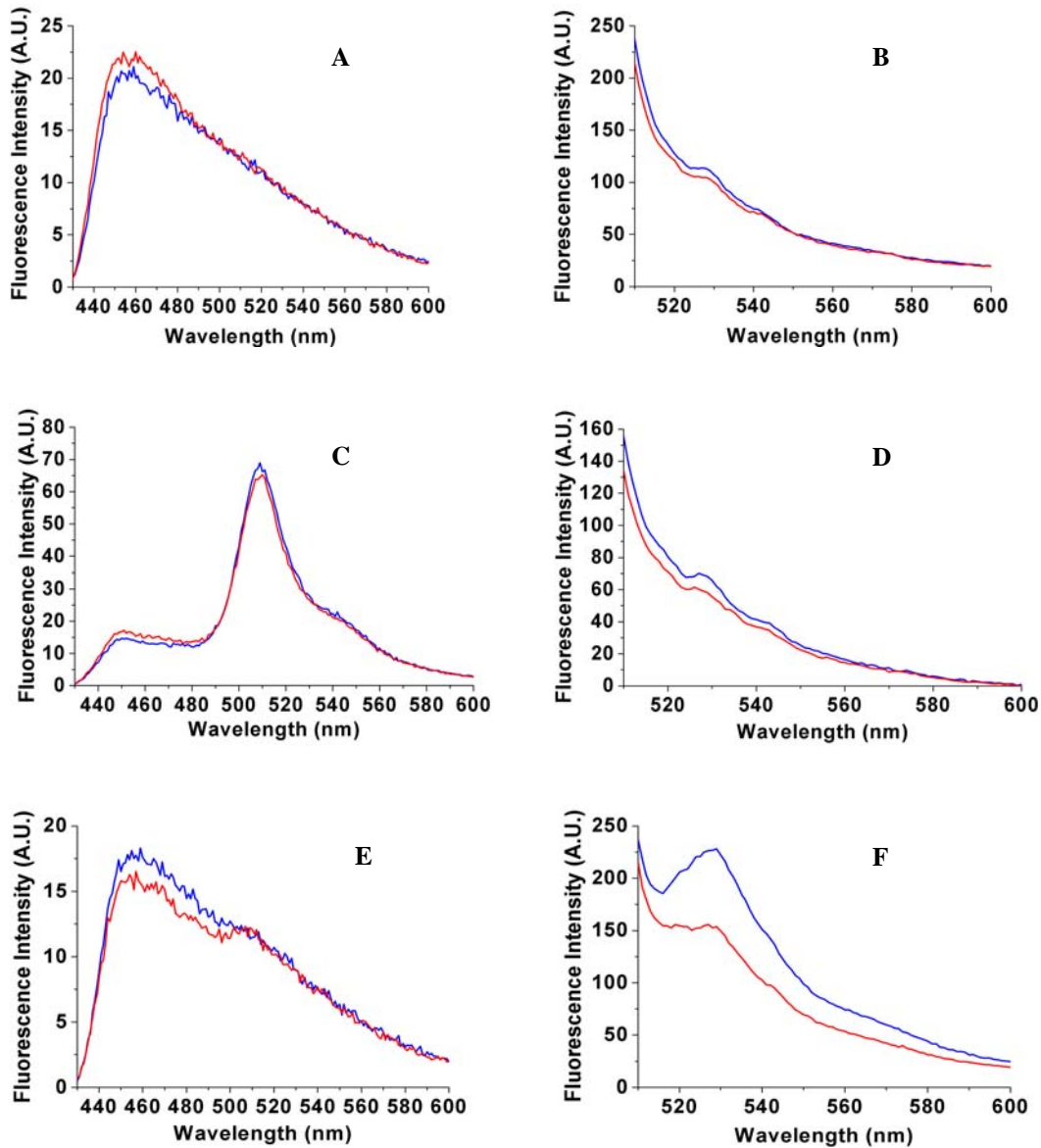


Figure Annex II : Spectra used for background and bleedthrough corrections. Suspensions of non transfected Vero cells (A and B) or Vero cells expressing either GFP₂ (C and D) or venusYFP (E and F) were excited at 390 nm (left panel: A, C and E) and subsequently at 498 nm (right panel: B, D and F), the excitation wavelengths for GFP₂ and venusYFP respectively. Emission spectra were acquired before (blue line) and after (red line) acceptor photobleaching. The spectra obtained were used to calculate the background and the bleedthrough with the programs Origin and Excel.

CURRICULUM VITAE

Name: Sophie Estelle Verrier

Date of birth: 28th August 1976

Place of birth: Decize, France

Education:

1982-1987	Primary school Saint-Just, Decize
1987-1991	Collège Maurice Genevoix, Decize
1991-1994	High school, Lycée Maurice Genevoix, Decize

Studies:

1994-1996	Université de Dijon - Pharmacy
1996-1998	Université de Dijon – Biology (DEUG)
1998-2000	Université de Toulouse – Biochemistry (Licence) Université de Toulouse – Structural Biochemistry (Maîtrise)
2000-2001	Diploma thesis in Pharmacology and Pharmacochimistry, Dept. of pharmacology and physico-chemistry of cellular and molecular interactions (CNRS/UMR 7034 – Université de Strasbourg)
2001-2005	PhD, Dept. of Neurobiology, Max Planck Institute for Biophysical Chemistry, Göttingen, Germany

LIST OF PUBLICATIONS

Verrier, SE., Barnewitz, K., Guo, C., Söling, H.-D., and Ferrari, D. M. (2006). The PDI-related protein Wind functions as a disaggregase in the processing of the 2-O-sulfotransferase Pipe. manuscript in preparation.

Verrier SE.*, Egner A.*, Müller T., Sölling HD. and Hell SW. Characterization of the Golgi apparatus cisternal morphology in live mammalian cell by two color 4Pi-microscopy. Work in progress.

Ouédraogo M., Lecat S., Gicquiaux H., **Verrier S.**, Gaire M., Mély Y., Takeda K., Galzi JL., and Bucher B. (2006). Novel internalization and trafficking properties of truncated and chimeric neuropeptide Y Y1 receptors. submitted manuscript.

Kawabe H., Rhee JS., Hirrlinger J., **Verrier SE.**, Varoqueaux F., Sonja Wojcik, Wang Y., Sudhof TC., Kirchhoff F., Rosenmund C., and Brose N. (2006). ERC Regulates Synaptic Short-Term Plasticity by Recruiting bMunc13-2 to Active Zones. submitted manuscript.

Verrier SE., Willmann M., Wenzel D., Fischer von Mollard G. and Söling HD. (2006). Members of a Mammalian Golgi→ER SNARE Complex Interact with the KDEL-Receptor and Subunits of the COPI Coatomer. submitted manuscript.

Neculai D.*, Neculai AM.* , **Verrier S.** , Straub K. , Klumpp K. ,Pfitzer E. , Becker S.(2005). Structure of the unphosphorylated STAT5a dimer. *J. Biol. Chem.*, 280(49):40782-7.

Egner, A., **Verrier S.**, Goroshkov A., Söling H.-D. and Hell S. W. (2004) 4Pi microscopy of the golgi apparatus in live mammalian cells. *J. Struct. Biol.*, 147(1):70-6.

Majoul I.,Goroshkov A.,Butkevich E. ,**Verrier S.**, Duden R. (2003). Live cell analysis of transport complex formation with FRET. *Proceedings of SPIE* Volume: 4967, Genetically Engineered and Optical Probes for Biomedical Applications.

Escricuet C., Gigoux V., Archer E., **Verrier S.**, Maignret B., Behrendt R., Moroder L., Bignon E., Silvente-Poirot S., Pradayrol L., Fourmy D. (2002). The biologically crucial C terminus of

cholecystinin and the non-peptide agonist SR-146,131 share a common binding site in the human CCK1 receptor. Evidence for a crucial role of Met-121 in the activation process. *J. Biol. Chem.*, 277(9):7546-55.